CARDIOVASCULAR INSTRUMENTATION

A thesis

submitted in partial fulfilment

of the requirements for the Degree

of

Master of Engineering (Electrical)

in the

University of Canterbury

by

P.J. BONES

University of Canterbury

1975

CONTENTS

CHAPTER		PAGE
	ABSTRACT	1.
1.	INTRODUCTION	2.
	1.1 The Cardiovascular System	2.
	1.2 The Development of Cardiovascular Instrumentation	10.
2.	ARTERIAL FLOW	15.
	2.1 Rheology and Dynamics of Blood Flow	15.
	2.2 The Effects of Atherosclerosis on Arterial Bloodflow	21.
	2.3 Blood Flow Measurement : The Ultrasonic Doppler Flowmeter	25.
3.	A METHOD OF ASSESSING THE CONDITION OF ATHEROSCLEROTIC ARTERIES	33.
	3.1 System Description	34.
	3.2 Digital Zero-crossing Detection	39.
	3.3 Design Considerations	48.
4.	THE HEART	51.
	4.1 The Performance of the Heart as a Pump	51.
	4.2 Parameters of Heart Performance	58.
5.	A METHOD OF CARDIAC EJECTION FRACTION ESTIMATION EMPLOYING A SPECIAL-PURPOSE CALCULATOR	66.
	5.1 Left Ventricular Volume Estimation from Cineangiocardiograms	66.
	5.2 Rectangular Rule Method - Employing Calculator	70.
	5.3 Input Transducers	75.
	5.4 Errors of the C.E.F. Calculation	79.
	5.5 Results using the C.E.F. Calculator	84.

(Contents, cont.)

CHAPTER		PAGE
6.	THE DESIGN OF THE C.E.F. CALCULATOR.....	88.
	6.1 Basic Description.....	88.
	6.2 Data Processing.....	95.
	6.3 Synchronous Control Unit (S.C.U.)...	104.
	6.4 Construction Details.....	111.
7.	THE CARDIAC EJECTION FRACTION AS A GUIDE TO SURGICAL PROGNOSIS.....	114.
	7.1 Methods.....	115.
	7.2 Results.....	117.
	7.3 Discussion.....	120.
8.	SUMMARY : CARDIOVASCULAR INSTRUMENTATION..	124.
	ACKNOWLEDGEMENTS.....	126.
	REFERENCES.....	127.
	APPENDICES.....	133.

ABSTRACT

A brief introductory treatment is made of the physiology and instrumentation of the cardiovascular system. Two areas are singled out for further investigation.

Arterial blood flow is investigated. In particular the effects of atherosclerosis on the pulse wave propagation through the arterial system are considered. A method for assessing arterial condition employing two ultrasonic Doppler flowmeters is proposed. A digital zero-crossing detection system is suggested as a means of producing a relatively simple and inexpensive instrument to provide real-time results.

The performance of the heart as a pump and the parameters used to assess this performance are considered. One such parameter is the cardiac ejection fraction, which relates the stroke and end-diastolic volumes of the heart's left ventricle. A new method of estimating left ventricular volume from single-plane cineangiocardiograms is described. Called the Rectangular Rule, this method approximates the volume to a series of circular discs. A special-purpose calculator has been developed to implement the Rectangular Rule and to make cardiac ejection fraction estimations. Results of studies made of patients indicate that the calculator produces results at least as accurate as those of an other popular method, and that the cardiac ejection fraction is a valuable guide to surgical prognosis.

CHAPTER 1

INTRODUCTION

1.1 THE CARDIOVASCULAR SYSTEM

The vital processes in living cells involve the utilisation of oxygen and nutrients and the simultaneous elimination of waste products. In the human body the cardiovascular system provides the means for this exchange to be carried out continuously. Blood, which contains oxygen, nutrients and waste products, is pumped around the system by the heart.

The heart contains four chambers (see Figure 1-1). The two atria act as 'primers' for the ventricles. Deoxygenated blood returns from the systemic circulation (head and body organs) and is pumped into the pulmonary circulation by the right atrium and ventricle. The pulmonary circulation consists only of the lungs, where the blood is supplied with oxygen and waste carbon dioxide is removed. The oxygenated blood is pumped into the systemic circulation and back around the body by the left atrium and ventricle.

Systemic Circulation

In the systemic circulation, blood is forced at high pressures (around 100 mm Hg) throughout a large volume of vessels against a considerable resistance. The nature of this part of the system means that it is of

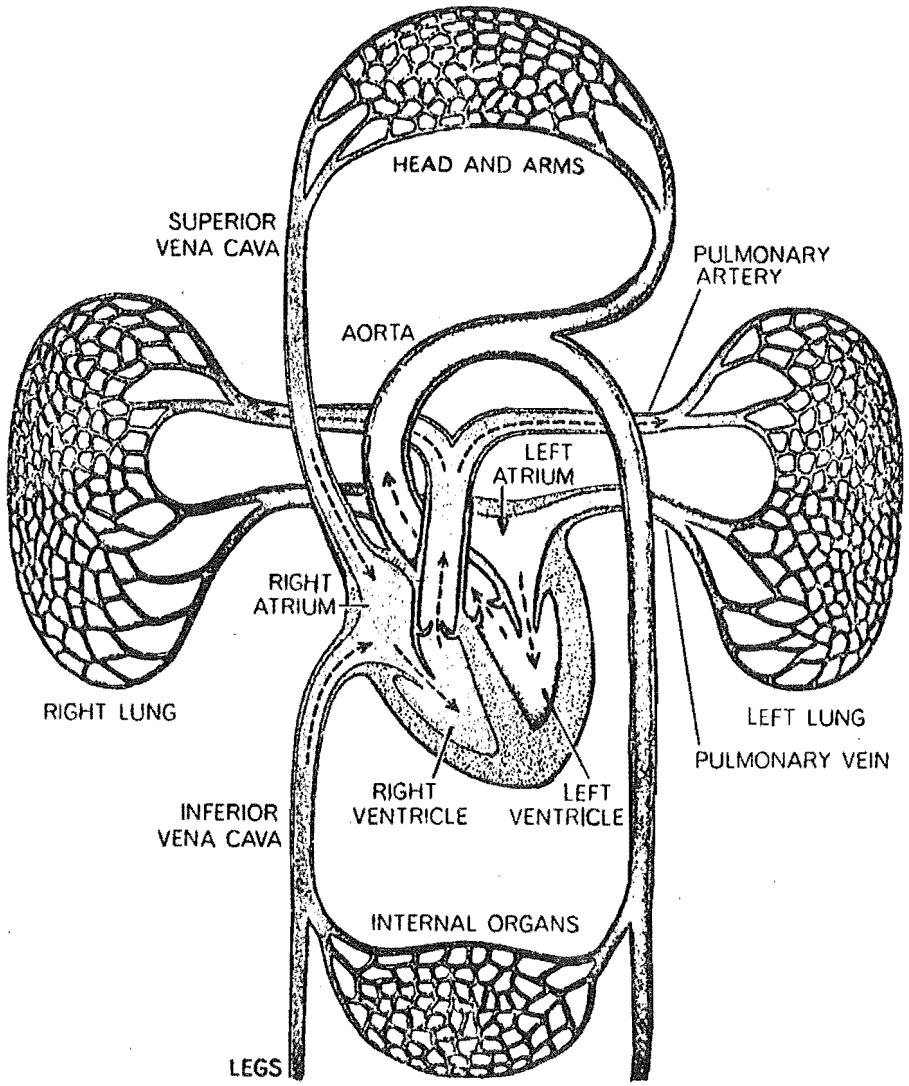

FIGURE 1-1. The cardiovascular system.

major importance in cardiovascular monitoring. The pulmonary circulation is operated at relatively low pressures and is therefore less critical.

The left ventricle pumps blood into the aorta and thence into other large arteries. These subdivide into smaller arteries and finally into minute capillaries. Exchange of oxygen, nutrients and wastes between the body tissue and the blood occurs by diffusion through the capillary walls. The capillaries recombine into venules and then into veins. The veins finally return to the heart.

Under steady state conditions the amount of blood flowing into the systemic circulation must equal the amount of blood flowing out. Thus the cross-sectional area and the flow velocity have an inverse relationship, as shown in Figure 1-2. Note also the change in pressures throughout the circulation. Only a small pressure gradient is needed to drive the blood along the arteries, but a large gradient in the small vessels.

The blood vessels vary widely in construction as well as in size. The arteries have thick walls of muscle and elastic tissue to withstand the high pressures. The elasticity of the walls acts to convert the intermittant flow of the aorta into the continuous flow of the capillaries. Capillary walls consist only of a thin permeable layer of smooth cells. Since the pressure in the venous system is low, veins and venules have relatively thin walls. However, there is a muscular layer which allows the veins to contract or expand and thus to change their storage capacity.

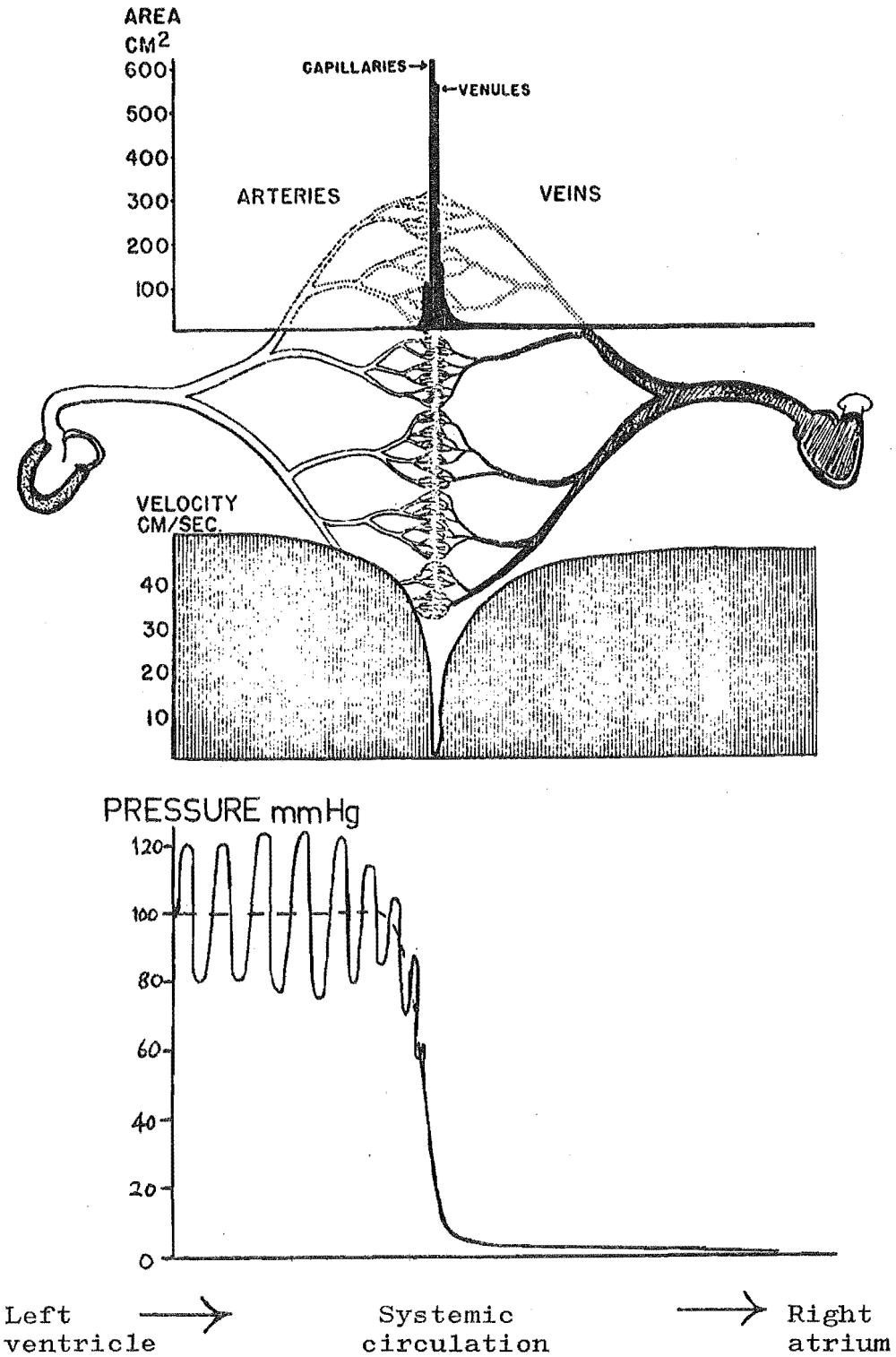

FIGURE 1-2. Vessel cross-sectional area, blood velocity and pressure in the systemic circulation.

Blood

Blood consists mainly of a faintly yellow fluid - plasma - in which are suspended numerous cellular elements, the blood cells. These are of three types: red and white blood cells and blood platelets.

The major function of the red blood cells is to transport haemoglobin, a complex compound which combines with oxygen. Enough haemoglobin is present for the transport of 20 ml of oxygen per 100 ml of blood. Normal red blood cells are biconcave discs, about 8 microns in diameter and 2 microns thick. The total number present in the blood (haematocrit) is regulated closely and will depend largely on the degree of physical activity of the person.

The Heart

The heart is constructed of two separated lattice structures of cardiac muscle, as shown in Figure 1-3. The two ventricles form one structure, the two atria the other. Fibrous tissue, supporting the four heart valves, connects the two structures. The valves are essential to maintain the directional pumping action of the heart. The amount of work which can be performed by muscle is determined by the amount of oxygen delivered to the muscle. Therefore for the cardiac muscle to cope with the varying load imposed by the cardiovascular system, it is supplied (normally) with a plentiful amount of blood direct from the aorta by means of the coronary arteries.

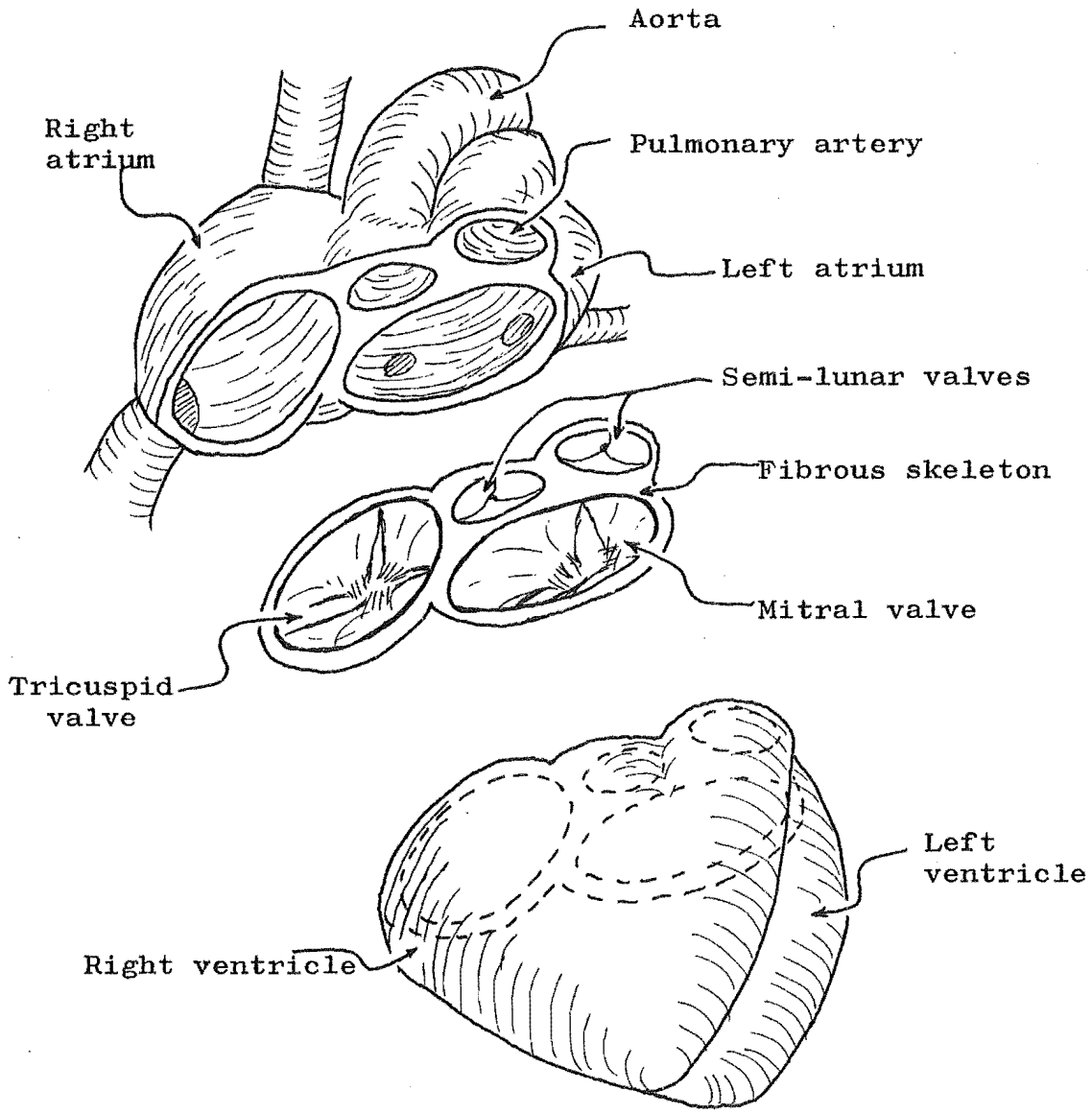

FIGURE 1-3. Heart anatomy.

Muscle contraction is stimulated by electrical impulses known as 'action potentials' which travel along the muscle fibres. Once excited, cardiac muscle remains in the contractile state for about 0.3 second. This allows time for the atria or ventricles to complete their contraction. Cardiac action potentials are produced spontaneously and rhythmically by a small piece of specialised muscle in the right atrium known as the sino-atrial node. The impulse travels throughout the atrial muscle and then is delayed by the atrio-ventricular node which provides the only electrical path between the atria and ventricles. The spread of the impulse throughout the ventricular muscle is aided by specialised conductive fibres, the Purkinje Fibres.

The cardiac cycle comprises a period of relaxation, called diastole, followed by a period of contraction, systole. Figure 1-4 illustrates the changes which occur throughout the cycle of a healthy heart. Blood flows continuously from the great veins into the atria (due to the venous pressure) and approximately 70% flows directly into the ventricles before the atria contract. Atrial contraction then causes the additional 30% filling. Thus the atria act as primers for the main ventricular pumps. The onset of ventricular contraction causes a steep rise in ventricular pressure as the atrio-ventricular valves close (see Figure 1-4). An additional 0.02 - 0.03 second is required before the ventricular pressure becomes sufficient to open the semilunar valves against the back pressure of the receiving arteries. Immediately,

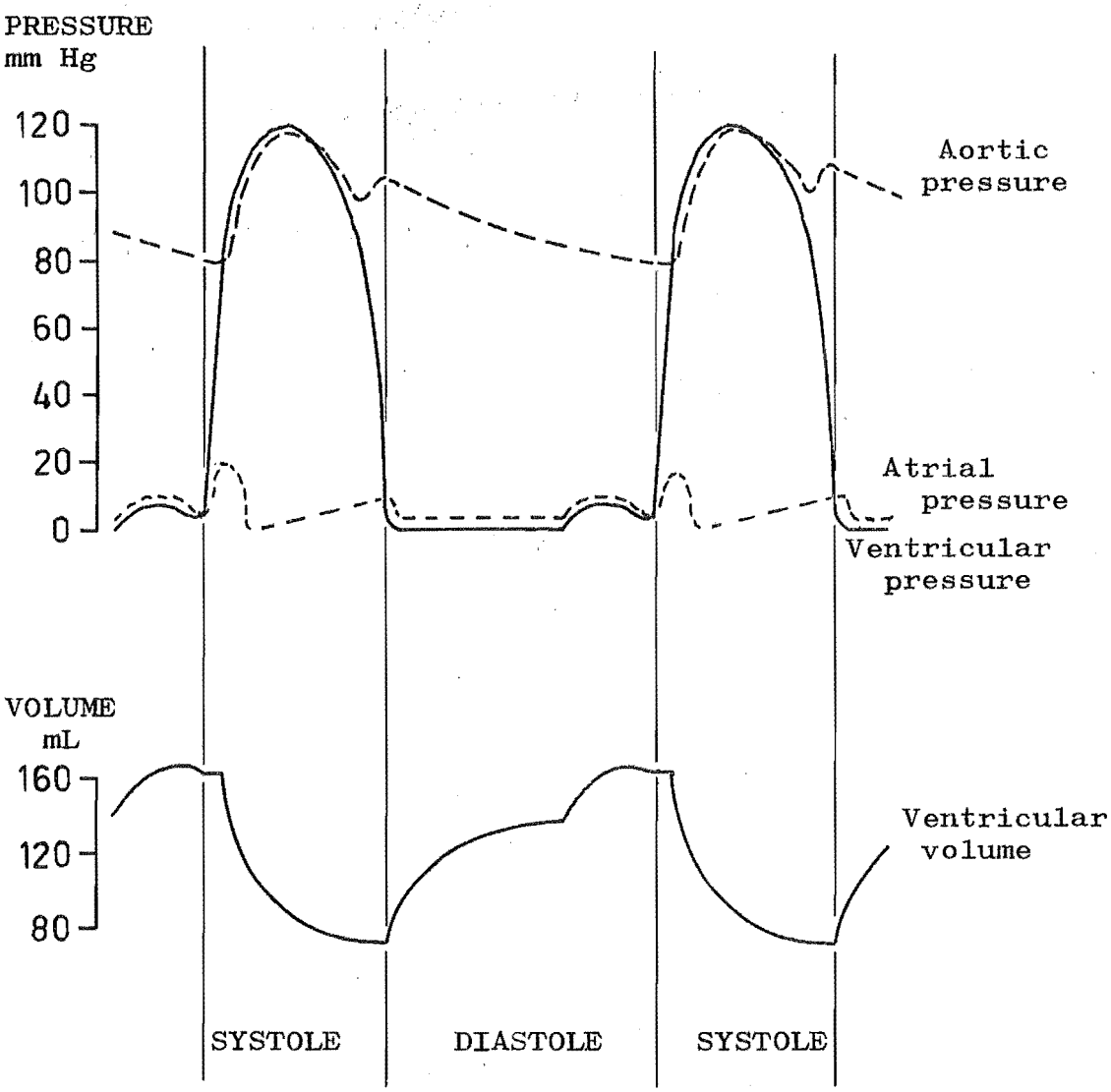

FIGURE 1-4. The cardiac cycle.

blood begins to flow out, as evidenced by the sharp decrease in ventricular volume. At the end of systole, ventricular relaxation begins suddenly, the internal pressure drops and the semilunar valves close. While the aortic valve is open, aortic pressure follows ventricular pressure. However, during diastole, with the valve closed, the pressure decreases as blood flows along the aorta into the systemic circulation.

1.2 THE DEVELOPMENT OF CARDIOVASCULAR INSTRUMENTATION

From very early times, man has known something about his anatomy. He has been able to carry out postmortem examination on his less fortunate fellows; physicians throughout the ages have carried out at least elimentary surgery; fairly obvious parallels were made with the anatomy of other mammals. Therefore he soon established the existence of the cardiovascular system, and recognised its basic function of moving blood around the body. Studies of blood under the microscope supplied missing information on its relation with other physiological systems, and the effects of various diseases on the blood and cardiovascular system were noted.

The amount of information the physician could gain from outside the living body, however, was severely limited. Without any diagnostic instruments, he could only palpate (feel with finger tips) the pulse, listen to the chest directly with his ear and observe external symptoms. The same procedures still form the basis of modern First Aid,

but enable only a general assessment of the patient's condition. The need was evident for some instruments to aid in monitoring the cardiovascular system.

The first instrument to appear was probably the stethoscope. The familiar instrument of today took some years to evolve from early 'ear trumpet' types. The stethoscope provides a mechanical amplification of the vibrations reaching the chest wall from blood and valve movements of the heart. Spectral analysis techniques are now being used to glean more information from phonocardiograms, which are recordings of the heart sounds.

Although the first efforts to measure arterial blood pressure were recorded in the 18th century, an indirect method for the physician to use did not appear until early this century. The method employed an inflatable cuff and mercury manometer. The cuff was inflated around the arm until the pulse could no longer be palpated; this was taken as the systolic pressure. Then the cuff was slowly deflated until the observed oscillations of the mercury column reached a maximum; this was interpreted as the diastolic pressure. This technique is known as sphygmomanometry and the only major changes have been in the method of obtaining the diastolic pressure.

The successful recording of instantaneous pressures has been very much a modern development. Intravenous catheters (small diameter plastic tubes) are normally used for this purpose. Either a fluid-filled catheter is employed and the pressure recorded by an electrical

transducer at the extra-corporeal end of the catheter, or the transducer is mounted in the catheter tip. The former type lack the high fidelity of the latter, as a consequence of the fluid coupling, but can be used for other purposes (such as injections) simultaneously with pressure monitoring.

In 1791, Galvani recorded his experiments with frogs in which he found that the application of electrical stimuli to muscle would evoke contractions. Most early research in the field was directed at responses to stimulation, but eventually the galvonometer (named after the original researcher) became sensitive enough to record potentials produced in muscle fibres between miniature electrodes. The development of the electrocardiograph (E.C.G.) was of major importance in cardiovascular instrumentation. E.C.G. signals are produced by currents induced in body tissue by the spread of the excitation potential across the heart muscle. The recording of these signals is now a standard technique in cardiac monitoring. As well as the standard 12-lead system of E.C.G. electrode positioning, systems have been devised which, either by analogue or digital means, produce a vector representation of the signals.[19]

The widespread use of x-rays in other fields lead to their use in cardiovascular application. The development of image intensifiers and techniques of catheterisation meant that any desired heart chamber or

blood vessel could be observed in detail by direct injection of radiopaque material. This process is known generally as angiography. The addition of a fast motion camera and T.V. monitor led to a full cineangiocardiographic facility capable of observing and recording the heart pumping action and condition of the coronary arteries.

New Developments

A large proportion of new developments in cardiovascular instrumentation have been directed towards two fields. The first is that of non-invasive monitoring; the aim has been to lessen the patient risk involved and the medical skill needed in performing monitoring techniques. The second field is in the analysis of measurements and recordings made, with development largely associated with the digital computer.

Probably the most significant recent advance in non-invasive techniques has been in the use of ultrasound. Ultrasound instruments for observing the heart's motion and condition in real time, and for recording instantaneous blood flows, are now in everyday use.[17,41] In neither case is it necessary for the patient to be subjected to any more discomfort or trauma than that involved in a normal medical examination. Chapter 2 of this thesis investigates arterial blood flow and the effects of a major cardiovascular disease, atherosclerosis. Chapter 3 describes the possible implementation of an inexpensive non-invasive instrument (based on ultrasonic flowmeters)

for detecting this disease.

The large amount of quantitation involved in cardiology has meant that the cardiologist has had to attain some skill as a mathematician and statistician. However outside help, in the form of digital calculators and computers, has enabled him to devote most of his time to his real task of patient treatment. Chapter 4 outlines the major parameters used in assessing the performance of the heart as a pump. Then Chapters 5 and 6 describe the development of a new method and special-purpose calculator to measure one of these, the cardiac ejection fraction. Chapter 7 presents the results of studies made of the cardiac ejection fractions of two groups of patients.

CHAPTER 2

ARTERIAL FLOW

A much simplified model of the cardiovascular system is a closed system of 'pipes' connected by a 'pump'. For the system to operate effectively, the pipes must be clear of obstructions, and the pump must provide an efficient conversion of energy into work and allow no backflow. The first of these factors, the condition of the pipes, mainly concerns the arteries. The flow through these vessels will be considered in this chapter.

2.1 RHEOLOGY AND DYNAMICS OF BLOOD FLOW

The analogy of arteries to pipes indicates that a suitable starting point in a discussion of blood rheology is to consider fluid flow through a pipe. Flow of the fluid occurs as a result of a pressure gradient along the pipe. The simplest analytical case is the ideal laminar flow of a homogeneous fluid in a smooth, rigid pipe.

For this simple solution, the flow is assumed to be steady, to have velocity components only in the direction of flow (laminar flow) and to be driven by a constant pressure gradient. The flow is symmetrical and the velocity varies across the pipe only by virtue of the fluid viscosity (constant). At the walls the velocity continuously reaches zero. Let the pressure difference

be ΔP along a length L of the pipe (see Figure 2-1 (a)). The pressure gradient = $\Delta P/L$. By considering a concentric cylinder of fluid, radius r, the velocity can be shown to be:

$$u = \frac{\Delta P}{4L\eta} (R^2 - r^2) \quad \ldots\ldots\ldots\ldots\ldots\ldots (2\text{-}1)$$

where: R = pipe radius,

η = viscosity of fluid.

(The derivation of this equation is completed in Appendix II).

Thus for this very idealised situation, the velocity profile is parabolic (see Figure 2-1 (b)). Integrating across the pipe cross-section, the total flow rate can be found:

$$Q = \frac{\Delta P . \pi . R^4}{8 . L . \eta} \quad \text{Volume/time} \quad \ldots\ldots\ldots (2\text{-}2)$$

This is known as the Poiseuille equation. Note that, according to this equation, flow is proportional to radius to the fourth power. This in part explains the large difference between the total cross-sectional areas of the arteries and the capillary beds, and the pressure gradients involved (refer to Figure 1-2).

A fluid is defined as a medium which is unable to sustain internal forces at rest. The ideal fluid considered above is a Newtonian fluid, in which the rate of fluid shear is proportional to the shear stress applied (velocity gradient equals rate of shear). Blood plasma exhibits some non-Newtonian properties, particularly at low

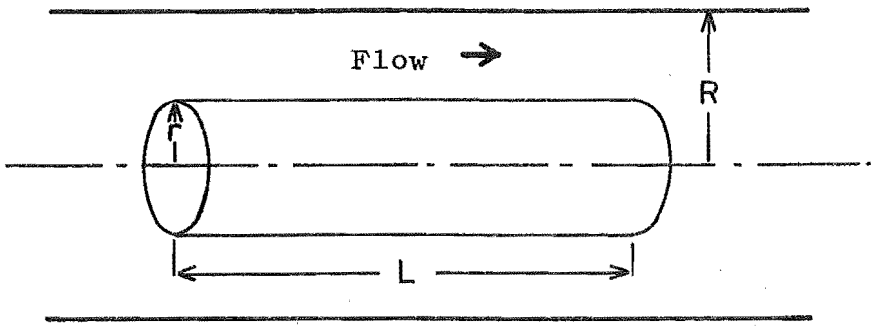

(a) Fluid flowing in cylindrical pipe.

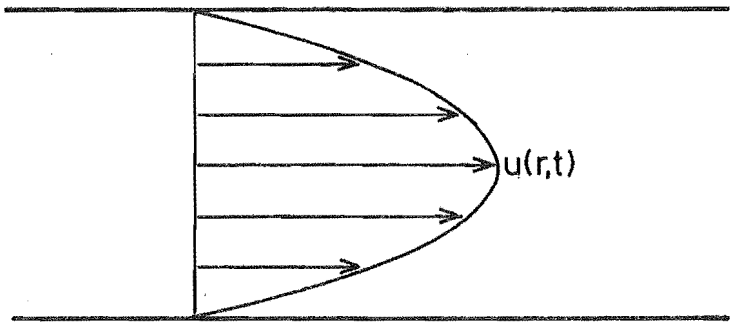

(b) Velocity profile of steady laminar flow of a homogeneous fluid.

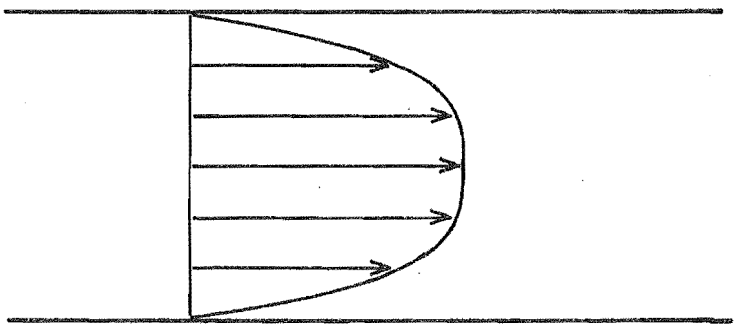

(c) A more realistic blood flow velocity profile.

FIGURE 2-1. Fluid flow velocity profiles.

rates of shear[48]. The existence of a yield stress (a stress below which no shearing occurs) has been suggested[6] and although this yield stress is probably extremely small in magnitude, it may have significant effects in small vessels. The non-Newtonian properties become insignificant at high rates of shear.[48]

The presence of a large percentage of red blood cells in the blood has a marked effect on the flow properties. Although the cells are flexible, they cannot sustain a shearing action, so they tend to move to areas of low rates of shear. As a result they gather in the centre of the vessel. This has the effect of increasing the fluid viscosity in this region and decreasing the viscosity near the vessel walls, producing a flattened velocity profile, as illustrated in Figure 2-1 (c). This profile is similar to that of a Bingham plastic.[48] The relative viscosity of blood is dependent on the haematocrit. The relationship is nearly linear in the normal range found in humans.

Blood flow is further complicated by its pulsatile nature and the visco-elastic properties of the arterial wall. The large pressure increase transmitted to the aorta during systole causes only the proximal vessel to distend immediately, due to the inertia of the blood in the aorta. Then the pressure pulse, and the resulting velocity pulse, propagate along the arterial tree. The velocity of the pressure pulse is in the region of 3 to 12 m/sec, but the mean blood velocity is only of the order of one hundredth of this value.[27,43] The amount of

distension of the arteries as the pulse passes is only of the order of 5 to 6% of their diameter because of the unusual rheological properties of the vessels.[37] Figure 2-2 shows typical blood flow versus time recordings at various arterial sites.[23]

The two major factors affecting the pulse pressure waveform and propagation velocity are:

1. stroke volume output of the heart,
2. compliance of the arterial tree

(compliance is the inverse of elastance). Once the pulse has been produced, its propagation is then only affected by the latter factor and minor interference from anatomical features (mainly reflections from junctions). In the absence of reflected waves, the value of c_p, the pulse wave velocity, is given by:

$$c_p = \sqrt{K/\rho} \qquad \text{.....(2-3)}$$

where: K = volume elastic modulus per unit length of artery,

ρ = blood denisty.[37]

The elastic modulus can be found in terms of the pressure and arterial dimensions:

$$K = \frac{PP.D}{2.\Delta D} \qquad \text{.....(2-4)}$$

where: PP = pulse pressure,

D = inner arterial diameter at diastole,

ΔD = increase in arterial diameter during systole.[22]

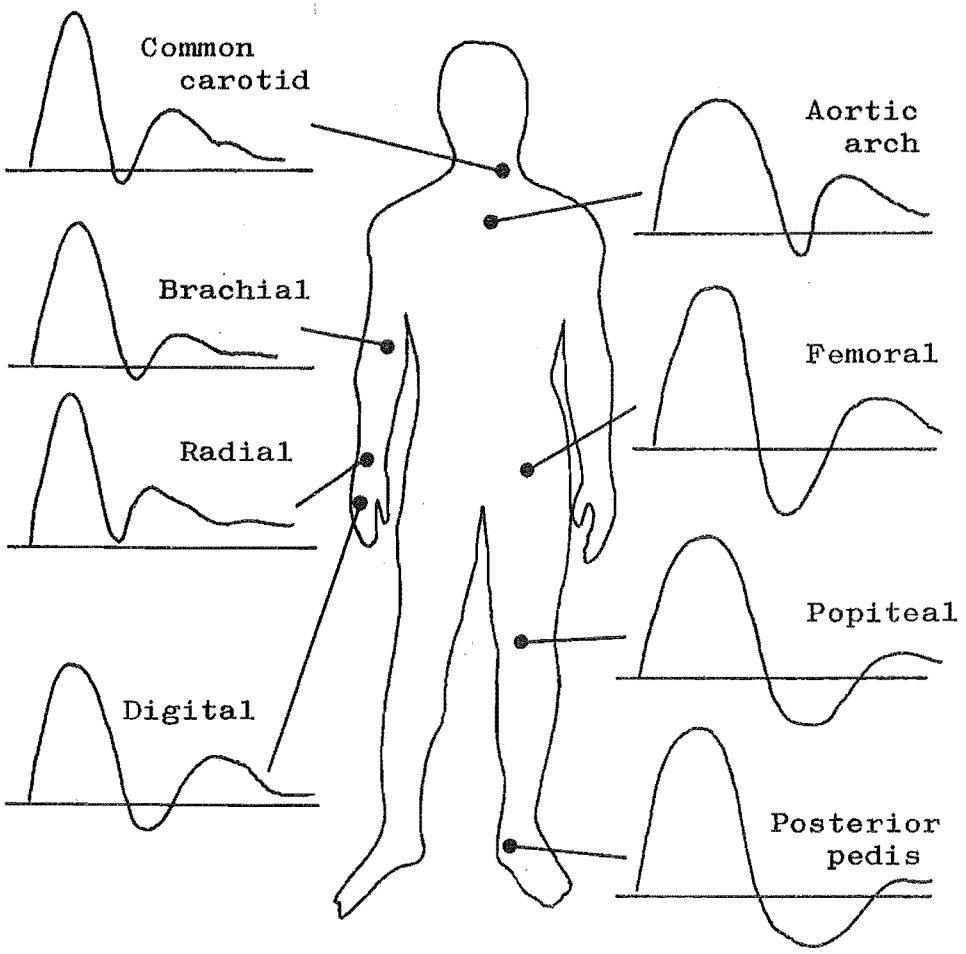

FIGURE 2-2. Typical blood flow velocity waveshapes at arterial sites.

Good correlation has been obtained between expected and experimental results for pulse wave velocity.[22,24]

The pulsatile nature of blood flow coupled to the very branched nature of the arterial tree has lead to investigations of the possibility of turbulent flow occurring rather than laminar flow. Just as some of the sounds of the phonocardiogram are definitely caused by turbulence in flow through the heart valves it is reasonable to expect the same phenomenon in the arteries. The general concensus of opinion is that conditions for turbulence occur, especially in the aorta where velocities are greatest, but fully developed turbulence may only occasionally occur since the periods of peak velocity are short.[37,48]

2.2 THE EFFECTS OF ATHEROSCLEROSIS ON ARTERIAL BLOOD FLOW

Atherosclerosis is a disease, principally of the large arteries, in which fatty deposits, known as plaques, appear in the artery wall inside the inner layer of smooth cells. These plaques contain a large amount of cholesterol. As well as causing restriction of the space available for blood flow, the lumen, the atheromatous plaques are usually associated with degenerative changes in the arterial wall. Often calcium precipitates to form hard calcified plaques. The result is general hardening of the arteries (arteriosclerosis). Almost half of all human beings die of arteriosclerosis; two thirds of these deaths are caused by blockage (thrombosis) of the very important coronary arteries.[27]

The first indication of plaque formation within the arterial wall is thickening of the inner layer (intima) and fragmentation of the inner elastic membrane. At this early stage, there is evidence of a slight increase in wall distensibility.[22,48] Once atherosclerosis is well developed, however, the intimal layer becomes fibrous resulting in an increase in the elastic modulus of the affected area. These changes occur to a lesser extent from normal aging, thus a plot of elastic modulus versus age shows a nearly linear relationship.[32] Advanced stages of atherosclerosis are characterised by severe calcification of plaques. The wall distensibility is further decreased and the calcified plaques often protrude into the lumenal space.

Atheromatous build-up is apparently particularly liable to occur in regions exposed to the full impact of the blood, such as at branches or points of abrupt curvature, so that it is probable that some mechanism of fluid dynamics contributes to formation.[48] If this effect is due to turbulence occuring at these points, this may provide an explanation for the localisation of plaque formation. Angiographic investigations of patients with coronary arterial disease at The Princess Margaret Hospital have shown that plaques tend to be localised in the majority of cases. The existence of turbulence immediately downstream of a stenosis (narrowing) has been predicted[28] and reported in peripheral arterial disease.[52] Turbulence caused by the initial mild stenosis may increase

the probability of further build-up at that point, rather than at some other point along the artery wall. It is also possible that plaque formation is more likely at points where the arterial wall experiences maximum flexing. This is especially relevant to the coronary arteries where considerable flexing occurs with the heart movement.

The arterial wall hardening associated with atherosclerosis has the effect of increasing K, the volume elastic modulus per unit length. Thus the same pressure changes cause less distension of hardened arteries than of the equivalent normal arteries. A corresponding increase in pulse wave velocity occurs, by Equation (2-3), since the blood density is essentially constant. This increase in velocity occurs only in the regions of elevated K, so the distributed or localised nature of the plaque formation is a factor in the measured transit time across a artery segment. The blood flow wave form is also affected by both the wall elasticity of the vessels through which it passes and the particular 'geography' of the plaque formation. Gosling *et al*. have documented these changes extensively with arterial segments of varying atheromatous involvement.[23] Examples from their findings are shown in Figure 2-3.

If complete occlusion of an artery occurs, collateral vessels will allow some flow past the blockage to the downstream area. Depending on the location of the occlusion and the length of time the collaterals have

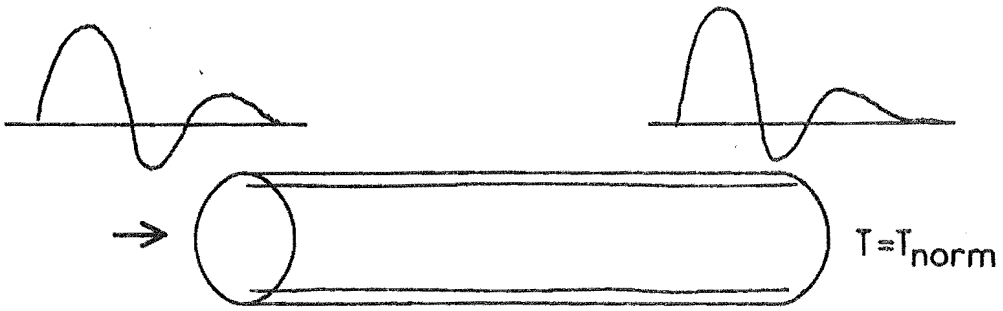

(a) A normal arterial segment.

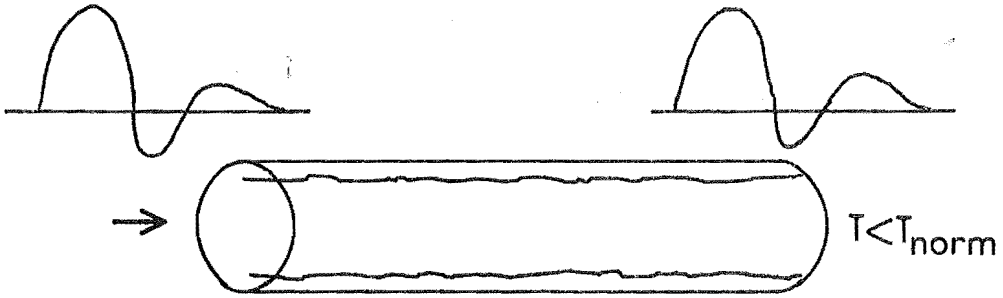

(b) General wall stiffening without marked narrowing.

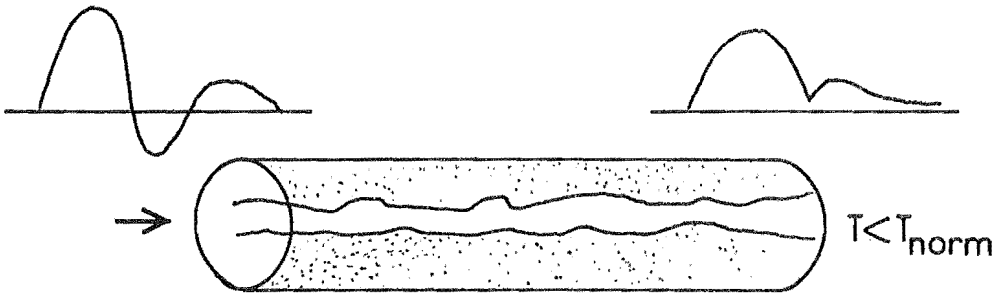

(c) General narrowing and wall stiffening.

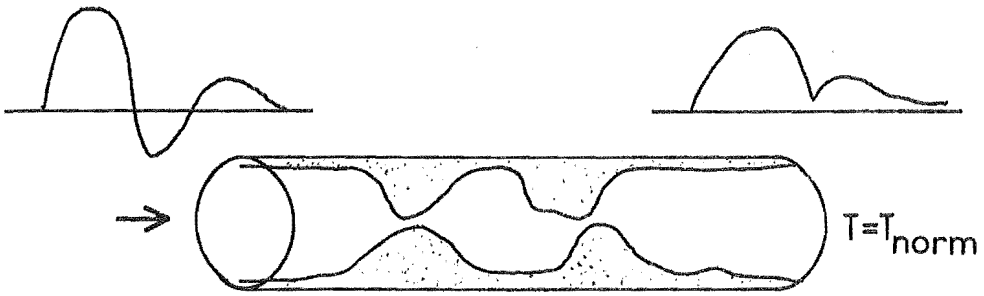

(d) Large plaques, but normal elasticity.

FIGURE 2-3. Effect of atheromatous conditions on waveshapes and transit times.

had to form, the collateral supply may be well formed or only consisting of very small vessels. The velocity of pulse wave propagation is independent of the vessel diameter, according to Equation (2-3). Therefore, assuming that the elastic modulus of the collateral vessels is similar to that of the main artery, the time taken for the pulse to pass the occlusion is mainly dependent on the length of the collateral supply. A larger than normal transit time for the pulse across an arterial segment can thus be taken as an indication of an occlusion.

Equation (2-2) shows that the actual flow occurring as a result of the passage of the pressure pulse is very dependent on the vessel diameter. Thus small collateral vessels will show a large resistance to flow, causing severe damping of the flow waveform. These effects have also been well documented (by correlating results with angiographic findings) and examples are shown in Figure 2-4.[23]

2.3 BLOOD FLOW MEASUREMENT : THE ULTRASONIC DOPPLER FLOWMETER

The measurement of blood flow is a much more difficult task than the measurement of blood pressure. Consequently, blood pressure became a recognised characteristic of the cardiovascular system well before blood flow. The first blood flowmeter which could follow fluctuations

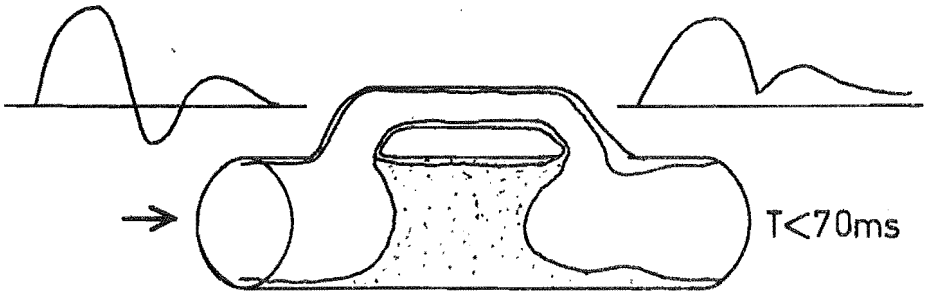

(a) Short and wide bore collateral supply.

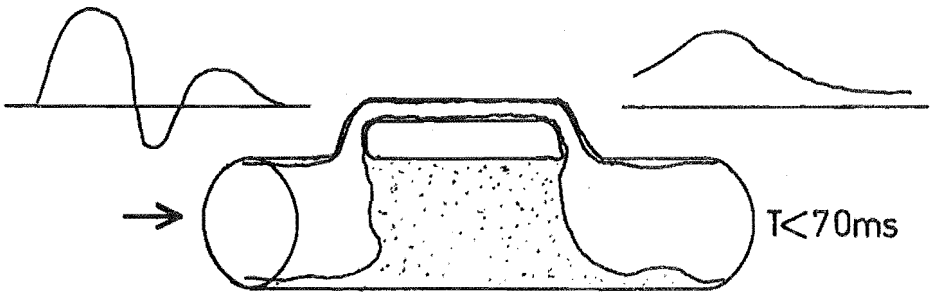

(b) Short and narrow collateral supply.

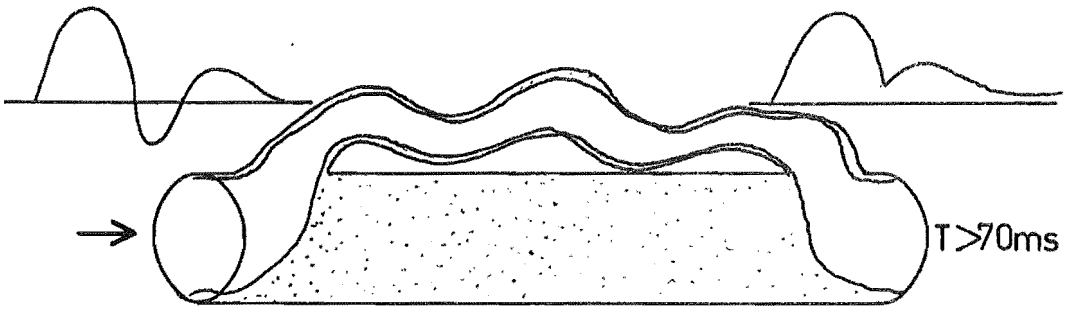

(c) Long and wide collateral supply.

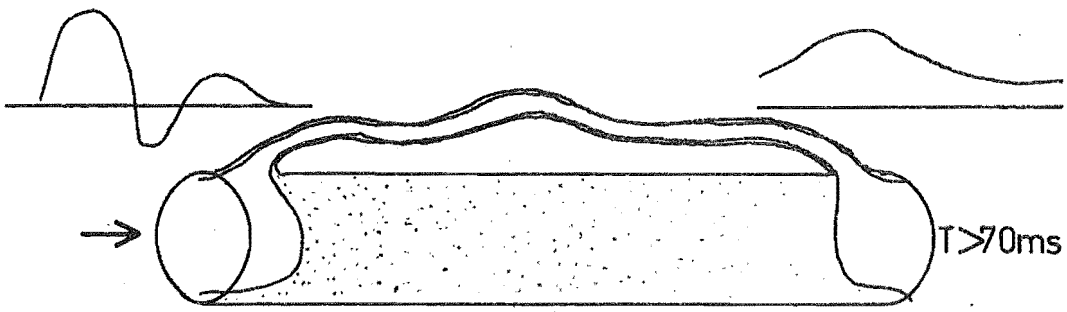

(d) Long and narrow collateral supply.

FIGURE 2-4. Effect of occlusion with collateral supply on waveshapes and transit times (in all cases, $T > T_{norm}$).

in flow with high fidelity, was the electromagnetic flowmeter, invented by Kolin in 1936.[33] This instrument has become one of the most widely used types of flowmeters although it is relatively invasive. A cuff transducer must be placed around the vessel to be measured, or a catheter transducer used.

The flowmeters which appear to have the most future as non-invasive instruments are of the ultrasonic Doppler type.[41] Many commercial ultrasonic Doppler flowmeters are available which allow the transcutaneous monitoring of flow velocity. The simplest of these generate continuous ultrasonic waves and receive back-scattered reflections with a double piezoelectric crystal transducer. Aspects of the operation of this continuous-wave Doppler flowmeter are considered in the following.

Ultrasonic Doppler Signals

The ultrasonic Doppler flowmeter was first described in 1961 by Franklin.[20] Conceptually, the operation is straightforward. Consider Figure 2-5, which shows a flowmeter probe directed transcutaneously at an artery. The frequency shift of the ultrasound reflected from moving blood cells in the artery and received by the probe is described by the Doppler shift equation:

$$\Delta f = \frac{2uF \cos \theta}{c} \quad \text{.....(2-4)}$$

where: Δf= frequency shift of reflected ultrasound,
F= frequency of transmitted ultrasound,

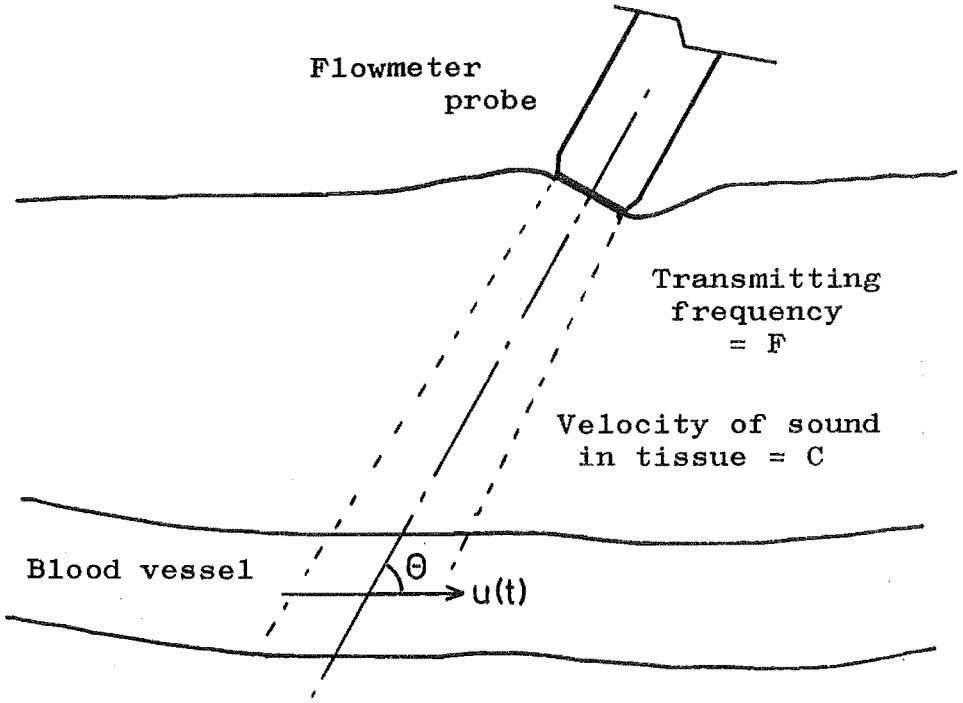

FIGURE 2-5. Operation of the ultrasonic Doppler flowmeter.

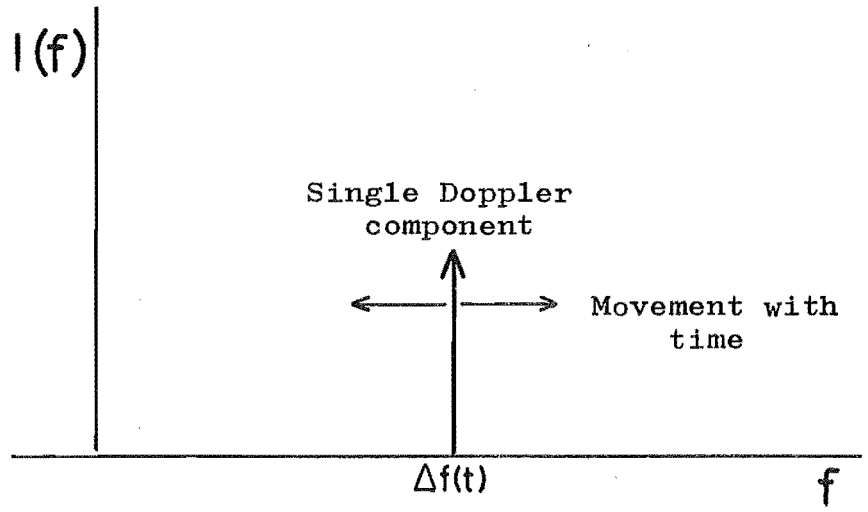

FIGURE 2-6. Doppler amplitude spectrum produced by uniform blood velocity.

θ = angle of inclination to the direction of flow,

c = velocity of sound in body tissue (approximately 1500 m/sec),

u = magnitude of blood velocity.

The choice of transmitting frequency, F, is based on a number of factors. The absorption of ultrasound as it passes through body tissue is dependent on frequency; the higher the frequency the more the absorption per unit distance. The sensitivity of the Doppler flowmeter to changes in blood velocity is directly dependent on F; by equation (2-4), Δf is proportional to F.u for given θ. Thus the choice of F is a compromise between maintaining a satisfactory signal-to-noise ratio (lower absorption means greater reflected signal returns) and satisfactory sensitivity. The normal range of frequencies used for Doppler flowmeters is 5 to 10 MHz.

Demodulation of the received signal from the flowmeter probe is necessary to recover the Doppler information, Δf. The signal is essentially frequency modulated (F.M.) and therefore can be demodulated by a standard F.M. demodulator.[35] However, modifications are necessary for distinction to be made between forward and backward flow in the resulting output signal. For the model case of a vessel containing blood flowing with a single velocity, the output from the Doppler flowmeter will be a single frequency component, with frequency Δf, and amplitude dependent on many factors related to the

flowmeter system and the strength of the reflected signal. If the single velocity of the blood is made a function of time, then the frequency of the Doppler component will become a corresponding function of time, $\Delta f(t)$, but the amplitude has no cause to change. This is illustrated in Figure 2-6.

Effect of Velocity Profile

Clearly the single velocity blood flow considered above is not a real situation; the range of velocities which occurs across the blood vessel gives rise to a Doppler frequency spectrum. Each frequency in the spectrum corresponds to a velocity, and the amplitude of the spectrum at that frequency is a function of the proportion of blood cells moving with the associated velocity. The ideal homogenous fluid flowing in a pipe, considered in Section 2.1, has a parabolic velocity profile, which can be shown to give rise to a flat frequency spectrum (see Figure 2-7(a)). Since the number of reflecting blood cells 'illuminated' by the ultrasonic beam at any time is essentially constant, the area under the amplitude spectrum remains constant as velocities change with time. These results are derived in Appendix III.

The real velocity profile occurring in arteries differs from the ideal parabolic profile (see Section 2.1), and therefore the flat Doppler spectrum is modified. Flattening of the profile in the centre of the vessel, where the maximum velocities occur, causes an increase

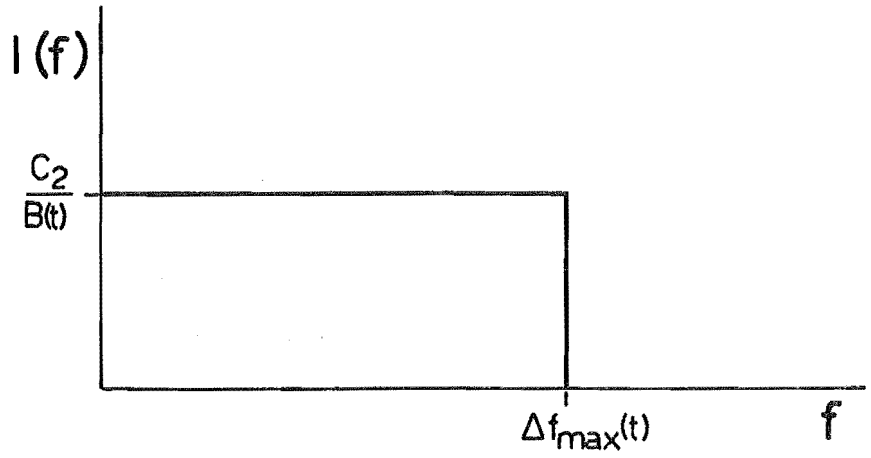

(a) Ideal parabolic blood velocity profile.

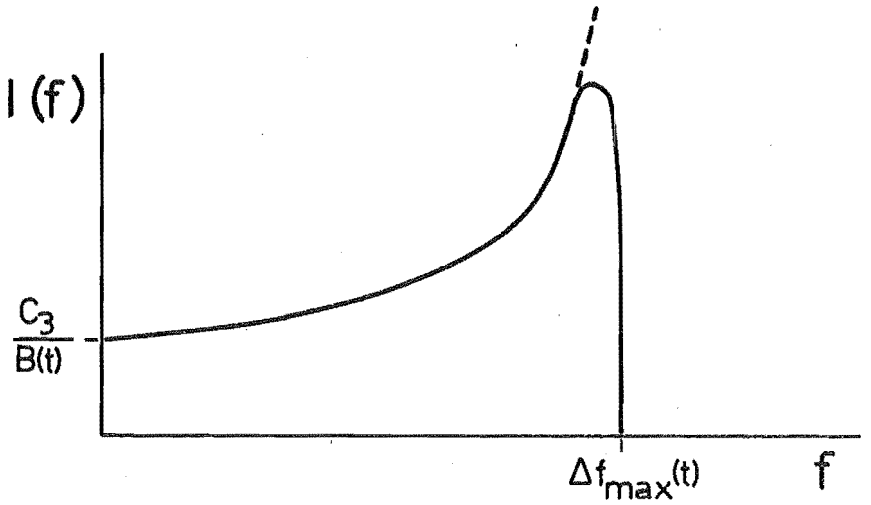

(b) 'Real' blood velocity profile.

FIGURE 2-7. Doppler amplitude spectra (full illumination of vessel cross-section).

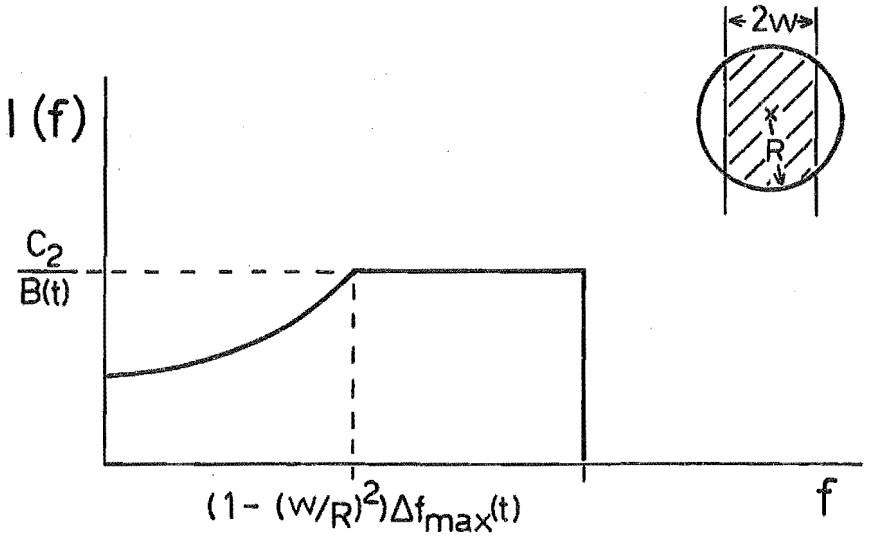

FIGURE 2-8. Narrow beam Doppler amplitude spectrum (parabolic velocity profile).

in the number of reflecting cells with these velocities and a corresponding peak in the amplitude spectrum (see Figure 2-7(b) and Appendix III).

Effect of Beam Width

The spectra discussed above have been derived considering that the entire cross-section of the blood vessel is illuminated by the ultrasonic beam. However in many cases this is not the case as the artery may be relatively large, and flowmeter probe developments have resulted in narrow beams. If a narrow beam is centred on a vessel with a parabolic profile, the spectrum produced is shown in Figure 2-8. Since less of the outer, slower blood cells are illuminated by the narrow beam, while the contribution from the highest velocity cells is retained, the spectrum is biased towards the frequencies in a band below Δf_{max}. This result is also derived in Appendix III.

CHAPTER 3

A METHOD OF ASSESSING THE CONDITION OF ATHEROSCLEROTIC ARTERIES

Atherosclerosis, in its severe forms, is recognised as being responsible for a large percentage of premature deaths. The gradual development of symptoms as a result of the gradual accumulation of atheromatous material has meant that detection usually only occurs at a relatively advanced stage. The early stages of the disease can be expected to be reversible to some extent, so great importance must be placed upon methods of early detection.

Some methods of arterial investigation, notably arteriography (angiography) and plethysmography, have been in use for some time, but are not suitable for performing this early detection. Arteriography is an excellent method of locating well-formed plaques, but involves exposing the patient to a relatively large radiation dosage, and thus is usually only employed in severe cases where surgery is contemplated. Plethysmography is only suitable for evaluating the mean arterial blood flow into a region of the body. The need is apparent, therefore, for a non-invasive, non-injurious method of detecting significant build-up of atheromatous material, suitable for application to relatively large populations.

The effects of atherosclerosis on the pulse wave velocity and shape have been discussed in Section 2.2, and the Doppler ultrasonic flowmeter in Section 2.3. A method has been described by Gosling et al.[22,23] which employed two Doppler flowmeters to monitor changes in the pulse wave as it moved along a selected artery. The Doppler signals were recorded on analogue tape and processed off-line. Two parameters, the propagation time of the pulse between the two sites and the "pulsatility index" of the two waveforms, were derived and correlated with results obtained from angiograms. The results were encouraging. The following is a description and analysis of a proposed system to apply the same method by different techniques. The purpose is to simplify the diagnostic procedure and give the clinician an immediate result, while using a relatively inexpensive and uncomplicated instrument. Since the development of the system has not reached the stage of circuitry design or construction, this chapter is limited to description and analysis of the system operation.

3.1 SYSTEM DESCRIPTION

The simplicity of the proposed system is mainly due to its digital nature. A block diagram of the major components is shown in Figure 3-1. Each of the two flowmeter probes transmits an identical continuous-wave signal at a frequency in the range of 5 to 10 MHz

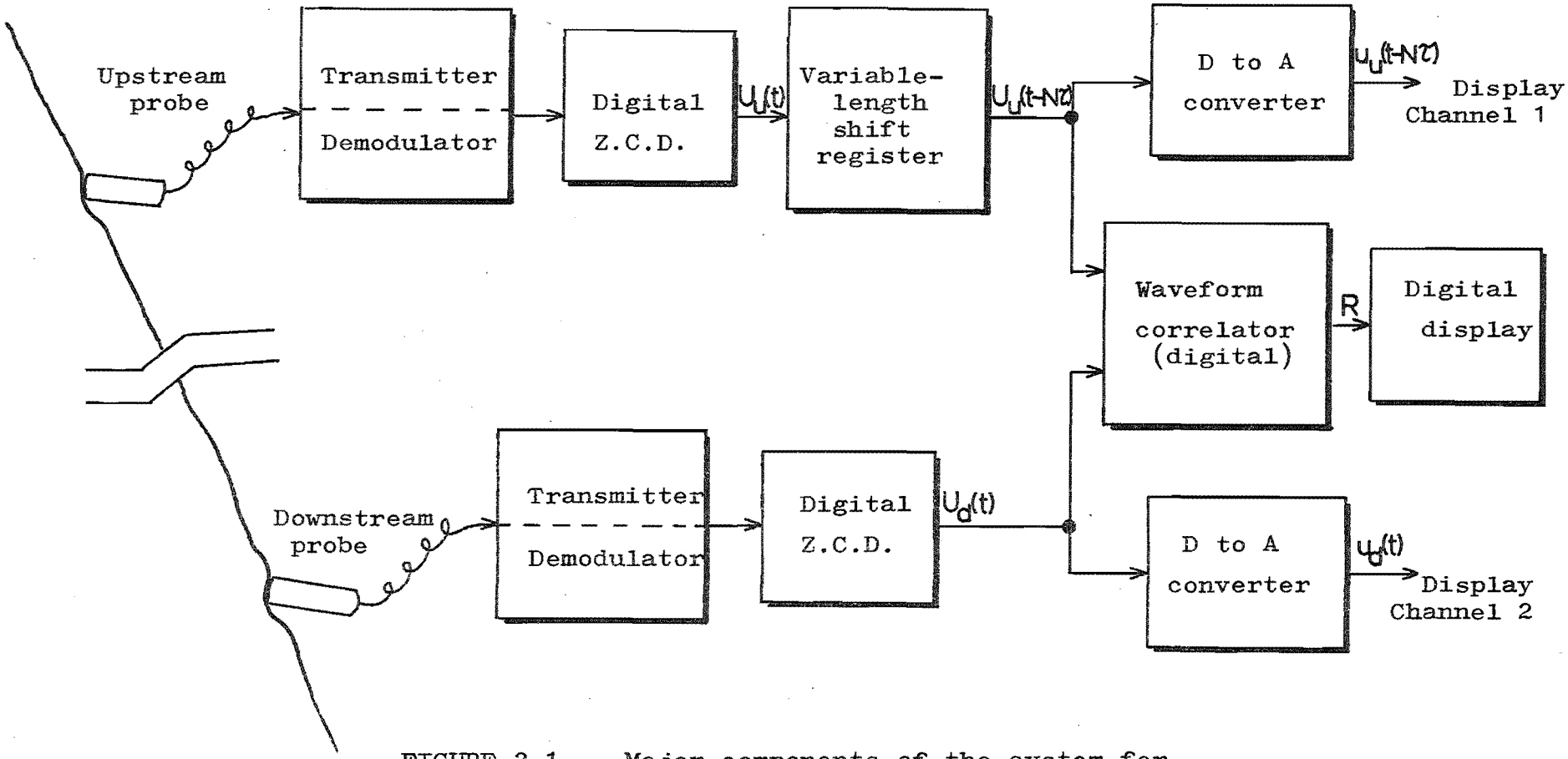

FIGURE 3-1. Major components of the system for assessing arterial condition.

(the lower frequencies give better penetration for observing deep arteries). The received signal from each probe is first demodulated, the result being a signal containing a spectrum of frequencies in the range 0 to 10 kHz, as discussed in Section 2.3. A digital zero-crossing detector (Z.C.D.) is used to sample a representative frequency Δf_c, from the Doppler signal, proportional to the blood velocity. The detector counts the number of zero-crossings in a preset sample time. Identical detection systems are used for both flowmeters.

At the end of each sample period (length, τ seconds), two numbers, one from each detector, are stored in a latch. The number from the upstream flowmeter, U_u, is shifted into the left end of a variable-length shift register. If the shift register is set to a length of N words, the rightmost word of the register at any instant t is $U_u(t-N\tau)$. This word can be compared to the present sample of the downstream flowmeter, $U_d(t)$. If N is set so that the leading edges of the delayed upstream pulse (corresponding to a sharp increase in $U_u(t-N\tau)$) and the real-time downstream pulse coincide, then $N\tau$ is the time delay of the pulse propagation between the two flowmeter sites. This process is illustrated in Figure 3-2. Clearly, since τ must be of finite size, then $N\tau$ is only an approximation to T.

An analogue display of the detected velocity waveforms is achieved by simple digital to analogue (D to A)

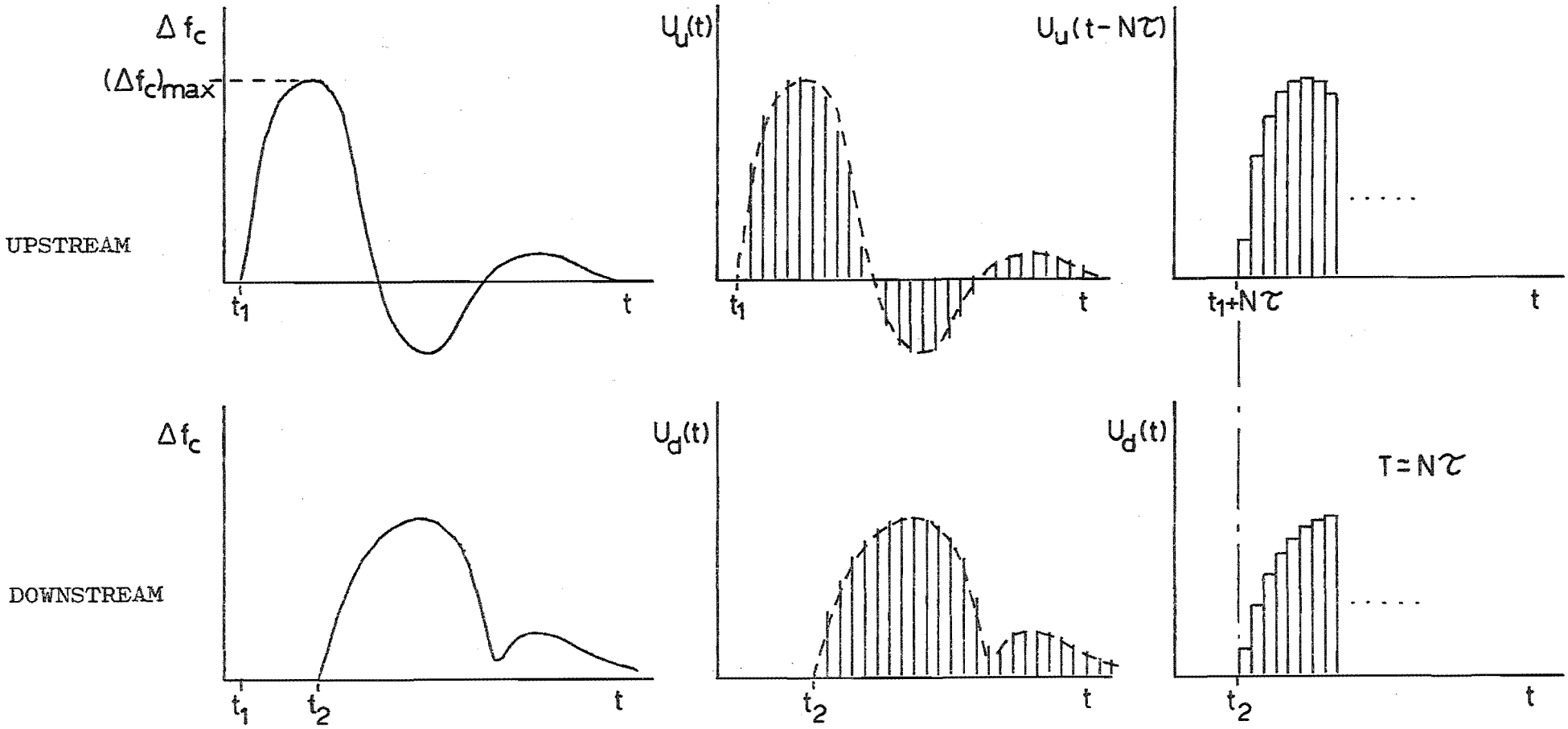

FIGURE 3-2. Processing of the detected pulse waves to measure the transit time T.

converters. A final low-pass filter on each channel will give a continuous curve for observation by oscilloscope, or recording by pen recorder. Thus the operator can observe the output waveforms on the oscilloscope, adjust N manually until the leading edges coincide, and read $T = N\tau$ off the dial.

As well as evaluating the transit time of the pulse wave between the two arterial sites, further information on the condition of the artery can be obtained from a comparison of the velocity waveforms. Changes in shape are related to the degree of arterial wall hardening and lumen obstruction as discussed in Section 2.2, and illustrated in Figures 2-3 and 2-4. Gosling et al.[22,23] used a digital computer to analyse the waveforms, the pulsatility index being based on harmonic content. It would be advantageous to be able to perform the comparison in real time at the bedside. This is possible with the system described here.

The displayed outputs from the Z.C.D.'s after D to A conversion are single line functions in time and so can easily be compared by eye on the oscilloscope. However, since a sampled digital representation of the waveforms is available at the outputs of the Z.C.D.'s, a direct comparison technique can be used to derive a measure of waveform correlation. An easily derived estimate of the correlation of the waveforms is the integral, over one period (period = time between heart beats), of the square of the difference between $u_u(t-T)$ and $u_d(t)$. This

"correlation factor", R, is given by:

$$R = \int_{1 \text{ period}} \left[u_u(t-T) - u_d(t)\right]^2 dt$$

If there are m samples taken in each beat period, then this integration can be achieved with the sampled data by:

$$R = \sum_{n=1}^{n=m} \left[U_u((n-N)\tau) - U_d(n\tau)\right]^2 \quad \ldots\ldots\ldots\ldots (3\text{-}1)$$

Clearly, R is only a significant correlation factor if the time delay, $N\tau$, is properly adjusted to be equal to the transit time, T. Also some normalisation of the waveforms is necessary. This could be achieved by adjusting the flowmeter gains until the displayed peak velocities approximate to a datum line on the oscilloscope screen.

3.2 DIGITAL ZERO-CROSSING DETECTION

Zero-crossing detection is a method of deriving a representative frequency, Δf_c, from a signal containing a spectrum of frequencies. It is only possible to retain a small amount of the information contained in an unknown signal with a Z.C.D. The frequency, Δf_c, is equal to half the number of zero-crossings of the signal (in the time domain) per unit time, and can only be obtained by averaging the signal over a finite time interval. However, if the signal's amplitude spectrum, I(f), is known, and stationary with respect to time, then information can be retained by the Z.C.D. process.

The received signal from the continuous-wave ultrasonic Doppler flowmeter, after demodulation, has been shown to have an amplitude spectrum dependent on the blood velocity profile across the observed vessel and on the beam width (Section 2.3). The magnitude of the mean (and maximum) velocity is a function of time, since arterial flow is pulsatile, but the profile is approximately constant. A constant shape of amplitude spectrum results. The time dependence of the velocity can be considered as an independent function, B(t) and the amplitude spectrum normalised as shown in Figure 3-3. Both the effects of flattened velocity profile and narrow flowmeter beam produce accentuation of the higher frequencies in the Doppler spectrum (refer to Section 2.3), as shown in Figure 3-3. This spectrum is similar to that found experimentally by spectral analysis.[50] Thus the signal processed by the Z.C.D. has an amplitude spectrum with predictable shape and with spread along the frequency axis governed by a function of time.

Flax et al.[18,50] have suggested that Δf_c is given by:

$$\Delta f_c = \left[\frac{\int_0^\infty \Delta f^2 \, I(f) \, df}{\int_0^\infty I(f) \, df} \right]^{\frac{1}{2}} \quad \ldots\ldots\ldots\ldots\ldots (3\text{-}2)$$

The test system of Figure 3-4(a) has been used to verify this equation for specific amplitude spectra. The Doppler spectrum resulting from a parabolic velocity profile is similar to that of white noise passed through a low-pass

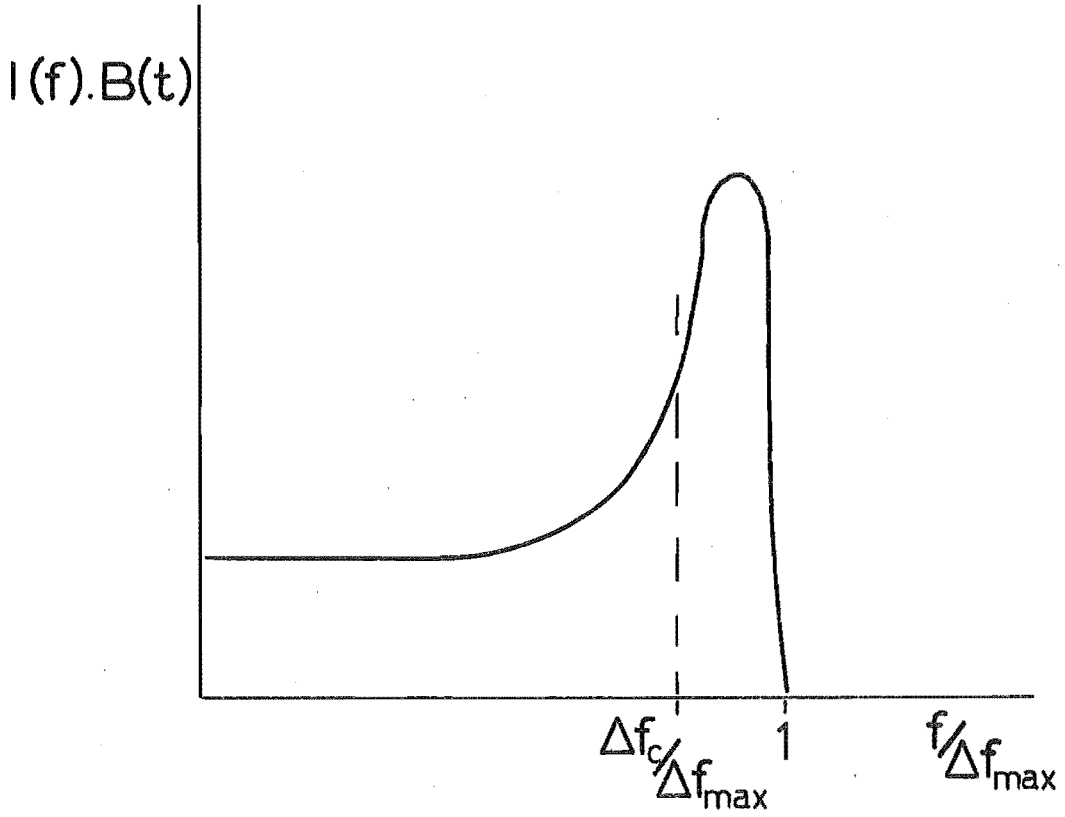

FIGURE 3-3. Normalised Doppler spectrum predicted in 'real' situation.

filter, with Δf_{max} corresponding to the cutoff frequency of the filter (see Figure 3-4(b)). Substituting into equation (3-2) gives:

$$f_c = \left[\frac{\int_0^{\Delta f_{max}} \Delta f^2 \frac{B}{\Delta f_{max}} \, df}{\int_0^{\Delta f_{max}} \frac{B}{\Delta f_{max}} \, df} \right]^{\frac{1}{2}}$$

$$= \Delta f_{max}/\sqrt{3}$$

With filter cutoffs ranging from 1 kHz to 10 kHz, results ranged from $\Delta f_c = 0.570 \, \Delta f_{max}$ to $\Delta f_c = 0.580 \, \Delta f_{max}$ ($1/\sqrt{3} \doteqdot 0.577$). Thus good experimental verification of equation (3-2) was found.

Applying equation (3-2) to the 'real' amplitude spectrum of Figure 3-3 can be expected to give a different coefficient, relating Δf_c to Δf_{max}, but one which is constant provided the spectral shape is constant. A coefficient of 0.7 to 0.8 appears likely.

Errors in Δf_c Estimation

There are a number of restrictions on the fidelity of the digital Z.C.D. output. The first of these is the inherent error in the measured Δf_c. This error can be considered to be caused by statistical 'noise' in the output. Flax *et al.*[18] have analysed this noise for the analogue Z.C.D., which uses a low pass filter to convert a train of pulses into an analogue voltage. Clearly,

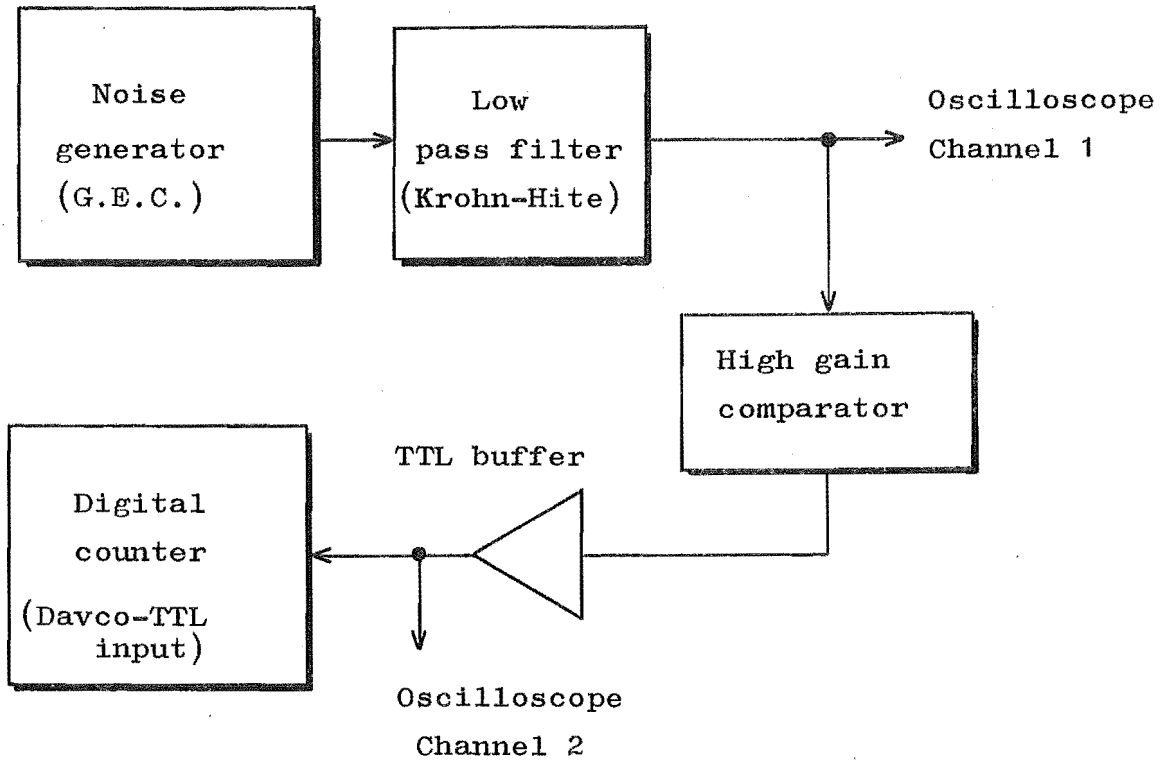

(a) Digital Z.C.D. test system.

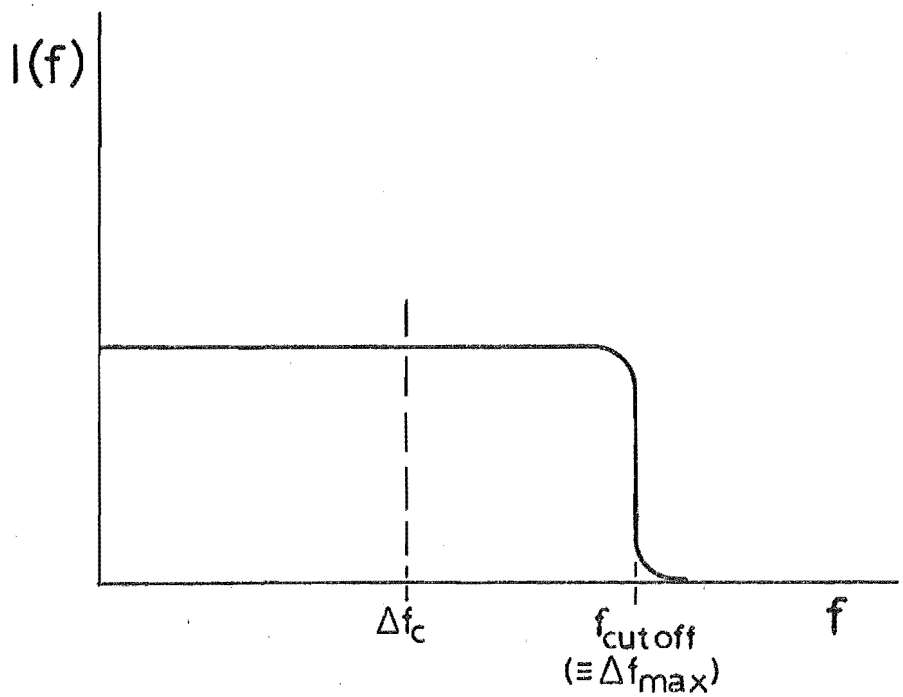

(b) Spectrum produced in test system.

FIGURE 3-4. Experimental evaluation of the digital Z.C.D.

if the time constant is large, the output voltage will tend to an accurate representation of Δf_c, as long as Δf_c does not change rapidly. This corresponds to a long sampling (counting) period of the digital Z.C.D. Similarly if the time constant/sampling period is small, the output will be able to follow rapid fluctuations in Δf_c, but any instantaneous estimation of Δf_c can be expected to be in error.

Zero-crossing detection of white noise results in a random pulse train, which can be described statistically by a Poisson distribution. For an analogue Z.C.D., the mean and standard deviation of the output is given by:

$$\left(\frac{\sigma}{\mu}\right)_{f_c} = (4\ \Delta f_c \beta)^{-\frac{1}{2}}$$

where: σ and μ = mean and standard deviation of the Δf_c estimations,

β = time constant of the Z.C.D.[18]

Experiments carried out with a digital Z.C.D. (the test system of Figure 3-4(a)) show that similar relations hold with β replaced by the sample time, τ . Figure 3-5 is a graph of the results, which indicate that the following approximate relation holds:

$$\left(\frac{\sigma}{\mu}\right)_{f_c} \doteq (5\ \tau\ \Delta f_c)^{-\frac{1}{2}} \quad \ldots\ldots\ldots\ldots (3\text{-}3)$$

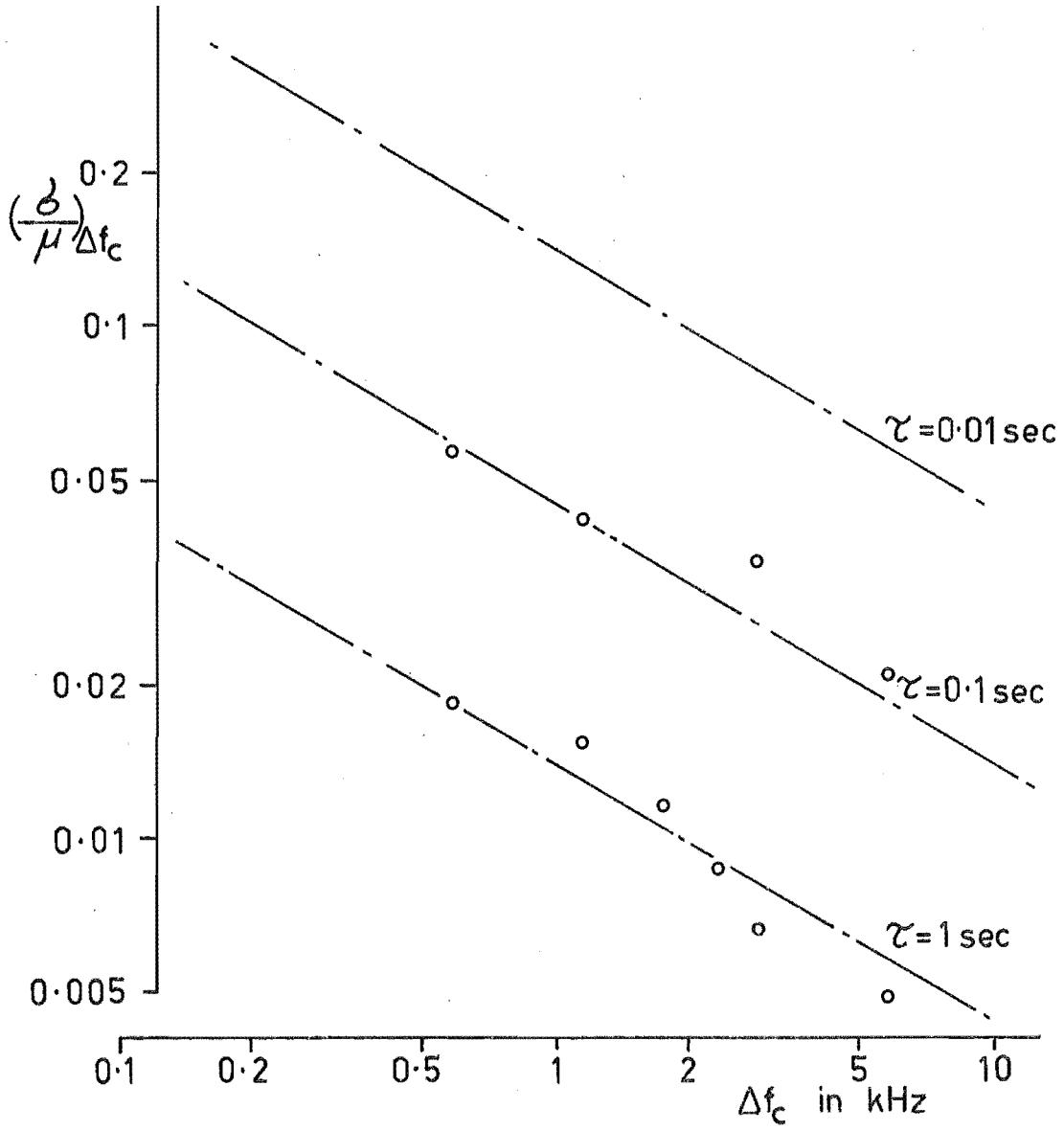

FIGURE 3-5. Digital zero-crossing estimation errors (Equation (3-3).

The assumption of the Doppler signal being band-limited white noise is a worst case in relation to errors in Δf_c. The modifications to the amplitude spectrum, causing accentuation of the high frequencies, effectively restrict the error, with Δf_c constrained within the peaked region. It is evident also, from Figure 3-5, that the largest error in Δf_c is likely at low values of Δf_c corresponding to low velocities. The application of the digital Z.C.D. suggested in this chapter is mainly concerned with observing the higher velocities during the passage of the pressure pulse. Thus the error is unlikely to cause significant output signal degradation.

Bandwidth Considerations

The Z.C.D. output depends on the whole frequency spectrum up to Δf_{max}. Therefore the instrument bandwidth must be sufficient to allow for the maximum blood velocity which is likely to occur. An empirical value for this is 8 times $\bar{u}$, the mean flow velocity over one cycle (mean flow divided by vessel cross-sectional area).[18] Thus, the maximum frequency component is:

$$(\Delta f_{max})_{max} = 8 \frac{2 F \bar{u} \cos \Theta}{c}$$

For a transmitting frequency (F) of 5 MHz, Θ of 45° and $\bar{u}$ of 40 cm/sec (large artery), the resultant maximum Δf_{max} is approximately 15 kHz. The amount of random noise present will depend on the bandwidth, so maximum signal-to-noise ratio will be gained by restricting the bandwidth to the

minimum required. The effect of too much restriction will be clipping of the Z.C.D. output peaks.

The artifacts caused by "wall thump" have been cited as a major restriction on the use of a Z.C.D. for Doppler signal processing.[23] Low frequency Doppler signals arise from ultrasound reflections, from the interface of the arterial wall with blood and with surrounding tissue, due to the vessel distension with pulse passage. The addition of a high-pass filter to the output of the demodulator, with sufficient stop band to attenuate these low frequency artifacts, will not degrade the digital Z.C.D. output except at very low flow rates. So, wall thump should not impose any restriction on the application of this method.

The digital Z.C.D. is conducting a sampling of the Doppler signal, which contains information on the flow velocity as a function of time. Essentially, therefore, u(t) is being sampled, and the requirements for minimum sampling rate must be satisfied for fidelity of the output. Each sample takes time τ to compute (count) yet the result is a single number (the total number of zero-crossings in that time) and so can be considered equivalent to an instantaneous sample taken at the $\tau/2$ time. This does not infer that perfect sampling is taking place, since there is uncertainty associated with the Δf_c estimate. The maximum frequency component which can be recovered accurately from a sampled waveform is less than half the sampling frequency (the Nyquist criterion)[35]; therefore the bandwidth of the system with respect to u(t) (this is

independent of the Doppler bandwidth) is governed by the time between samples, which may be made nearly equal to τ.

3.3 DESIGN CONSIDERATIONS

The advantages of the proposed system, employing a digital zero-crossing detector for the purpose of assessing atherosclerotic arteries, lie in its simplicity and ability to produce useful results, in real time, at the bedside. To ensure the simplicity of the design and yet preserve an accurate output, careful choice of design parameters must be made. Some of these parameters are considered below.

Demodulator Bandwidth

Restriction of the demodulator bandwidth is necessary at low frequencies to remove wall thump artifacts from the Doppler spectrum, and at high frequencies to gain the maximum signal-to-noise ratio. The frequencies concerned can be expected to be in the vicinity of 200 Hz and 15 kHz respectively, but need to be accurately determined. It would be advantageous to have these values adjustable according to the particular vessel under observation and the age and condition of the patient.

Sample (Count) Time, τ

τ is clearly the most important parameter of the system, since it is related to the expected error of Δf_c and the u(t) bandwidth restriction. Other considerations in the choice of τ include the resolution of T estimations

($T \doteq N\tau$), the minimum velocity resolution and the proliferation of digital hardware.

Both the statistical error in the Δf_c estimation and the output bandwidth restriction (due to insufficient sampling rate) will cause degradation of the output waveform. The statistical error decreases with increasing τ and with increasing Δf_c; the sampling restrictions increase with increasing τ. The method relies on the comparison of waveforms during the pulse passage, when velocities are greatest, so the higher Doppler shift frequencies can be considered of maximum importance. This would suggest that τ selection is best made on the basis of u(t) bandwidth (Δf_c errors are least at high Δf_c). For example, τ = 10 msec gives a theoretical u(t) bandwidth of 50 Hz. The error in Δf_c estimation (based on the worst case of a flat amplitude spectrum, Equation 3-3) is then:

$$\left(\frac{\sigma}{\mu}\right)_{f_c} < 0.1, \text{ for } \Delta f_c \geq 2 \text{ kHz}.$$

The same choice of τ (10 msec) will achieve a resolution of 10 msec for the T estimation (found to within $\pm$ 5 msec). The minimum velocity resolution corresponds to the minimum frequency of zero-crossings which will produce just 1 crossing during time τ, so:

$$(\Delta f_c)_{min} = 1/\tau = 100 \text{ Hz}.$$

The amount of digital hardware required is dependent on the

maximum frequency of zero-crossing to be handled. For τ = 10 msec, Δf_{max} = 15 kHz, and $\Delta f_c = 0.75\ \Delta f_{max}$, the maximum number is 2250, corresponding to a capacity of 12-bits needed for each channel.

Shift Register Size, N

The shift register is used to store a series of words sequentially, acting as a variable-length buffer. The maximum register length, N_{max} words, must be sufficient for the maximum pulse transit time expected, T_{max}. Thus:

$$N_{max} = (T_{max}/\tau) \text{ integer}$$

The results of Gosling et al.[23] suggest that allowing for T_{max} = 100 msec would be adequate. For τ = 10 msec, N_{max} = 10, so the necessary shift register capacity is 10 x 12-bit words.

D to A Converter Filter Cutoff

A converter suitable for transforming the digital Z.C.D. output into an analogue waveform for display, is the weighted resistor, summing amplifier type. A low-pass filter is needed to smooth the resulting stepped waveform. The maximum frequency component of u(t) able to be recovered is governed by τ, so the low-pass filter ideally should remove any frequencies above $1/2\tau$ Hz. In practice, a cutoff frequency lower than this may be necessary to allow for the non-ideal filter properties.

CHAPTER 4

THE HEART

The heart must perform its pumping action continuously since cessation for only a short time means certain death. The pumping action can be monitored in many ways and many parameters of performance measured. These parameters enable correct diagnosis and accurate location of lesions to be made. In deciding whether surgery is the appropriate course of treatment for a patient with an ailing heart, however, the cardiologist needs some indication of post-operative prognosis (the probable success of the operation). The factors affecting the heart's performance and some of the most useful parameters (including the C.E.F.) are considered in this chapter.

4.1 THE PERFORMANCE OF THE HEART AS A PUMP

When a person is at rest, the heart must only pump 4 to 6 litres of blood each minute. However, during rigorous exercise it may be required to pump as much as 5 times this amount. The pumping action of the heart is regulated by two basic means: intrinsic auto regulation in response to changes of volumes of blood flowing into the heart; and reflex control by nerves. Degradation of heart performance is caused by heart malfunctioning.

Intrinsic Autoregulation

The Frank-Starling Law[27] states that: the greater the heart is filled during diastole, the greater will be the quantity of blood pumped into the aorta during systole. Thus the heart can adapt to a widely varying input of blood.

The primary mechanism for this autoregulation can be seen in the relationship of muscle length to muscle tension, arising from feedback in the contracting microsystem (see Figure 4-1[27]). When the muscle is at its normal relaxed length at the end of diastole, the contracting force starts at the maximum available and decreases as the fibre lengths decrease. If, however, the heart is filled to a greater extent, the muscle will be stretched at the beginning of systole, with some resting tension (preload). As contraction occurs, a large contracting force is available over a greater range of length, thus more work is performed and a greater amount of blood is ejected.

An important consequence of the autoregulation mechanism is that the heart function is almost independent of the aortic pressure (afterload). Also it allows other body organs to control their blood supply by simply altering their vascular resistance to flow and thus the venous return.

Control by Nerves

The heart is supplied with two types of control signals, from sympathetic nerves (excitory) and parasympathetic nerves (restraining). These nerves are distributed mainly near to the sino-atrial and atrio-ventricular nodes and so

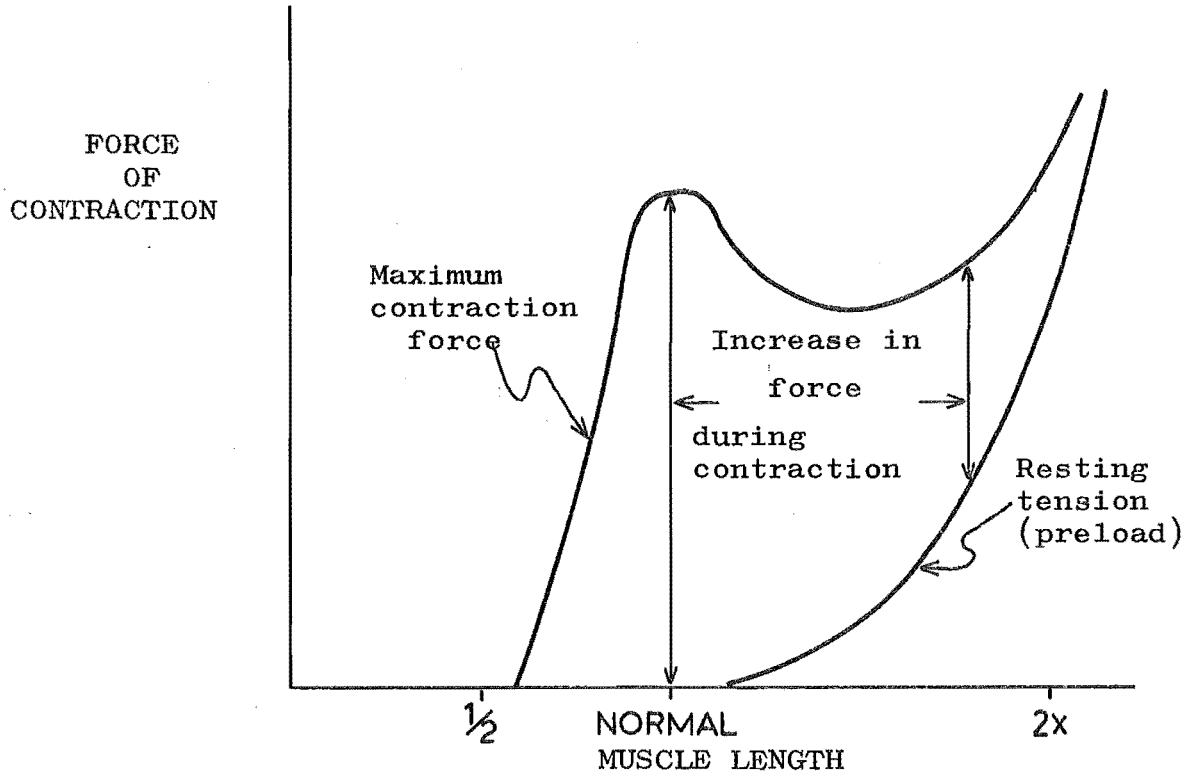

FIGURE 4-1. Relation of force of contraction to muscle length.

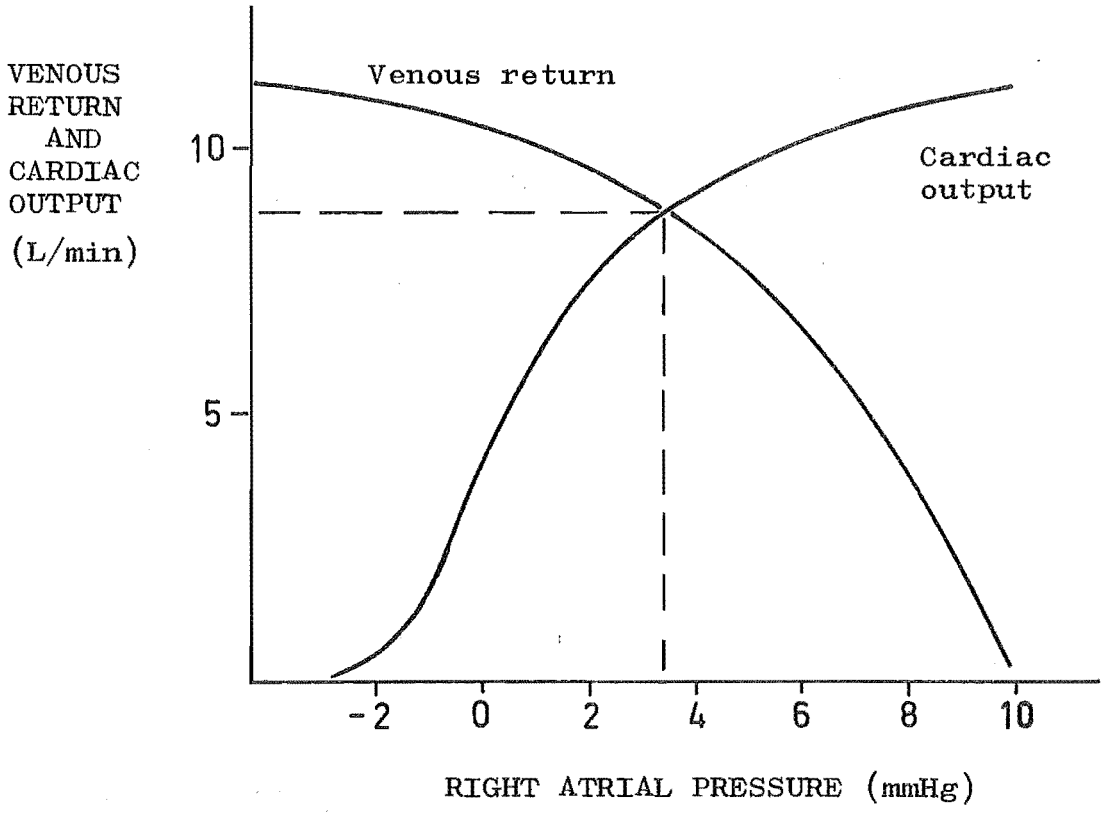

FIGURE 4-2. Cardiac function curves.

act to modify the electrical stimuli to the heart muscle. Stimulation of the sympathetic nerves causes an increase in the rate of the S-A node and an increase in conduction in the A-V node. As a result the heart pumps faster and with increased force of contraction. Parasympathetic stimulation has essentially the opposite effect. Very strong action of the latter nerves may cause the heart to stop for a short period.

Cardiac function curves are used to predict the response of the heart to both external and internal changes. The curves of venous return and cardiac output are related to the right atrial pressure, which is essentially the preload (see Figure 4-2[27]). The steady state operating point of the heart function at any time is the point of intersection of the two curves, since the rate of flow into the heart must equal the rate out (averaged over a cycle).

Heart Malfunctions

There are three main types of heart mulfunctions. They are: malfunctions relating to

(1) excitation mechanisms,

(2) valves and

(3) muscle.

These three, their effect on pumping action and their surgical treatment, will be considered briefly here.

(1) Excitation mechanisms. Excess dilation (stretching) of the heart, blockage of the Purkinje fibre system or response to various drugs, can cause the atria

or ventricles to contract rapidly. The lower frequency and coordinated contractions (up to 200 or 300 beats per minute) are called flutter and very high frequency and random contractions, fibrillation. These malfunctions result from the one action potential re-exciting muscle which has had time to relax from the contractile state. Pumping action may be seriously impaired or lost altogether if these conditions persist. Consequently, one quarter of all persons die in ventricular fibrillation.[27] A very large pulse of direct current passed through the ventricles can stop fibrillation by simultaneously exciting all the muscle (defibrillation).

Another excitation malfunction, atrioventricular block, occurs if the action potentials are prevented from reaching the ventricles from the atria. The Purkinje fibres will then excite the ventricles spontaneously, but at a much lower rate (15 to 40 times per minute) and unsynchronised with the atrial rhythm. The cardiac output is clearly reduced by the low beat rate and lack of coordinated priming by the atria. An inserted electronic pacemaker may be used to relieve this condition.

(2) Valve malfunction. Efficient heart functioning relies much on the operation of the A-V and semilunar valves (refer to Figure 1-3). Valve malfunctioning occurs in two possible ways. Either the valves fail to close properly and allow blood to flow with the reverse pressure gradient across the 'closed' valve, or they fail to open sufficiently and blood flows through with difficulty causing a large

pressure drop. These conditions are known as incompetence and stenosis, respectively, and may occur singly or together in any of the four heart valves.

Since backflow occurs when a valve is incompetent, a heart with this malfunction must expend more work to achieve normal cardiac output. Similarly a stenotic valve demands more cardiac work. Thus these hearts tend to have considerably thickened muscle. They also tend to become dilated to achieve maximum effect from the Frank-Starling mechanism. Malfunctioning valves can be repaired in some cases, but the success achieved with implantable valve prostheses has meant that replacement is often the preferred treatment.

(3) Muscle malfunction. Diseases of the heart muscle are known as myocardial diseases. These diseases directly effect the contractility of the muscle. The most common is ischemia (insufficient blood supply) caused by occlusion or thrombosis of the coronary arteries, resulting from atherosclerosis (described in Section 2.2). When the blood supply to cardiac muscle is diminished beyond a critical level, the muscle not only becomes nonfunctional but actually begins to die. This occurs in a matter of hours in total ischemia. Dead muscle is replaced by fibrous tissue which tends to stretch, instead of contract, during systole.

Clearly, myocardial diseases have a direct effect on the pumping performance of the heart, by reducing the work

performed per beat from a given end-diastolic volume. The Frank-Starling mechanism compensates by increasing venous return and thus the end-diastolic volume, and attempts to return the cardiac output to normal. The success of this depends on the area and condition of the diseased muscle. If good collateral blood supplies to the ischemic area have had time to form, the compensation may maintain normal cardiac output. However, the heart will remain in a dilated state and will not be able to cope with large transient fluctuations in demand, and is always susceptable to further disease. Secondary effects of myocardial disease may also occur: excess dilation of the heart provides the conditions for the occurrence of ventricular fibrillation and a branch of the Purkinje fibre conduction system may be blocked if it passes through a diseased area.

Surgical techniques are now available for treatment of some patients with myocardial disease. Bypass grafts can be made to the coronary arteries to restore blood supply to ischemic muscle areas. As well, areas of dead muscle may be removed and the edges of good muscle areas rejoined. These surgical operations require the action of the heart to be taken over by an external mechanical system and involve considerable trauma to the patient, therefore only patients with a considerable amount of preserved cardiac function are considered suitable candidates.

4.2 PARAMETERS OF HEART PERFORMANCE

The evaluation of new and existing parameters of heart performance, and their methods of measurement, has been the subject of much recent research. The standard measurements and tests carried out will probably indicate the existence of a heart malfunction once it is relatively well established, but may not enable the cardiologist to make a precise diagnosis. For example, increased heart size, elevated diastolic pressure and a low cardiac output at rest are well known and characteristic findings in left ventricular failure. However this failure may have resulted from one or a combination of many causes, and, before failure symptoms appeared, there may have been no indication of how well the compensatory mechanisms were coping. For these reasons, new parameters of heart performance have been suggested and a summary of these is made below. All the parameters relate to the left ventricle (L.V.).

Stroke Volume (S.V.)

The stroke volume is the difference between the volume of blood contained in the L.V. in diastole and in systole with units of millilitres. If a heart has properly functioning valves, then the stroke volume is equal to the cardiac output (C.O.) divided by the heart rate. Both these parameters are only of limited use in assessing the condition of cardiac muscle since the compensatory mechanisms

act to restore a normal C.O. Together, however, S.V. and C.O. are of use in the diagnosis of valvular disease. Significant differences found between C.O. and S.V. x H.R. (H.R. is the heart rate), where C.O. and S.V. have been obtained independently, is evidence of the occurrence of regurgitant flow. The regurgitant flow volume per beat is given by:

$$V_R = (S.V. \times H.R.) - C.O.$$

In practice, C.O. can be measured by the Fick expired air method or dye dilution method, and S.V. by angiography or ultrasound time-motion study.[17,25,40]

End-diastolic Volume (V_D)

The end-diastolic volume is the maximum volume of blood the L.V. contains during the cardiac cycle. V_D (and C.O.) are often normalised to the patient's body surface area and expressed in units of ml/M^2 ($L/min/M^2$). In man without clinical evidence of heart disease, V_D has been shown to be 70 ± 20 ml/M^2.[31] An increase in V_D occurs when the heart becomes dilated, as in most cases of valvular and myocardial disease. Thus a significantly large value for normalised V_D (V_D sometimes reaches four or five times normal) lends weight to a diagnosis of these diseases.[15]

Left Ventricular Pressure

The two main parameters of interest related to left

ventricular pressure are the end-diastolic pressure (E.D.P.) and the maximum rate of increase of pressure (dP/dt). The units are mmHg and mmHg/sec, respectively. A rise of V_D for any reason can be expected to be accompanied by a rise in E.D.P. In fact it is an increase in venous pressure (and thus in E.D.P.) which initiates the Frank-Starling mechanism by increasing the preload on the cardiac muscle. However, E.D.P. not only reflects V_D, but also the compliance and overall degree of filling of the vascular bed (control of vascular resistance is one method the cardiovascular system uses to respond to changes in demand).[8]

At the beginning of systole, the ejection of blood from the left ventricle cannot commence until enough pressure is developed to open the aortic valve against the aortic pressure. Therefore the initial ventricular muscle contraction is isometric (tension is developed without a change of length), since blood can be considered as incompressible. Observation of the ventricular pressure curve (refer to Figure 1-4) shows that the point of maximum dP/dt occurs during this isometric part of the contraction, so dP/dt has been suggested as parameter of muscle contractile tension.[21,40]

Studies of patients undergoing cardiac catheterisation at The Princess Margaret Hospital have shown that in a significant number of cases, a rise in E.D.P. follows the intraventricular injection of contrast material. It has been suggested[3] that the procedure might serve as a

' stress test' for the heart and that the increase occurring may have significant correlation with the degree of coronary artery disease (see Chapter 7).

Velocity of Fibre Shortening v_{fs}

The rate at which the muscle fibres in the left ventricular wall decrease in length during contraction is proportional to the rate of decrease of the ventricle's diameter. Thus v_{fs} is usually measured by making observations of changes in the diameter and is expressed in units of circumferences/sec. The force-velocity curve for an isolated muscle strip shows an inverse, nearly hyperbolic, relationship between the tension developed (clearly dependent on the load) and the velocity of shortening (see Figure 4-3).[4] The maximum velocity of shortening, known as v_{max}, is the intercept of the force-velocity curve on the velocity axis, corresponding to conditions of no load on the muscle. v_{max} has been suggested as another parameter of muscle condition.[4,30,39,42]

Various methods can be employed to estimate v_{max}. The muscle fibre tension (force) can be found from the intraventricular pressure, the ventricular diameter and the wall thickness, and is usually estimated by a combination of angiography and pressure measurement during cardiac catheterisation. The velocity of shortening at any instant can be estimated by angiographic observation of wall movement or of volume changes, or directly from the pressure recording by the relation:

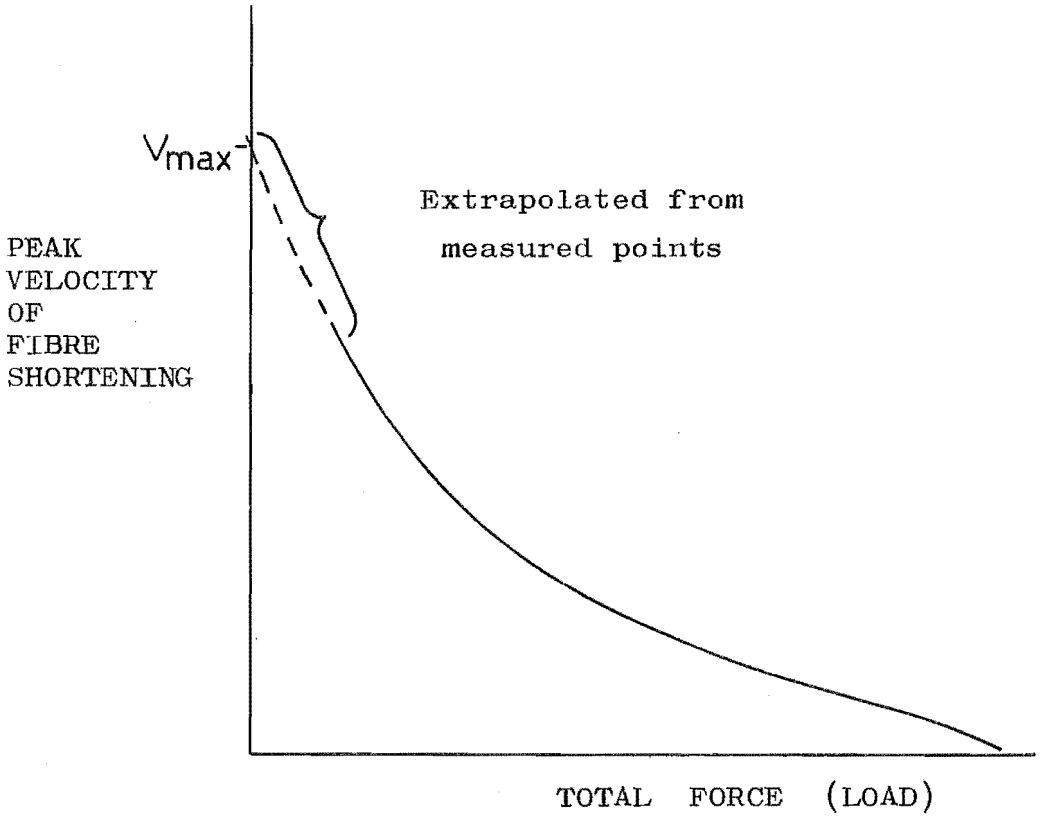

FIGURE 4-3. Force/peak velocity curve of cardiac muscle.

$$v_{fs} = (dP/dt)/ K.P$$

where K is a constant of geometric and elastic properties and is probably between 28 and 40.[30,39] Results from the three methods have been shown to give good agreement.[39] Once the naturally occurring portion of the force-velocity curve has been evaluated, a model of the muscle contractile mechanism must be assumed in order to extrapolate the curve and find v_{max}. The choice of model is apparently crucial for meaningful estimations of v_{max}.[2]

Cardiac Ejection Fraction (C.E.F.)

The cardiac ejection fraction (often called systolic ejection fraction or simply ejection fraction), is the ratio of stroke volume to end-diastolic volume. Thus:

$$\begin{aligned} C.E.F. &= S.V./V_D \\ &= (V_D - V_S)/V_D \quad \ldots\ldots\ldots\ldots (4\text{-}1) \end{aligned}$$

C.E.F. is usually expressed as a percentage, and has been found to have values of 67 $\pm$ 8% (mean $\pm$ 1 standard deviation) for man with no clinical evidence of heart disease.[15] This parameter is sensitive to changes in heart functioning since the stroke volume, which has a wide spread of values, is normalised by the end-diastolic volume, which also varies considerably between patients. A reduced C.E.F. can occur with either a reduced S.V. delivered from a normal V_D, or a normal S.V. delivered from an increased V_D (dilation). The cardiac function curve

(refer to Figure 4-2) relates cardiac output (proportional to S.V.), to right atrial pressure (reflecting input pressure to the system and the resulting V_D), so C.E.F. represents the slope at any given operating point. Since the slope of an 'output' versus 'input' curve of a system is the 'gain' of the system, C.E.F. can be considered an indicator of the muscle's capability to do work.

In patients with valvular incompetence (backflow), S.V. is not the volume of blood ejected during systole, but rather the volume which the heart could eject if the valvular lesion were repaired. Herein lies the prognostic value of the parameter. Chapter 7 considers the measurement of C.E.F. as a guide to prognosis of patients contemplated for open-heart surgery. Other investigators have also found a depressed C.E.F. to be associated with reduced survival in medically treated patients with valvular and myocardial diseases.[34,51]

Index of Myocardial Contractility

Myocardial contractility is normally defined as the amount of contractile work able to be performed by the heart from a given amount of initial fibre stretching (preload). Many indices of this quantity, which, because of its abstract nature, cannot be measured directly, have been suggested. Such an index must be independent of both the preload and afterload on the muscle throughout the possible operating range in order to accurately reflect

the muscle condition. The most popular of these suggested indices are related to dP/dt[21,40], v_{max}[4,39,42] or C.E.F.[8,14,15,40] However Blinks *et al.*[2] have found these indices to be dependent to some extent on either preload or afterload, by making a very detailed analysis of the contractile process. Probably the best test for the significance of any of these parameters is to see if they correlate significantly with clinical evidence of the heart condition, in studies made of a large sample of patients, in which the protocol of testing is carefully laid down to control variations in preload and afterload.

CHAPTER 5

A METHOD OF CARDIAC EJECTION FRACTION ESTIMATION EMPLOYING A SPECIAL-PURPOSE CALCULATOR

The need for the development of an instrument to measure ejection fractions from cineangiocardiograms was suggested by Dr F.T.L. Hull, consultant cardiologist to The Princess Maragret Hospital. Although methods have been suggested and used in the past, most were either laborious to apply or required the use of sophisticated computing equipment. In the following, the various methods of left ventricular volume estimation (necessary in order to estimate C.E.F.) are investigated, and a method developed for use with a special-purpose calculator (the Rectangular Rule method) is described. A prototype calculator has been evaluated in use at The Princess Margaret Hospital. The development of this prototype and a modified final instrument has been supported financially by the National Heart Foundation of New Zealand.

5.1 LEFT VENTRICULAR VOLUME ESTIMATION FROM CINEANGIOCARDIOGRAMS

The basic cineangiographic technique of observing body organs *in vivo* was first experimented with in the late 19th century.[38] Since then many improvements have been

made so that films are now produced showing clear outlines of the heart chambers. Many establishments have biplane cineagiographic facilities, which allow two projections of the left ventricle, the anterio-posterior (A-P) and left -lateral (L) projections, to be observed simultaneously. However, locally only single-plane facilities exist. The equipment needed for single-plane angiography is half that needed for biplane and the patient's radiation dosage is similarly reduced.

The angiographic projections (and thus the films) are distorted as a result of the non-parallel nature of the incident x-rays. The magnification of any portion of the abject depends on its distance from the projection plane, as given by:

$$M = s/_{s-p}$$

where: s = x-ray source to projection plane distance,

p = object to projection plane distance,

M = ratio of projected length to actual length.

Since all points on the ventricular outline do not lie on a plane parallel to the projection plane, distortion of the projected outline occurs. Geometric methods have been described for distortion correction of biplane angiograms and the evaluation of a spatial L.V. axis.[12] In the single-plane case it is only possible to apply an overall magnification correction (see Section 5.5).

Methods

A method of estimating the volume of a 3-dimensional object from 2-dimensional projections must make some assumptions about the object's shape and orientation. The success of the method depends on the justification of the assumptions.

Several methods currently in use approximate the left ventricle by a reference ellipse-based shape. In the biplane case the L.V. is assumed to be an ellipsoid and the volume estimated by evaluating the three axes' lengths.[1,12,13,14,44] For single-plane projections the L.V. is approximated by an ellipse rotated about its major axis (forming a prolate spheroid).[14,44,45]

The other type of method currently used is based on the Simpson's Rule for numerical integration. The L.V. volume is divided into a number of equal width segments by means of measuring successive cross-sectional widths at fixed intervals across the projection(s).[5,12] For biplane measurements, the cross-sections of the segments are assumed to be elliptical and the two axes' lengths found from the two projections. In the single-plane case, circular cross-sectional are assumed.

A summary of the methods which have been described is tabled in Figure 5-1. The various calculation formulae used and references are included.

Commercial Equipment

At the time of writing, there exists only one commercially available system for estimating L.V. volume

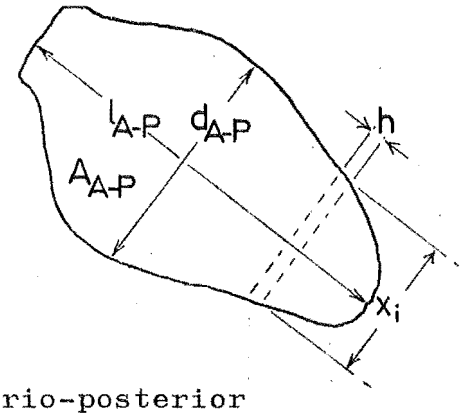

Anterio-posterior projection

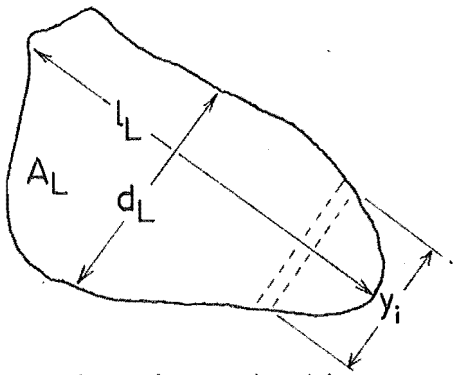

Lateral projection

Method	Formula	References
Biplane ellipsoid-3 axes measurement	$V_{L.V.} = \frac{4}{3}\pi \cdot \frac{l_{A-P}+l_L}{4} \cdot \frac{d_{A-P}}{2} \cdot \frac{d_L}{2}$	12, 14.
Biplane ellipsoid-Area-longest length	$V_{L.V.} = \frac{4}{3}\pi \cdot \frac{2A_{A-P}}{l_{A-P}} \cdot \frac{2A_L}{l_L} \cdot \frac{1}{2}$ l=longest of l_{A-P}, l_L.	1, 13, 14.
Biplane Simpson's Rule	$V_{L.V.} = \frac{\pi h}{3}\left[\sum_{i}^{\text{odd}} x_i y_i + \sum_{j}^{\text{even}} x_j y_j / 2\right]$	5,12.
Single-plane ellipse-Area-longest length	$V_{L.V.} = \frac{4}{3}\pi \cdot \left(\frac{2A_{A-P}}{\pi l_{A-P}}\right)^2 \cdot \frac{l_{A-P}}{2}$	14, 44, 45.
Rectangular Rule	$V_{L.V.} = \frac{\pi h}{4} \sum_{i} x_i^2$	

FIGURE 5-1. Methods of left ventriculr volume estimation from cineangiocardiograms.

from cineangiocardiograms and for deriving cardiac parameters. This is the Hewlett-Packard 5693A Angio-Analyser,[11] which is used in conjunction with the H-P 5690B Catheter Laboratory System.[16] The ventricular outlines are manually traced by an electronic pen and displayed on a separate storage oscilloscope screen. Derivation of volumes and cardiac parameters is achieved by software processing in the system's central computer. The system is quite flexible and should give good results, but it is very expensive: $17,000(USA) for the H-P 5693A, and $58,000 (USA) for the H-P 5690B (1974 prices).

5.2 RECTANGULAR RULE METHOD - EMPLOYING CALCULATOR

The method chosen for the C.E.F. calculating system has been named the "Rectangular Rule" (R.R.). The basis of the method is the division of the projected area (L.V. outline) into equal width rectangles and the assumption of circular cross-section (see Figure 5-2). The rectangular approximation to the area can be shown to be a modification of the first-order numerical method known as the Trapezoidal Rule (see Appendix IV). If each rectangle (length x_i, width h) is rotated about its minor axis, a circular disc is formed of volume,

$$V = h\, x_i^2/4.$$

The summation of the volumes of revolution of each rectangle is the volume estimation (see Figure 5-2). Thus,

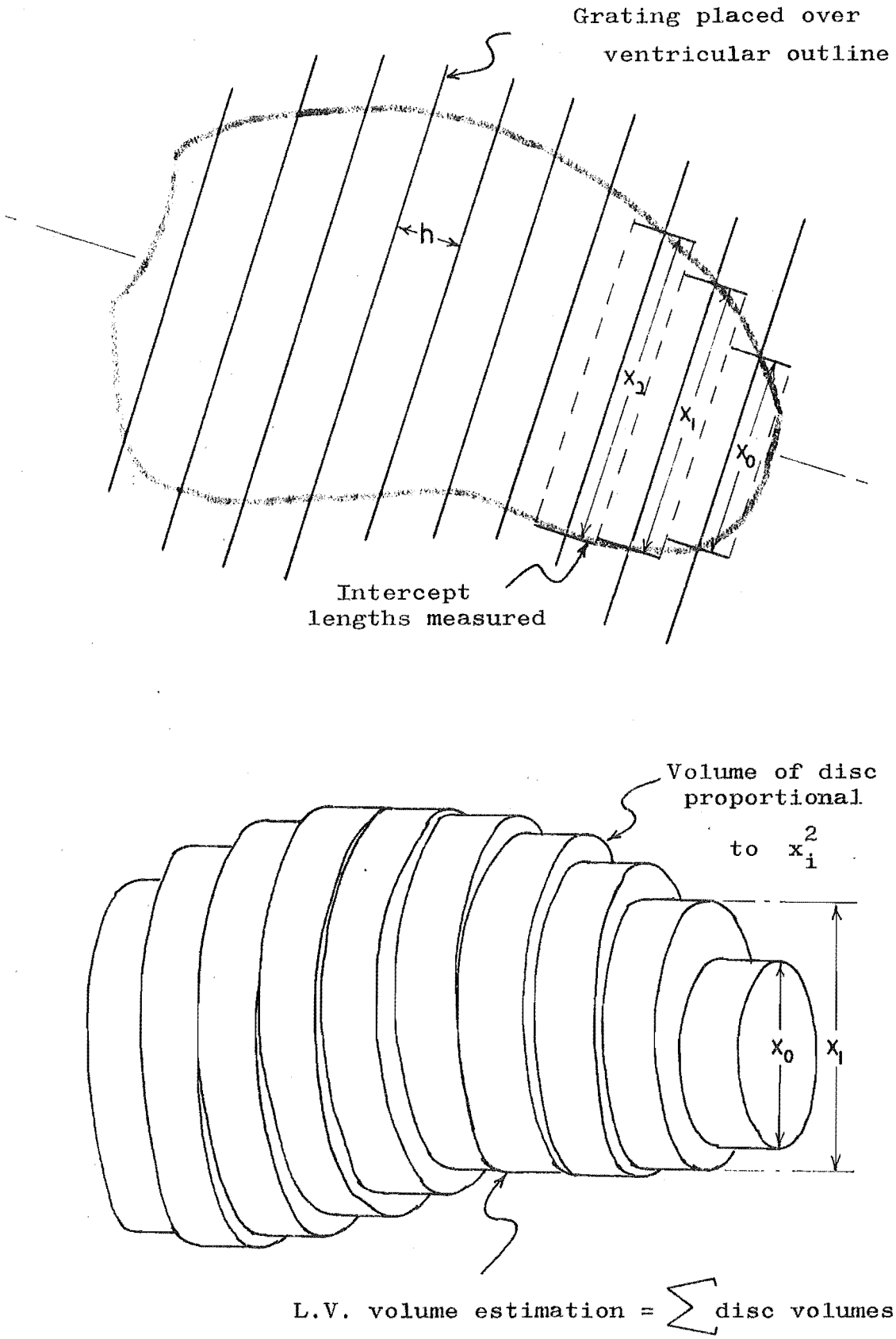

FIGURE 5-2. The Rectangular Rule method of ventricular volume measurement.

$$V_{LV} = (h / 4) \sum_{i=1}^{N} x_i^2 \quad \text{.....(5-1)}$$

The function of the calculating system, in applying the R.R. method, is to process data representing the lengths of the rectangles. These lengths can be considered as the intercepts on the ventricular outline of a set of equal spaced lines (grating). The orientation of this grating must be approximately perpendicular to the major axis of the L.V. outline for the circular cross-section assumption to apply. This axis, although difficult to define uniquely, normally passes through the mid-aortic valve and ventricular apex points.

The calculation of C.E.F. from L.V. volumes is governed be equation (4-1), rewritten here:

$$\text{C.E.F. } (\%) = \frac{(V_D - V_S)100}{V_D}$$

It can be seen that there is no direct dependence of C.E.F. on the volumes, only on the ratio of volumes. Thus the constants in the volume summation, Equation (5-1), can be ignored and a number representing the volume found by:

$$V_{LV} = \sum_{i=1}^{N} X_i^2 \quad \text{.....(5-2)}$$

where X_i is a number representing the distance x_i. An input transducer is used to convert the continuous lengths into discrete data. The calculator performs Equation (5-2) for both volumes, stores the resulting numbers and produces a percentage C.E.F. These processes are

illustrated in Figure 5-3 by means of flow charts. The major component of the calculator is an accumulator, the content of which is called A. The multiplication by 100 and division by V_D are performed by simplified processes (see Figure 5-3) to reduce the complexity of the calculator hardware. The hardware design employed is described in Chapter 6.

The R.R. method was chosen for the following reasons:

1) it offers a good compromise between speed (this includes ease of use) and accuracy;
2) the number of independent length measurements taken for each volume estimation ensures that the estimation accuracy does not depend directly on the accuracy of any one measurement;
3) a relatively straightforward and inexpensive calculating system is adequate for data processing.

The only method in popular use for volume estimations from single-plane cineangiograms appears to be the area-length elliptical method (refer to Figure 5-1). This method, first suggested by H.A. Dodge,[12,13] is popularly named after him. The Dodge estimation is directly dependent on a single measurement taken of the L.V. longest length (corresponding to the ellipse major axis). Thus errors in definition of the ventricular outline, a major restriction of all angiographic techniques, can be expected to have a more detrimental effect on the Dodge results than on the R.R. estimation. Direct calibration of estimations

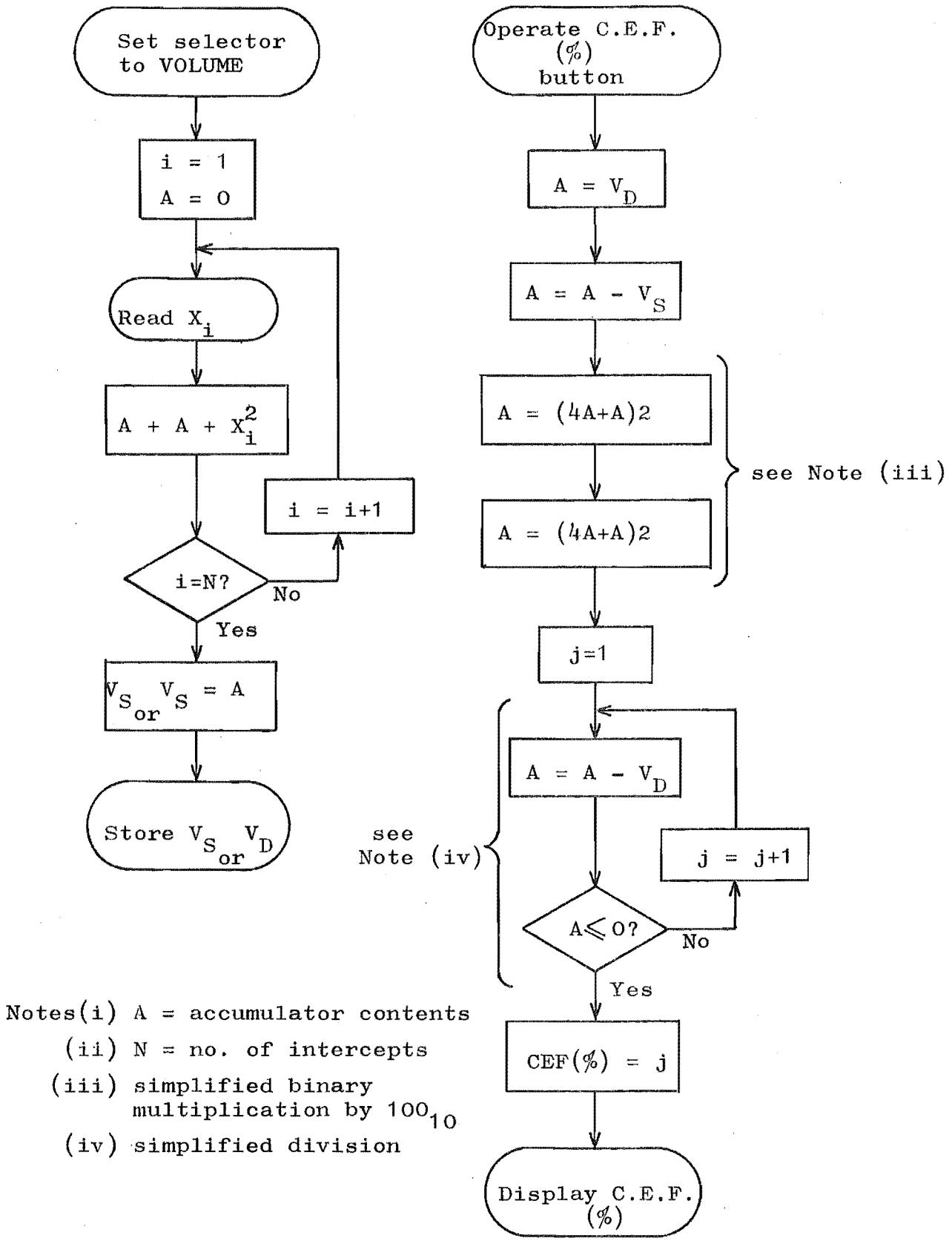

Notes (i) A = accumulator contents

(ii) N = no. of intercepts

(iii) simplified binary multiplication by 100_{10}

(iv) simplified division

FIGURE 5-3. Flow charts of the C.E.F. calculation process.

Left: volume estimation.

Right: C.E.F. from stored volumes.

with actual volumes is very difficult to obtain, although studies have been made on postmortem hearts[12] and comparisons made with cardiac outputs.[13,15,25,29] These results are encouraging for single-plane methods in general.

5.3 INPUT TRANSDUCERS

The Rectangular Rule method of volume estimation from cineangiograms depends upon a number of length measurements. The intercepts must be converted to suitable data for input to the calculating system and control signals sent to allow reception of the data. A wide range of input transducers are suitable to perform these functions. Four possible systems are described here.

Manual Calipers

Manual calipers allow a very simple and direct conversion of length to a binary coded data word for input to a special-purpose calculator. The jaws of the calipers are set to each intercept length and a signal is sent to the calculator to receive the data word (see Figure 5-4(a)). A coded strip attached to the movable jaw and an optical system supply the 4,5 or 6-bits (depending on accuracy required) of the data word.

Processing of more than several angiograms at any one time with this transducer involves an amount of tedium, so the design of the caliper handle, movement and control pushbutton is an important consideration.

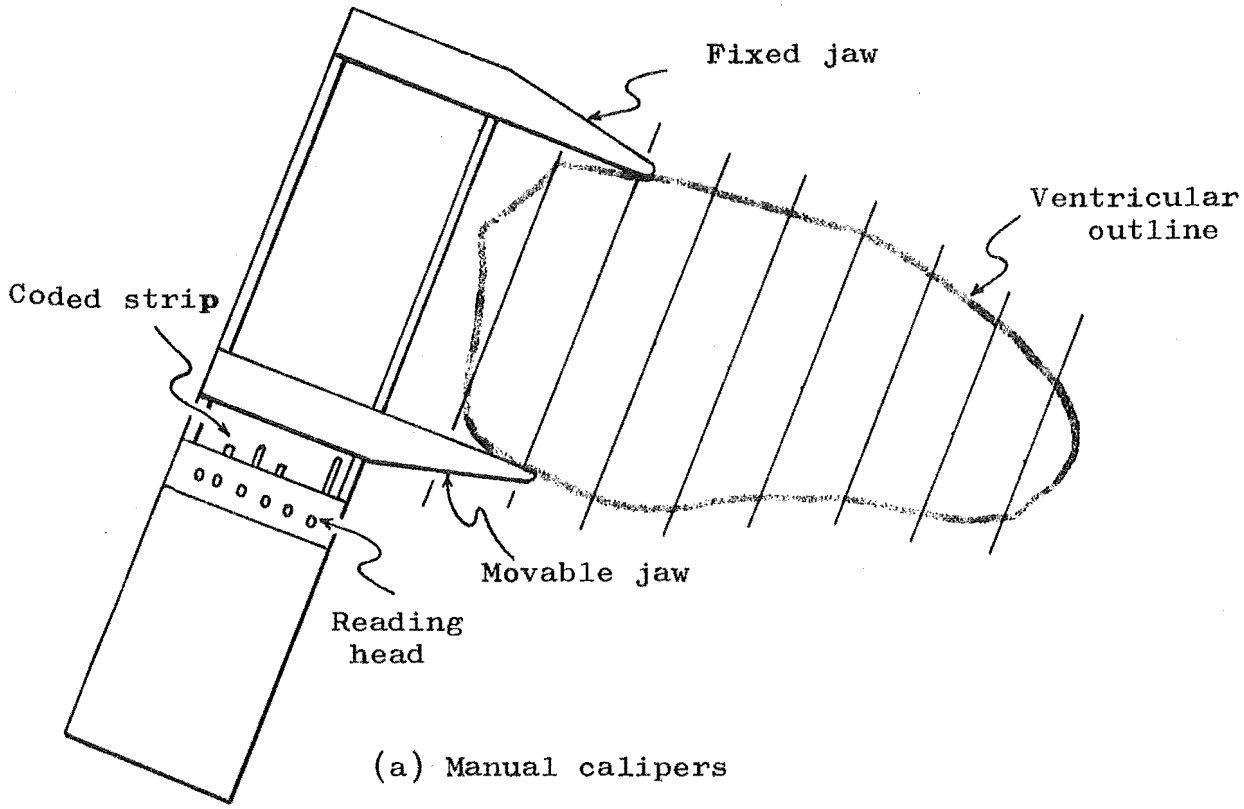

(a) Manual calipers

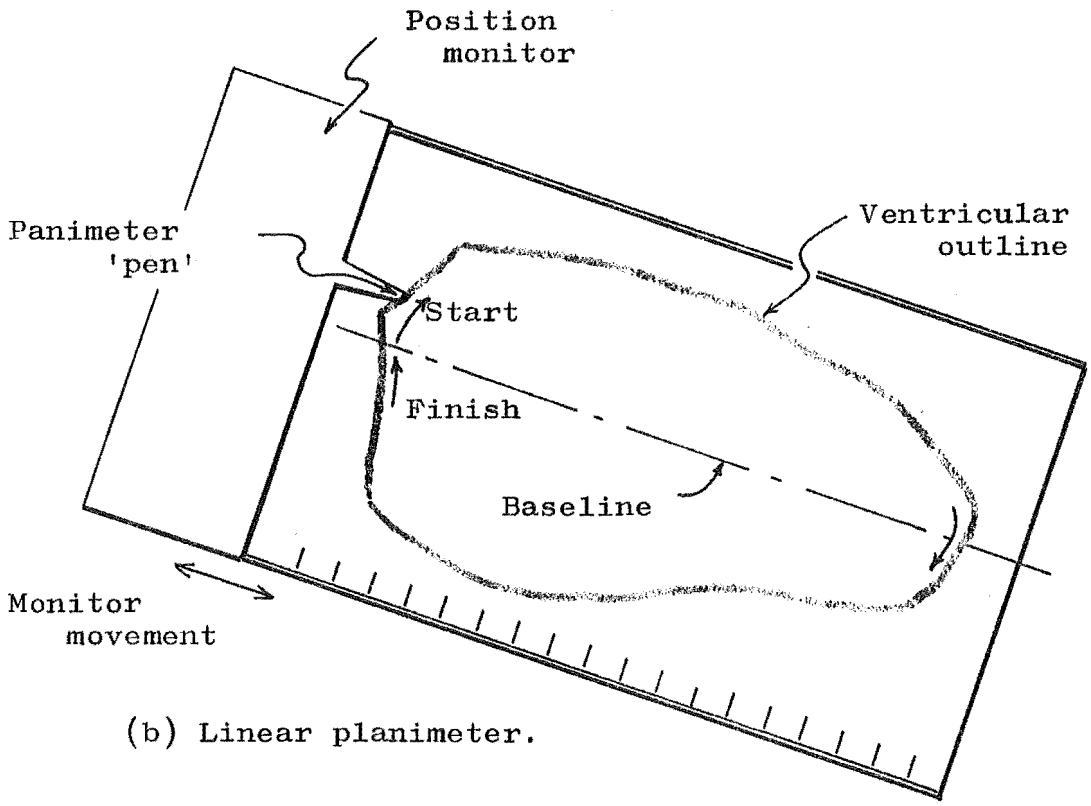

(b) Linear planimeter.

FIGURE 5-4. Input transducers.

Linear Planimeter

A planimeter is an instrument for mechanically measuring areas. 'Linear planimeter' is a coined name for a form of planimeter which uses extra information to enable a volume estimation to be made by the Rectangular Rule. The extra information is obtained by setting up a reference grating.

In practice an axis line and starting point for outline tracing are set up (see Figure 5-4(b)). An encoding system, similar to that employed by the calipers, is used to monitor the position of the tracing 'pen' in the direction perpendicular to the axis line. As the pen is traced across the top portion of the outline, a position data word is stored for each point corresponding to a grating intercept. Then as the pen returns along the bottom portion, differences between the top and bottom positions are recorded as the required intercept lengths. Only the tracing needs to be performed manually.

The linear planimeter system is suitable for use with a relatively complex calculator (perhaps a micro-processor with limited random-access memory) or as a peripheral to a computer system.

Scanning System

A scanning system suitable for L.V. volume estimation from angiograms is one which transforms the ventricle outline into an array of stored points and then processes the data. It could be a mechanically scanned light beam,

a scanned screen and sonic pen or a storage oscilloscope and light pen. Most scanning system rely on manual outline tracing,[11,46] but recently semi- and fully automatic methods of finding outlines have been described.[26,47] All scanning systems employ computers.

Some form of scanning system (sometimes known as a "digitising screen") is a possible future development locally. The system would have many applications in cardiovascular measurements, for example the analysing of time waveforms, as well as the use outlined here. Commercial systems are available (the H-P system mentioned in Section 5.1 uses a scanning system), but tend to be very expensive.

Densitometry

As well as finding ventricular outlines, densitometric techniques can derive cross-sectional information from single-plane angiograms. The variation in brightness across the angiogram is assumed to be directly related to the distance which the x-rays travel through radio-opaque material. An interactive system to derive ventricular cross-sections, using an I.B.M. 1800 computer, has been described.[46]

The availability of cross-sectional information would greatly improve the accuracy and usefulness of the Rectangular Rule method (and any similar methods). However, artifacts caused by imperfect mixing of contrast material and the difficulties of calibrating the intensity

versus depth relation have yet to be overcome.[9,46,47]

Choice of Input Transducer

A summary of the four systems described above is contained in Figure 5-5. The availability of a suitable processing system is the major factor involved in the choice of input transducer. If access were available to a mini computer (almost all computing systems appearing in New Zealand hospitals are of the mini type), one of the latter two sophisticated systems may be appropriate. However, with no computer system conveniently accessible, the special-purpose calculator seems the best alternative. The demands made on computer time in the hospital environment also stress the value of other inexpensive stand-alone systems. The manual calipers were chosen for both the prototype and final calculator developed for The Princess Margaret Hospital.

5.4 ERRORS OF THE C.E.F. CALCULATION

A rigorous analysis of the errors in this calculating system must consider every step in the process from the generation of the x-rays to the display of the output C.E.F. information. The propagation of errors in the calculator and input transducer can be analysed accurately and tests made to find typical errors. However, the error inherent in the cineangiographic process, the estimation of volumes from single projections and the tracing of the ventricular outline, are virtually impossible

TRANSDUCER TYPE	SETTING UP	OPERATION	SYSTEM REQUIREMENTS
Manual calipers and grating	Outline tracing. Grating orientation and position	Adjust calipers for 10 readings, push button for each	Special-purpose calculator (inexpensive)
Linear planimeter	Outline tracing. Base line orientation	Follow outline with planimeter point	Relatively complex calculator or interfaced with small computer
Scanned outline	Possibly outline tracing, rest automatic	Draw outline with light pen	Complex scanning system interfaced with computer
Densitometry	Optical processing of cineangiograms Calibration procedure	Automatic or interactive	Complex scanning system interfaced with computer

FIGURE 5-5. Summary of input transducers suitable for implementing the R.R. method.

to analyse. The most significant of these is the error involved in single-plane estimations. For the purpose of C.E.F. calculation, the difference between the cross-sectional shape of the L.V. before and after systole is the critical factor. Results indicate that this difference is not significant.[8,12,13,14]

Once the L.V. outline has been traced from the cineangiogram, the errors occurring from that point onwards can be placed within definite limits. In the following, three types of computation error (inherent, roundoff and truncation) will be considered and their propagation in the calculation process analysed.[36]

Inherent Errors

Inherent errors are errors in data values. The inherent error in data passed to the calculator from the input transducer is due to the quantisation of continuous length information into a binary-coded word. A 6-bit input word is used, so the maximum jaw width is divided into $2^6 = 64$ intervals. The inherent error of each input word, X_i, is between $-\frac{1}{2}$ and $+\frac{1}{2}$ of one quantisation interval. The maximum relative error (absolute value) of X_i is thus:

$$\left| \frac{e_{X_i}}{X_i} \right| \leqslant {}^{1}/_{64} = 0.78\%$$

Clearly this inherent error decreases as the number of bits in the word increases.

Roundoff Errors

Roundoff errors are caused by limitations in the available word length within the computation system. The information entered from the input transducer is hardware squared, producing an effective word length of 12-bits. The least significant 4-bits of this are chopped off, since this only produces a maximum relative error of $-\frac{1}{2}^8 = -0.39\%$. All information is preserved in the rest of the calculation, by expanding the word length to 19-bits, so no further roundoff errors are produced.

Truncation Errors

The truncation of an infinite mathematical process produces this type of error. The Trapezoidal Rule, and thus the Rectangular Rule, are first-order numerical integration methods and have truncation error if estimating the area under a curve of degree-2 or higher. The error can be shown, by means of a Taylor Series expansion, to be proportional to h^2.[36] Thus this error is minimised by using a finely spaced grating (small h). A grating pitch which allows at least 8 intercepts across the L.V. outline reduces the error to a negligible amount.

Another source of truncation error in the C.E.F. calculation process is the simplified division: $(V_D-V_S)100$ by V_D (refer to Figure 5-3). This final step is performed by a counted subtraction method and the error resulting is between 0 and + 1% in the displayed percentage.

Error Propagation

When two numbers, each with a specified error, are added together, the result has an error equal to the sum of the two input errors. Propagation of the inherent data errors in this way is the major source of error in the calculation process.

The input words, X_i, are squared and added into an accumulator to find the volume estimate (refer to Figure 5-3). Each X_i has a maximum relative error of $\pm$ 1/128, so each X_i^2 has a maximum relative error of $\pm$ 1/64, by application of the appropriate propagation formula.[36] Applying the same principle to the summation of X_i^2 gives the same maximum relative error for the resulting volume estimate. However there is only an extremely small probability of such an error magnitude occurring.

It can be assumed that the distribution of the continuous variable x_i is linear across the interval represented by X_i and that each reading is independent. By further dividing the basic quantisation interval, the probability of the inherent error being within certain bounds can be analysed. Making four such divisions allows a ninety five percent confidence level to be placed on a maximum relative error of $\pm$ 1/128 for V_D and V_S (see Appendix V). Thus:

$$\left|\frac{e_{V_D}}{V_D}\right|, \left|\frac{e_{V_S}}{V_S}\right| \underset{95\%}{\leqslant} 1/128$$

The numerator, NUM, of the C.E.F. equation (Equation (4-1)) will be considered first in analysing the errors in performing that equation. The subtraction of V_S from V_D is achieved without roundoff error, and the multiplication by 100 is exact. Therefore, the only errors propagated are those of the stored V_S, V_D values. For subtraction, the absolute values of relative errors are added, so:

$$\left|\frac{e_{NUM}}{NUM}\right| \leqslant \left|\frac{e_{V_D}}{V_D}\right| + \left|\frac{e_{V_S}}{V_S}\right|$$

$$\leqslant_{95\%} 1/64$$

The error introduced by the truncated division process and the earlier roundoff error must be added to the numerator error. Thus the maximum error of the displayed percentage can be expressed:

$$2.56\% \leqslant_{95\%} e_{CEF} \leqslant_{95\%} -1.95\%$$

5.5 RESULTS USING THE C.E.F. CALCULATOR

The prototype C.E.F. calculator has been in service at The Princess Margaret Hospital for eight months at the time of writing. It has operated satisfactorily during this time and results have been consistent. Studies have been made (by the author) of the cineangiograms of patients who underwent catheterisation in the 1973-74 period. The clinical aspects of the results are discussed in Chapter 7. However, proof of the accuracy of the estimations relative

to the actual physical volumes of the L.V. is difficult to obtain. Some measure of proof is obtained by the correlation of the calculator's estimations with those obtained by other methods.

Comparison with the Dodge Method

The most popular method of volume estimation in use is the single-plane elliptical method (area-length) outlined in Section 5.1, known as the "Dodge Method". The Cardiology Department at Greenlane Hospital, Auckland, uses this method for purposes of ejection fraction estimation. The results for ejection fraction estimated by Dodge and by the calculator, for the Group I patients of Chapter 7, are plotted in Figure 5-6. The two methods show very good correlation ($r^2 = 0.98$). The line of regression has the equation:

$$\text{Dodge E.F.\%} = 0.67\% + 0.99\ \text{C.E.F.\%}$$

Therefore, the methods can be considered to give results which are statistically equivalent.

Comparison with Cardiac Output

If significant correlation was found between L.V. volumes found by angiographic techniques and those by other independent techniques, this would suggest that the former methods were accurate. An independent measurement suitable for this correlation, is the cardiac output by one of several methods. The parameters needed for the comparison are the stoke volume (derived from V_D and V_S), the cardiac output and the heart rate:

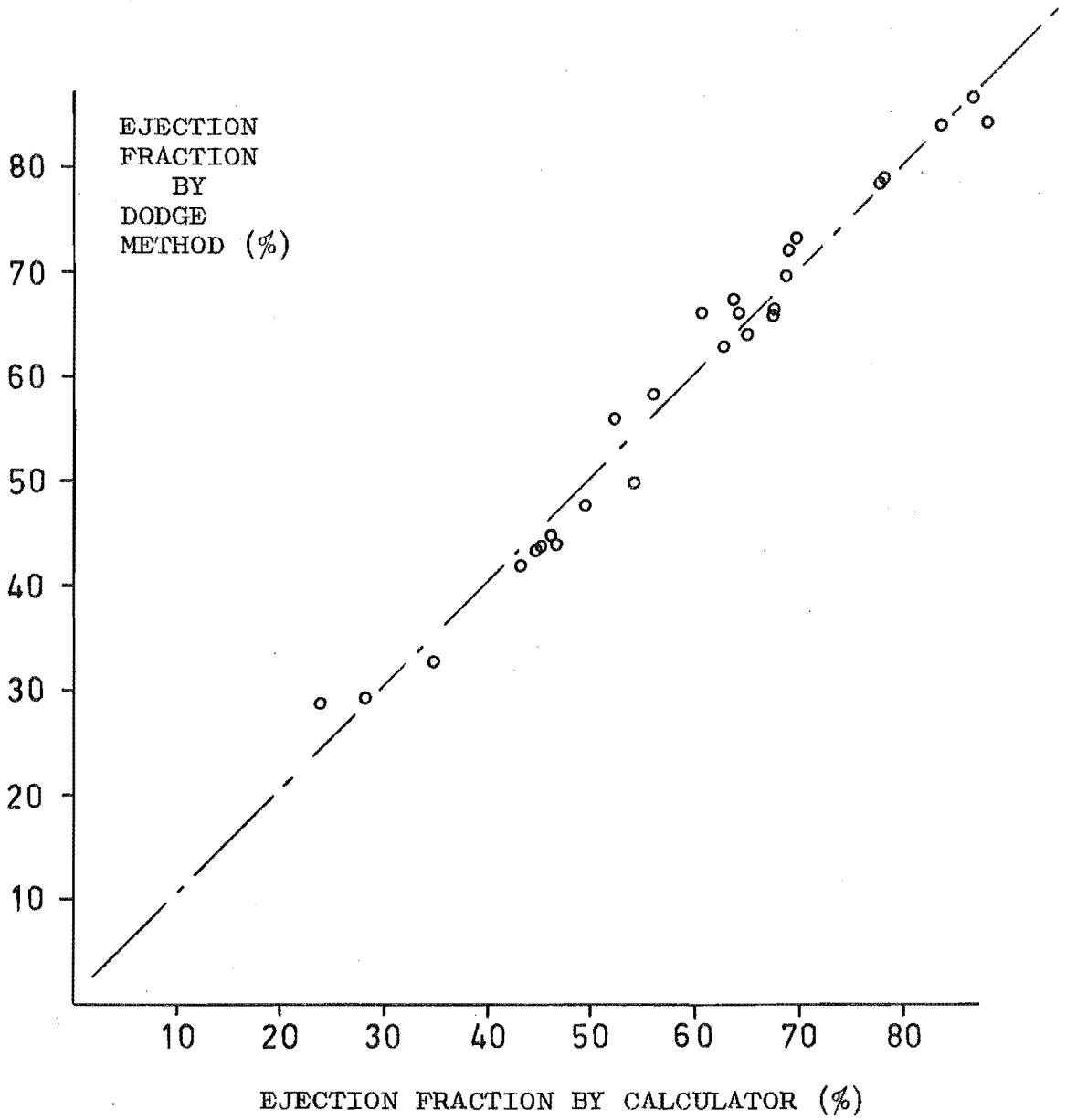

FIGURE 5-6. Comparison of ejection fractions estimated by the Dodge method and calculator (Group I patients).

$$S.V. = V_D - V_S$$

$$= C.O. / H.R.$$

The results of this comparison can only be significant if the patients concerned have normally functioning valves. If any regurgitation occurs then the second of the relations above does not hold.

At the present time no calibration apparatus is attached to the angiographic equipment at The Princess Margaret Hospital, so it is not possible to obtain calibrated stroke volumes. However this facility will be added in the near future and the study outlined above carried out. In the meantime, results show that the calculator is at least as accurate as the widely accepted Dodge method, and easier to apply.

CHAPTER 6

THE DESIGN OF THE C.E.F. CALCULATOR

A special-purpose calculator designed to apply the Rectangular Rule method had to meet certain requirements if it was to be a valuable hospital instrument. Operation had to be straight forward and efficient (in terms of a cardiologist's time and effort); results needed to be displayed prominently and unambiguously; the digital circuitry had to be simple enough to make the system relatively inexpensive, without sacrificing accuracy. An initial test system, constructed in late 1973, demonstrated the ability of the basic design to provide an effective volume estimation. Following this the prototype calculator was developed in a suitable form to evaluate the performance in the hospital environment. Only minor modifications have been necessary in the final calculator design.

6.1 BASIC DESCRIPTION

The manual calipers constructed as the input transducer for the system are shown in Figure 6-1. The device is designed to be held by the handle with the left hand. The left thumb is used to operate the single push button mounted at the top of the handle. The jaw separation is

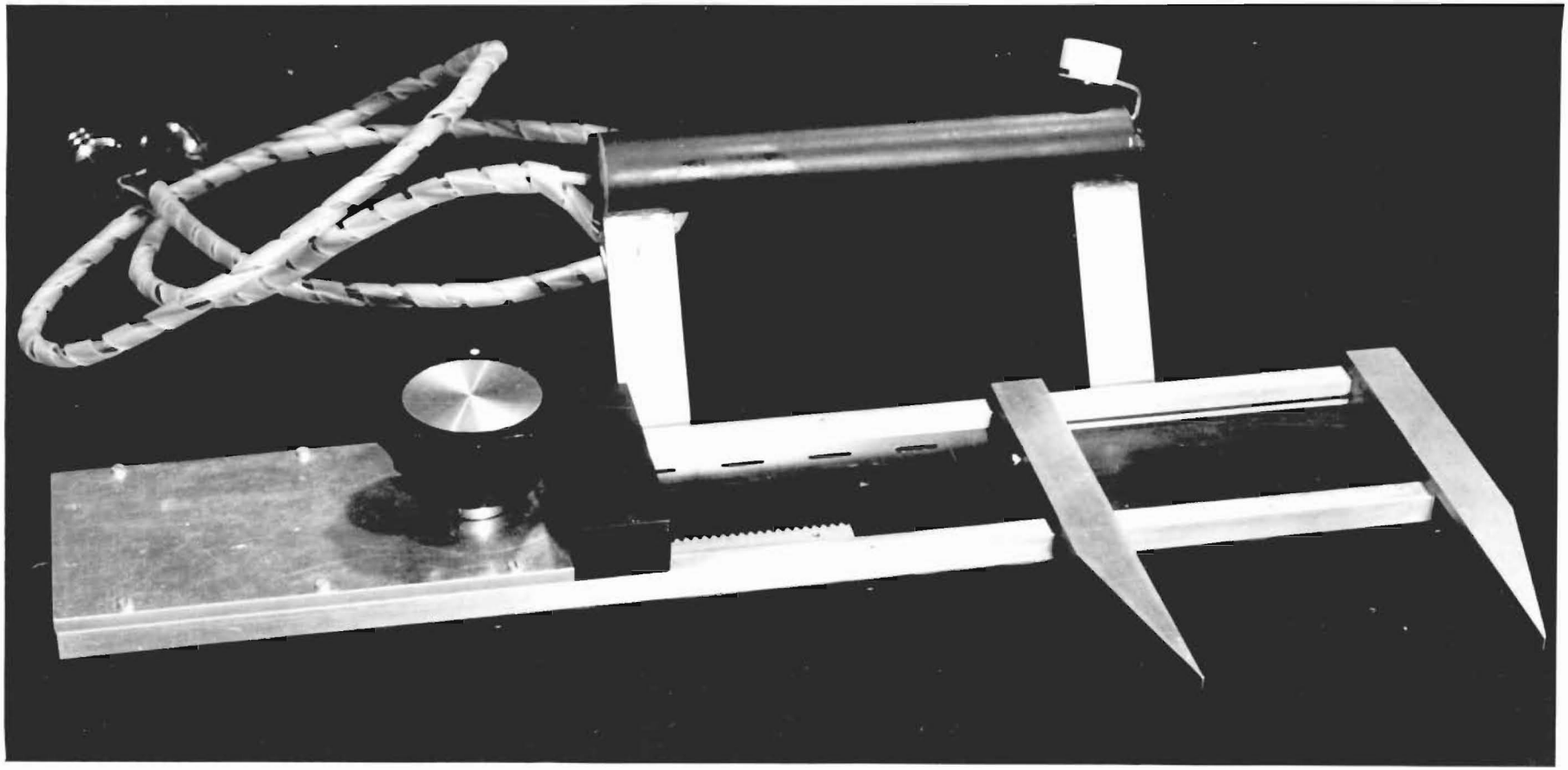

FIGURE 6-1. Manual calipers.

adjusted, by means of a large knob, with the right hand. A set of miniature filament bulbs and phototransisters straddle a slotted strip (coded in Gray binary code) attached to the movable caliper jaw. A flexible lead connects these components to the calculator cabinet and circuitry, producing an input Gray code binary word corresponding to the jaw position.

The calculator performs the following functions in response to the controls on the calculator front panel and input device:

(1) performs area or volume summations;
(2) stores two values representing the systolic and diastolic areas or volumes;
(3) displays either of the two stored values;
(4) calculates the C.E.F. from the stored values, and displays this as a percentage;
(5) clears the display and internal accumulator.

Figure 6-2 shows the calculator front panel. Each of the functions (2) to (5) above are achieved with a single button push. Function (1) is performed by operation of the caliper push button.

The configuration of the calculator is illustrated by block diagram in Figure 6-3. The majority of data processing is carried out by the C.P.U. (central processing unit). The special-purpose nature of this calculator has enabled the C.P.U. design to be relatively simple since it has only to perform a limited number of

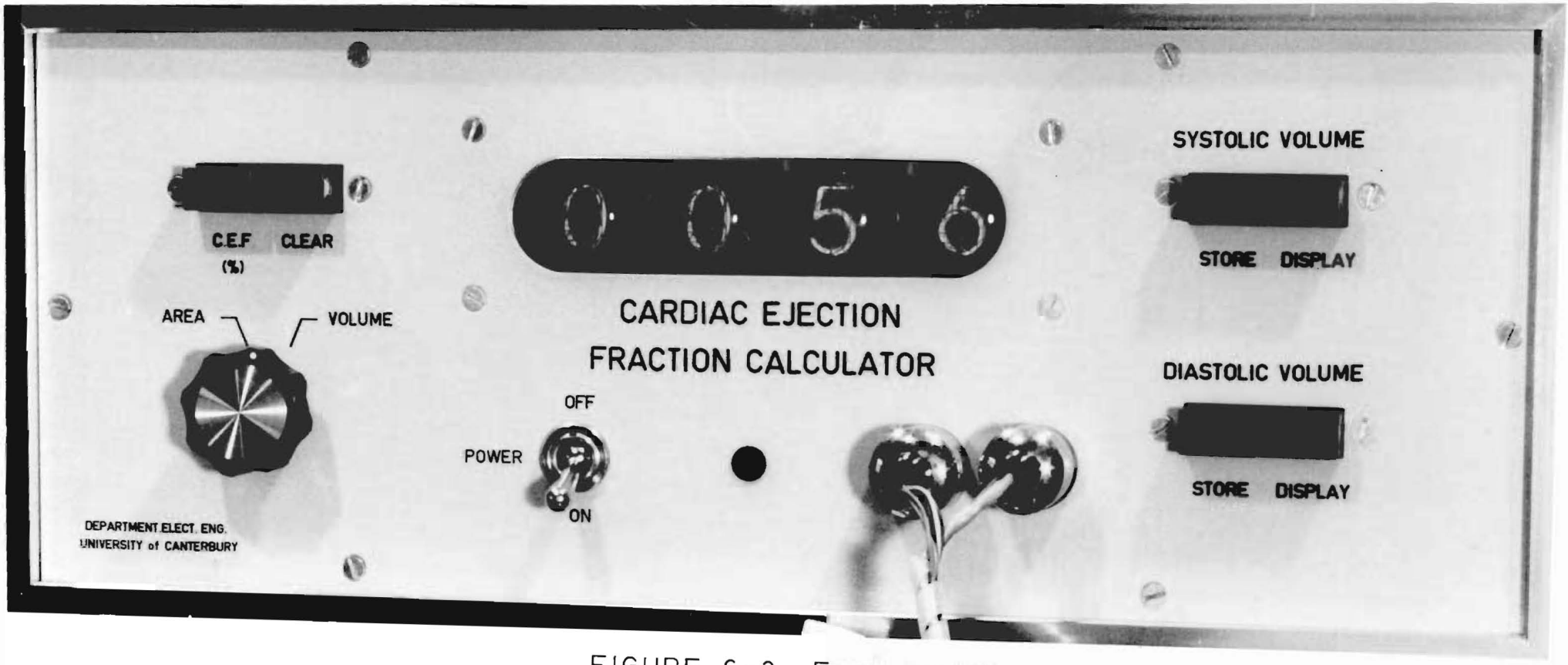

FIGURE 6-2. Front panel.

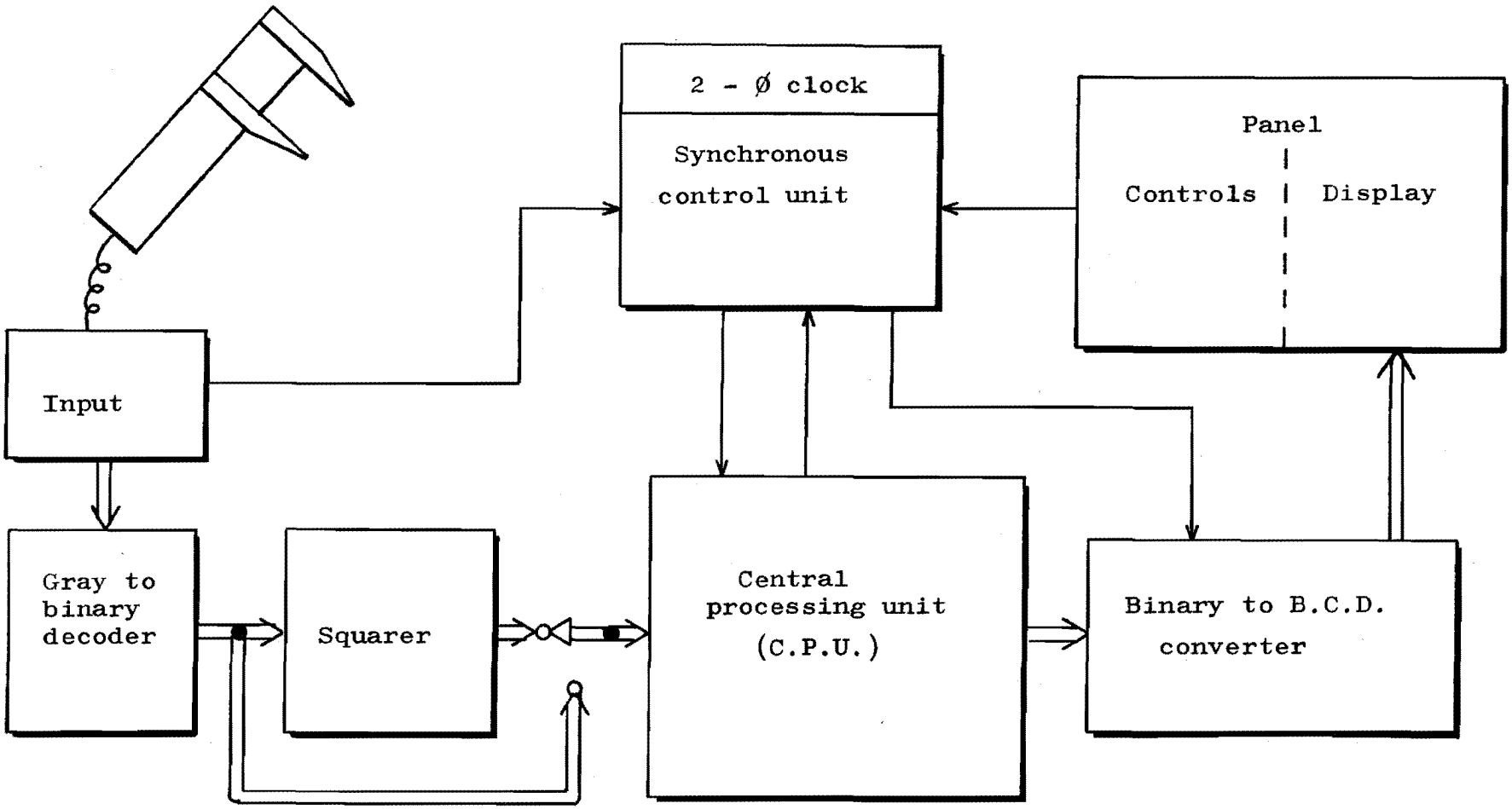

FIGURE 6-3. Major components of the C.E.F. calculator.

operations. Two operations, which might be included in the C.P.U. repertoire in a general purpose machine, are performed externally and independently. These are the squaring of the input word, and final conversion from binary to binary-coded decimal. All computation is by positive integer binary arithmetic.

Each input Gray coded 6-bit word from the calipers and associated circuitry is first decoded to a 6-bit binary integer. If an area summation is to be performed, the 6-bit binary word is accepted directly by the C.P.U. The C.P.U. output is a 12-bit binary integer (corresponding to a maximum decimal integer of 4095_{10}) and thus a 4-digit decimal display is required. The conversion from binary to binary-coded decimal (B.C.D.) is achieved by a simplified 'count up and compare' process. The binary/B.C.D. conversion unit also performs the percentage count in the simplified division process used to find the C.E.F. (refer to Figure 5-3). The data processing components of the system are described in detail in Section 6-2.

The calculator components are controlled by a synchronous control unit (S.C.U.) and a two-phase clock. The two phases of the clock, ϕ_1 and ϕ_2, have the same repetition frequency and differ in phase by 180 degrees (see Figure 6-4). The state of the S.C.U. and its output control lines change synchronously in response to ϕ_1, while ϕ_2 clocks all data processing operations selected by the present S.C.U. state. The design of the S.C.U. is completed in Section 6.3.

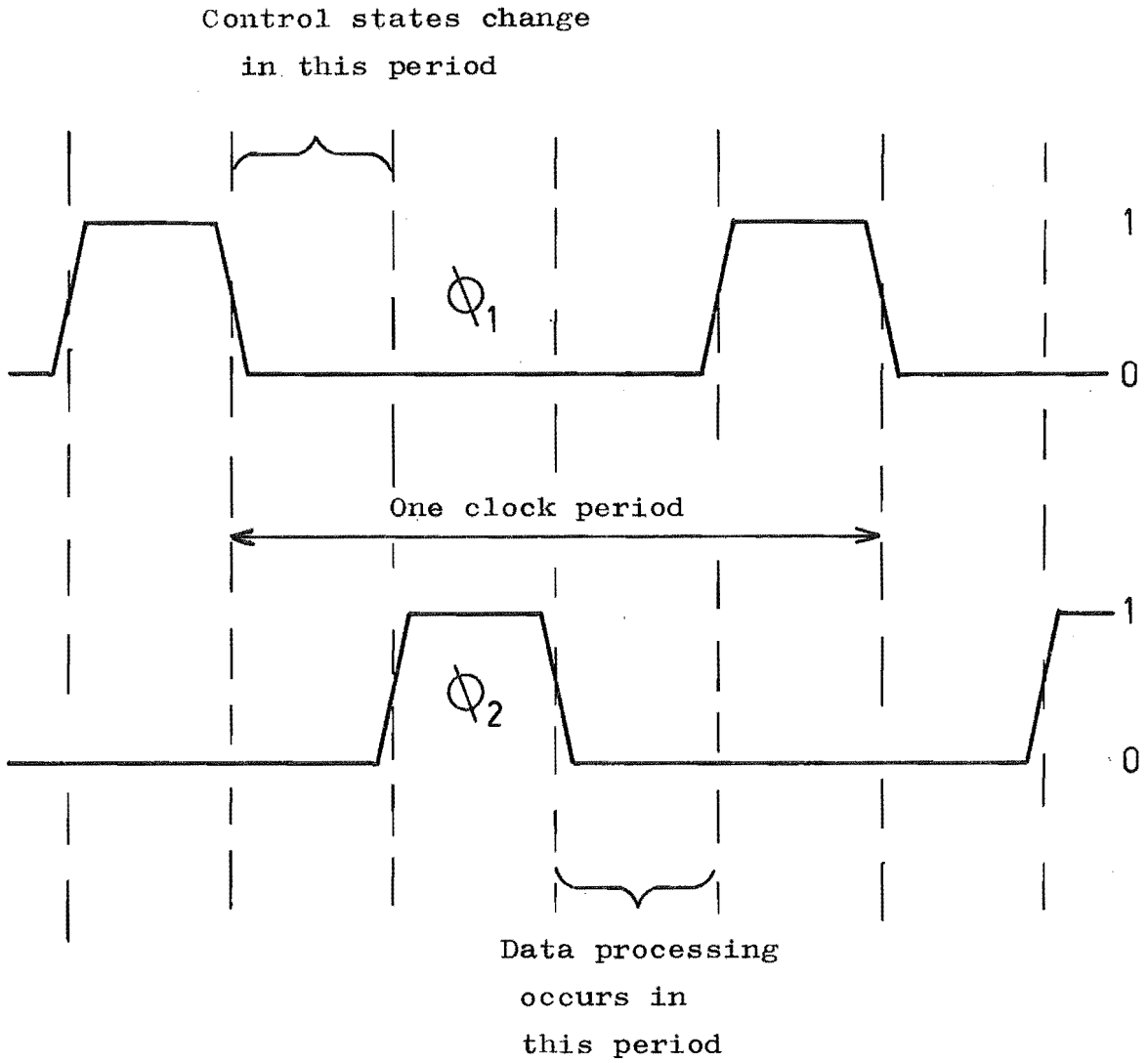

FIGURE 6-4. Two-phase clock.

Several methods of hardware implementation were possible for the C.E.F. calculator. One was the use of a L.S.I. (large-scale integration) calculator circuit, similar to those used in most modern pocket calculators. These have the advantage of being very flexible in operation, operating at low power consumption and having miniature size. However, for this special-purpose application, either a considerable amount of auxillary circuitry or a programmable read-only memory would be needed to control the operations. Only if the production of a number of identical systems was envisaged, would this be a practical and economic solution.

In lieu of using a L.S.I. device, then, it was possible to utilise the range of M.S.I. and S.S.I. (medium-scale and small-scale integration) circuitry available in various digital families. Transistor-transistor logic (TTL) was chosen. Disadvantages of the relatively high power consumption and low fanout capability of TTL devices were outweighed by advantages of low cost and ready availability.

6.2 DATA PROCESSING

The data processing components of the calculator are those which directly perform operations on the data in its digital form of 0's and 1's. All data transfer and processing is carried out in parallel in this system. Thus 6 lines are needed to carry 6-bits of information, and

to add two 6-bit words together requires a 6-bit full-adder circuit. Parallel operations require some proliferation of processing hardware but considerable savings in control hardware.

Input Decoding

In the input transducer distance information is transformed into a digital word. Gray (or cyclic) code is used to avoid errors in this transformation. Consider the switching point between 7_{10} and 8_{10}, for example:

in binary: 000111 to 001000

in Gray code: 000100 to 001100

In the binary case, if any one of the bits switches before the others (due to some mismatch in the optical switching circuitry or inaccuracy in the slotted strip), the output may be one of a range of words from 3_{10} (000011_2) to 15_{10} (001111_2) at the switching point. In Gray code, however, only a single bit switches at each switching point (bit 3 in this example), so the output word can only be interpreted as belonging to one of the adjacent intervals.

The decoding from the 6-bit Gray code word $g_5g_4g_3g_2g_1g_0$ to 6-bit binary word $a_5a_4a_3a_2a_1a_0$ (positive integer) is achieved by 5 EXCLUSIVE-OR logic gates. The governing Boolean expressions are:

$$a_i = g_i + a_{i+1}, \quad i = 0,1,2,3,4$$

$$a_5 = g_5$$

OUTPUT BITS											
11	10	9	8	7	6	5	4	3	2	1	0
	a_5		a_4		a_3		a_2		a_1		a_0
									$a_1 \cdot a_0$		
								$a_2 \cdot a_0$			
							$a_2 \cdot a_1$				
					$a_3 \cdot a_2$	$a_3 \cdot a_1$	$a_3 \cdot a_0$				
			$a_4 \cdot a_3$	$a_4 \cdot a_2$	$a_4 \cdot a_1$	$a_4 \cdot a_0$					
	$a_5 \cdot a_4$	$a_5 \cdot a_3$	$a_5 \cdot a_2$	$a_5 \cdot a_1$	$a_5 \cdot a_0$						

(a) The weighted partial products for the 6-bit input, 12-bit output squaring system.

$$15_{10} = 001111_2$$

7	6	5	4	3	2	1	0
	1		1		1		1
					1		
			1	1			
	1	1	1				
1	1	1	0	0	0	0	1

$$(15_{10})^2 = 225_{10} = 11100001_2$$

(b) An example of the partial products method of squaring.

FIGURE 6-5. Squaring by the partial products method.

Squaring

Squaring is performed by a partial products method of multiplication. In this method, every digit in each number is multiplied by every digit in the other, and the resulting weighted products are summed. Thus, in decimal:

$$15_{10}^{2} = 25_{10} + 50_{10} + 50_{10} + 100_{10}$$

$$= 25_{10} + 2 \times 50_{10} + 100_{10}$$

Similarly, in 6-bit binary squaring, partial products are added together with each weighted as shown in Figure 6-5. The partial products of digits of different significance (e.g. $a_3 \times a_1$ or $a_0 \times a_2$) are shifted one-bit left (a one-bit shift left is equivalent to multiplication by 2) instead of being added twice.

Multiplication of two binary digits is equivalent to performing the AND operation, so 15 AND gates are used to produce the partial products. Note also that:

$$a_i \text{ AND } a_i = a_i . a_i = a_i$$

The squaring of decimal 15 in its binary form is shown as an example in Figure 6-5.

Central Processing Unit

The C.P.U. consists of an accumulator, two storage registers, a four-way selector (4:1 multiplexer) and an adder. These elements are connected as shown in Figure 6-6. The only arithmetic process performed directly is addition of the selector output, $Y_{18} \ldots Y_0$, to the accumulator

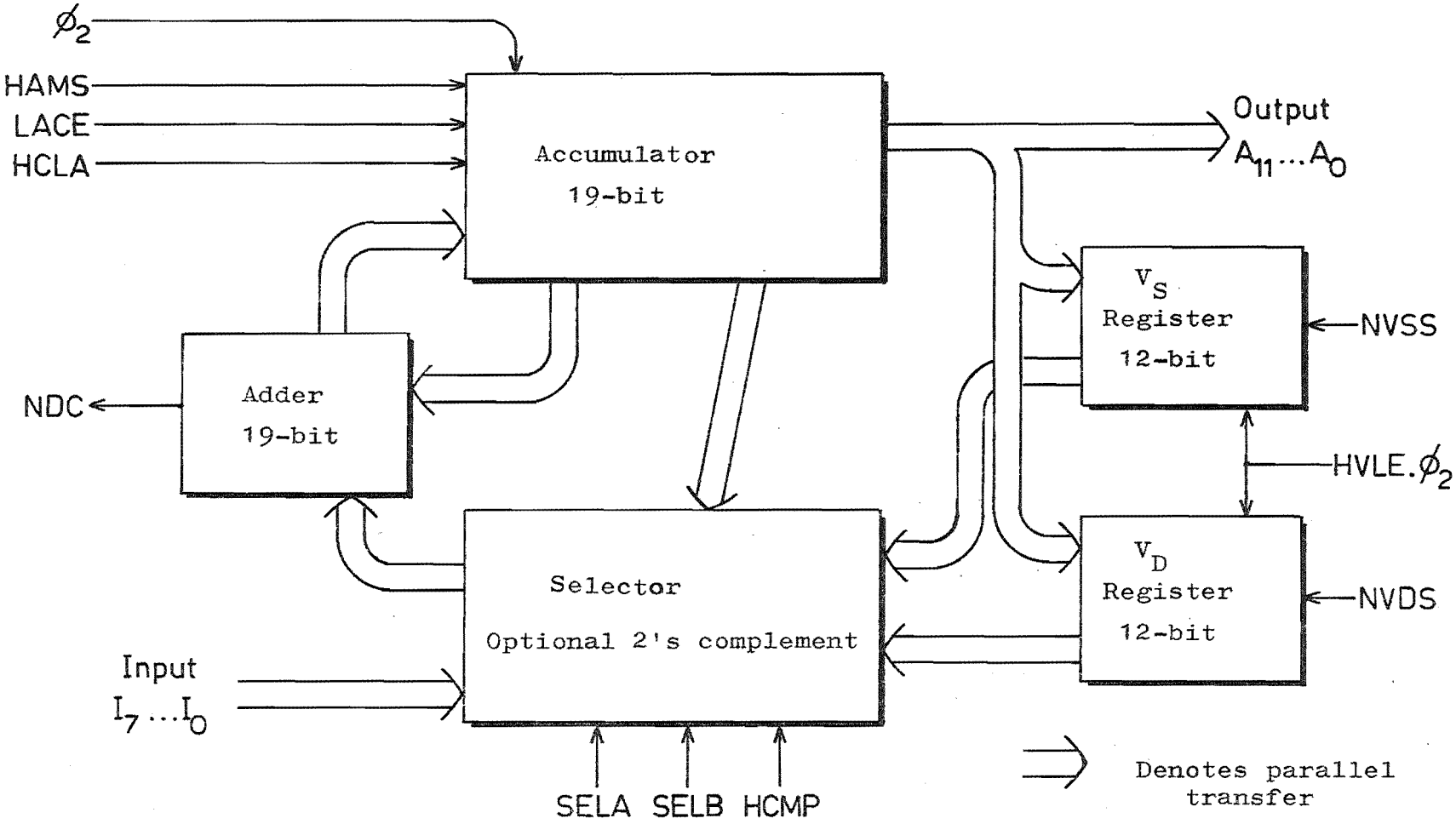

FIGURE 6-6. The central processing unit.

contents, $A_{18}....A_0$. Subtraction is performed by 2's complement addition (the 2's complement of a binary number is obtained by changing all 0's to 1's and 1's to 0's and adding 1 to the least significant bit).[10] The only C.P.U. data input is $I_7...I_0$, the eight most significant bits of the squarer output, and the only data output is $A_{11}...A_0$, the least significant 12-bits of the accumulator contents. The output is converted to B.C.D. and displayed as a 4-digit decimal number. All operations involving the C.P.U. are clocked by $\emptyset_2$, under the control of the S.C.U.

The accumulator is a 19-bit parallel-load, shift-left register. It is clocked by $\emptyset_2$ under control of 3 signals (LACE, HAMS and HCLA, refer to Appendix VI). The selector address is a 2-bit word, SELB SELA, and the output is either complemented (HCMP=1) or non-complemented (HCMP=0). The storage registers are each 12-bit latches with input $A_{11}....A_0$ and outputs to the selector. These registers store the numbers representing the volumes V_S and V_D under control of $\emptyset_2$ and three signals (HVLE, NVSS and NVDS). The selector inputs are V_D, V_S, I, and A(2), where A(2) is the accumulator contents shifted 2-bits left (A_i is transferred to Y_{i+2}).

Figure 6-7 is an illustration of C.P.U. operation. The C.E.F. is calculated from values of V_D and V_S already stored in the appropriate registers. For the purpose of the example, only the least significant 9-bits of the accumulator are utilised. When the last (repeated) operation of the C.E.F. calculation sequence is reached

OPERATION	ACTIVE CONTROL LINES	SELECTOR	ACCUMULATOR CONTENTS	
			DEC.	BINARY
Clear accumulator	HCLA		0	000000000
Load V_D (5_{10})	LACE	V_D	5	000000101
Subtract V_S (2_{10})	LACE, HCMP	V_S	3	000000011
Add A(2) to A	LACE	A(2)	15	000001111
Shift 1-bit left	LACE, HAMS	-	30	000011110
Add A(2) to A	LACE	A(2)	150	010010110
Shift 1-bit left	LACE, HAMS	-	300	100101100
Subtract V_D	LACE, HCMP, HCNT	V_D	295	100100111
Subtract V_D	LACE, HCMP, HCNT	V_D	290	100100010

The last operation is repeated until the accumulator contents reach zero. The number of repititions is counted and displayed. The result in this example is 60 (%)

FIGURE 6-7. Illustration of C.P.U. operation: C.E.F. calculation with stored values, $V_D = 5_{10}$, $V_S = 2_{10}$ (9-bit accumulator only).

(subtraction of V_D from A), the control signal HCNT enables the binary/B.C.D. converter to count the number of subtractions performed until the accumulator contents reach zero. This number is displayed as the resulting percentage C.E.F. (refer to Figure 5-3, for a flow chart representation of the calculation sequence).

Binary/B.C.D. Converter

A 'count up and compare' process is employed to convert the C.P.U. output $A_{11}....A_0$ to B.C.D. This method achieves an exact conversion with a relatively small amount of hardware. The conversion speed is low, but this is unimportant in this application. With a clock speed of 10 kHz, the display of the largest storable number ($2^{12} - 1 = 4095_{10}$) occurs in less than 0.5 sec, which is quite acceptable. Other advantages of the method are the virtually automatic nature of the conversion and the ability to perform the percentage count with the same hardware.

A schematic diagram of the binary/B.C.D. converter is shown in Figure 6-8. Initially the counters are both reset to zero by the HCLD control and $\emptyset_2$. The clock $\emptyset_2$ is enabled to both counters and they commence to count up, one in binary, the other in B.C.D. The input binary integer is subtracted, by 2's complement addition, from the binary counter output (also a binary integer). When the counter output reaches the magnitude of the input, the carry out of the adder (LCVE) goes to 0 and inhibits any

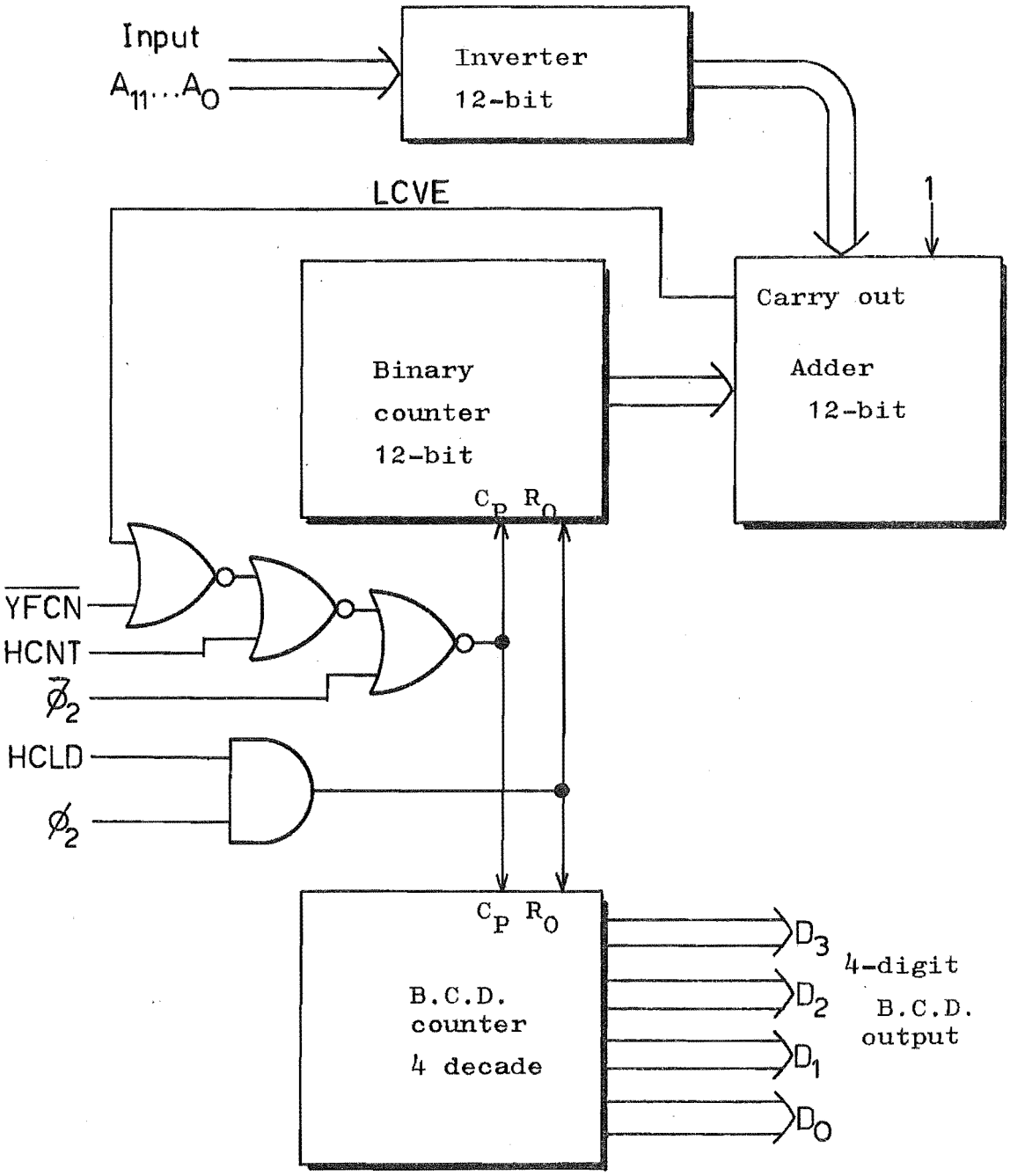

FIGURE 6-8. Binary to B.C.D. convertor.

further clocking of the counters. If the input is increased (during a volume summation) LCVE returns to 1 until the conversion is again completed.

When a percentage count is performed a different mode of operation is used. Initially the counters are reset to zero. HCNT goes to 1, while the repeated subtractions are made in the C.P.U., overriding LCVE. ϕ_2 clocks both the subtractions and the B.C.D. counter and the counter's displayed output is the calculated percentage C.E.F.

6.3 SYNCHRONOUS CONTROL UNIT (S.C.U.)

An important feature of a system designed for a specific application is that a minimum of user directions are needed for task performance. Some internal control machine is required, therefore, to replace the programme or key functions of a general-purpose system. A synchronous state machine was chosen to control the C.E.F. calculator.

A representation of the general state machine is shown in Figure 6-9.[7,10] Three basic blocks, one memory and two transform (combinational logic), with various connecting paths, make up the general machine. The state of the machine at any time is the output of the memory block, S. The next-state function defines the next state (which will become the present state in the following state time) in terms of the machine input, Q, and the present state, S. Thus:

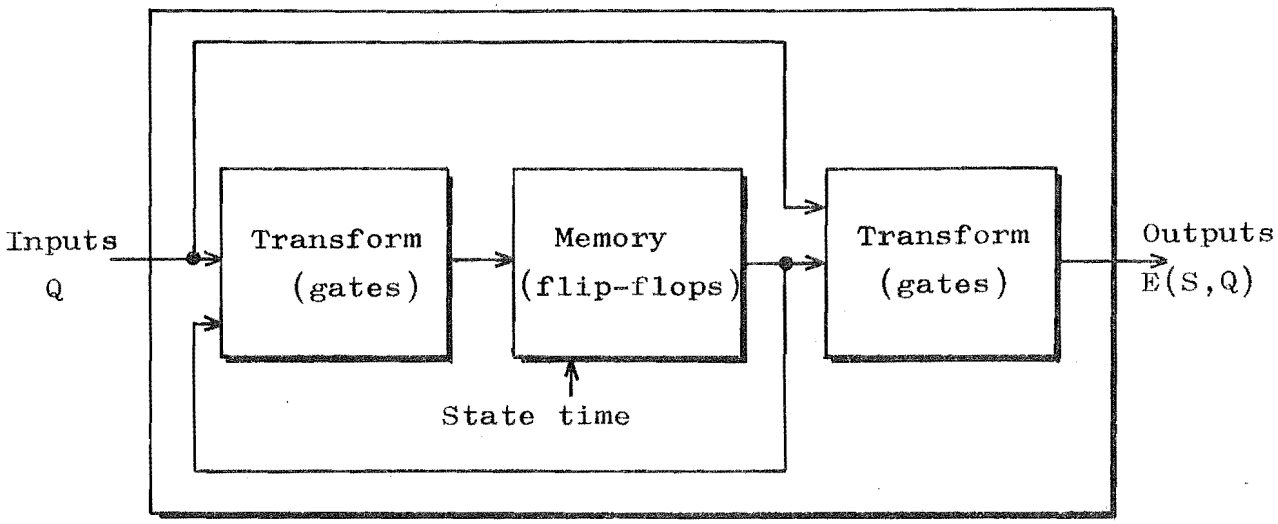

FIGURE 6-9. The generalised state machine.

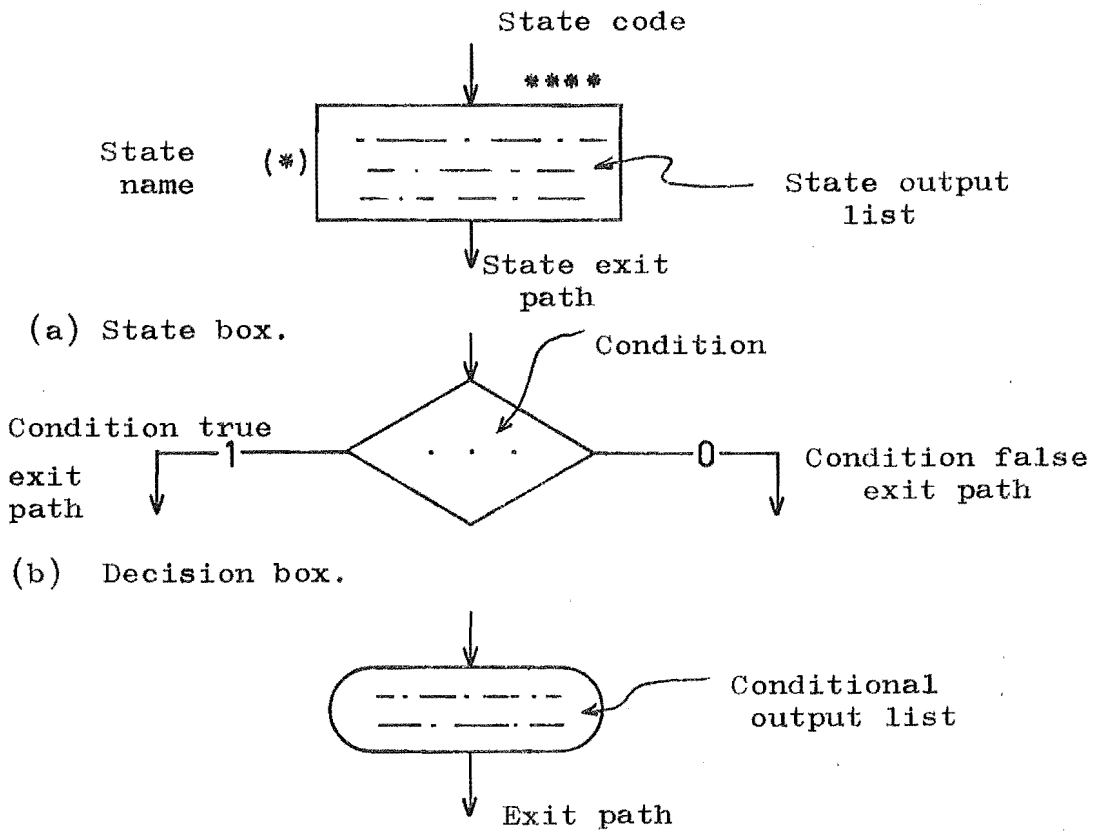

FIGURE 6-10. The three basic ASM chart elements.

$$S' = S'(Q,S) \qquad \text{(next-state function)}$$

Similarly the output, E, depends on the input and present state, so:

$$E = E(Q,S) \qquad \text{(output function)}$$

The next-state and output functions together define the machine operation.

The first steps in the design of a synchronous state machine involve deciding the number and sequence of states to be used, and their relation to inputs and outputs. This portion of the design was carried out by means of an ASM (algorithmic state machine) chart. The synthesis of the machine, after its functioning was defined by the ASM chart, involved choosing state codes (state assignment) and logic implementation (transforming the chart description into logic gates). Then the machine was tested by means of a computer simulation program.

ASM Chart

The ASM chart is a diagrammatic description of the output and next-state functions of a machine. This method of design has been used extensively by the designers employed by Hewlett-Packard (a major producer of calculators) and has been published by C.R. Clare.[7] The three basic elements of the ASM chart are shown in Figure 6-10. One state box, along with its unique code, is associated with each machine state. The exit path from a state box may go directly to another state (or to itself) or to more than one state by means of decision boxes (similar in principle

to the operational flow chart). Outputs may be associated directly with a state or conditionally with a decision box (the latter case is shown as a conditional output box).

The aim in choosing the configuration of the ASM chart is to minimise the number of elements necessary to uniquely define the desired machine operation, and thus minimise the combinational logic needed to implement the next-state and output functions. The 'optimum' ASM chart derived for the calculator's control machine is shown in Figure 6-11. It has 11 states, (a) to (k), state (a) being the 'rest' state. Two flags (YF1 and YFCN) were included in the chart to interface external asynchronous control signals (from the manual pushbuttons) with the synchronous machine. The various mnemonics used in the chart, and throughout this chapter, are listed in Appendix VI.

State Assignment

A series of JK flip-flops was chosen for the memory block of the control machine. The JK is the most general of the clocked flip-flops suitable for synchronous operation. The ASM chart has 11 states, so 4 JK flip-flops are needed to provide 4-bit codes (D C B A). The flags also require one flip-flop each, and can be considered as part of the memory block.

The assignment of a code to each state is probably the most important step in the machine design process. An understanding of the entire synthesis process is necessary since the choice of assignment greatly affects the

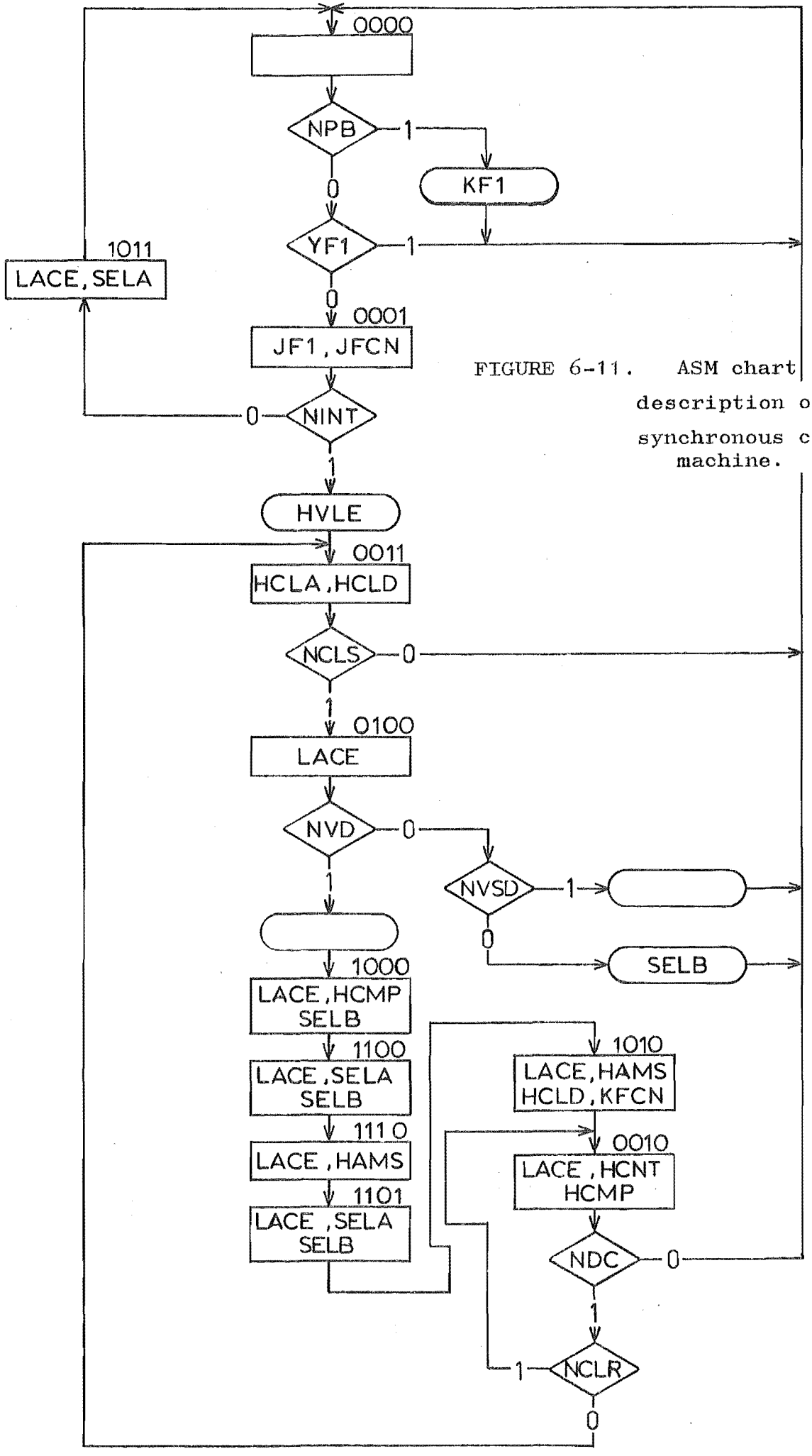

FIGURE 6-11. ASM chart description of the synchronous control machine.

complexity of the logic implementation. Moreover, there are many workable assignments, each with unique next-state function and output function. A large amount of research has been directed towards state assignment but no methods of general solution have emerged which do not involve a lengthy computer 'trial-and-error' search.[7,10] However, methods do exist for a state-by-state approach. Two of these, the reduced dependency and minimum state locus methods,[7] were employed in performing the S.C.U. state assignment. Both methods consider the change in code between two adjacent states and attempt to minimise the probable contribution to the complexity of the next-state function of that change. The resulting assignment is represented, by Karnaugh Map,[10] in Figure 6-12. It is not necessarily optimum, but is at least a reasonable minimum. (Note that, with 16 possible codes and 11 states, there are $^{16}p_{11} = 1.7 \times 10^{11}$ possible assignments).

Logic Implementation

The implementation of the ASM chart is achieved by a number of transformations. From the chart, tables are drawn up of the next-state and output functions. The next state of a JK flip-flop is determined by the J and K inputs in the present state time, so a transition table is needed to derive JK input functions, J(Q,S) and K(Q,S), from S'(Q,S). The next transformation, to gate-orientated equations, is probably best achieved by way of Karnaugh maps with map-entered variables.[7] The implementation process is illustrated for the next-state function in Figure 6-13.

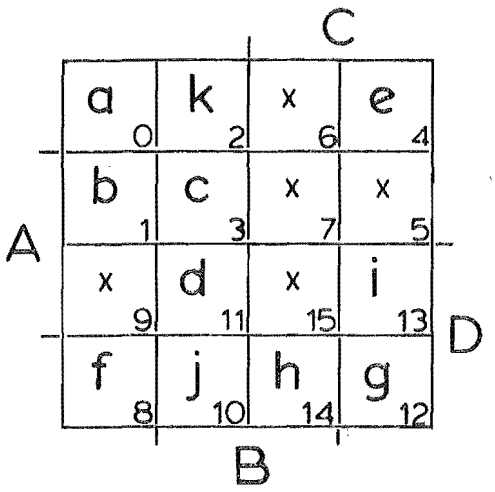

State code = D C B A

FIGURE 6-12. State assignment for S.C.U. (refer to Figure 6-11).

Transition	J	K
0 → 0	0	x
0 → 1	1	x
1 → 0	x	1
1 → 1	x	0

x denotes don't care

(a) J K flip-flop transition table

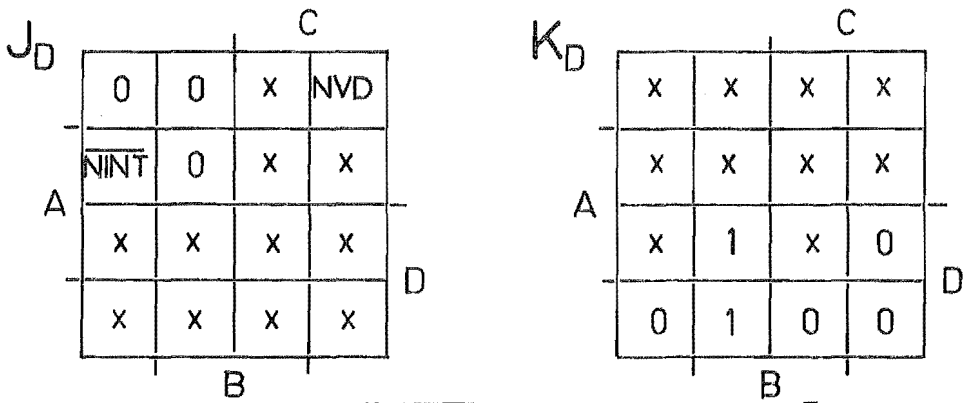

$J_D = C.\ NVD + A\ \bar{B}.\overline{NINT}$ $\qquad$ $K_D = B\bar{C}$

(b) JK input maps and Boolean expressions (flip-flop D).

FIGURE 6-13. Implementation of the next-state function from the ASM chart.

The end result of performing the above process for the control machine was a list of Boolean equations, one for each J and K input and one for each output. Further simplification was carried out on the basis of terms shared between equations and rearranging to suit the gate types available, before a completed logic design was produced.

Test Program

To avoid costly errors occurring in the printed circuit board constructed to implement the control state machine, the machine design was tested by means of a computer program. FORTRAN language was employed, but real integer arithmetic was used instead of the logical operators available in FORTRAN. All variables were restricted to values of integer 0 or integer 1, corresponding to the two logical states. The operators used are listed below:

```
NA = IABS (IA - 1)        (Ā= NOT A)
IC = IA * IB              (C= A.B)
IC = IABS(NA * NB-1)      (C= Ā.B̄ = A + B)
```

A listing of the program is included in Appendix VII, along with some examples of the results obtained. The simulation of the control machine was entirely successful and so the construction of the hardware version was completed.

6.4 CONSTRUCTION DETAILS

Almost all the circuitry included in the calculator

is made up of TTL devices, packaged in 14, 16 and 24-pin dual-in-line packages. These are soldered onto 6 double-sided printed circuit boards. The division of components between boards was made on the basis of minimising the number of board-to-board connections needed and each board layout was designed to minimise the length of conductor completing each connection. A 5 volt DC regulated power supply delivers approximately 2.5 amps to the total TTL circuitry. As well, a 300 volt unregulated DC supply is provided to drive the 4 cold-cathode indicator tubes which provide the 4-digit decimal display.

The pushbuttons on the calculator front panel and the modified microswitch on the manual calipers (refer to Figures 6-1 and 6-2) are all single pole double throw switches. If these switches were connected directly to the synchronous control unit, switch bounce (which occurs to some extent in all switches) may cause operations to be performed more than once. For example, 1 addition operation of a volume summation takes the calculator less than 0.3 microseconds to perform (at a clock frequency of 10 kHz), whereas switch bounce often occurs over a period of milliseconds. To avoid this problem, all switches are connected to the other circuitry by R-S flip-flops implemented by pairs of NAND gates. These flip-flops are mounted on one board, along with the 4 decoder-driver packages needed to drive the indicator tubes, and the clock generating circuitry. This board requires many

connections to the front panel and so is mounted parallel and close to the panel. The other boards are mounted in a rack facing the rear, alongside the power supply unit.

CHAPTER 7

THE CARDIAC EJECTION FRACTION AS A GUIDE TO SURGICAL PROGNOSIS

The evaluation of left ventricular function by angiocardiography in the cardiac catheterisation laboratory is a major part of the preoperative assessment of patients being considered for open-heart surgery. After the catheterisation is carried out at The Princess Margaret Hospital, the angiocardiographic films and results of other investigations of the patient are considered by a committee of cardiologists. The committee decide if the patient is suitable to refer to one of the surgical units (Auckland, Wellington and Dunedin at the present time). A similar consideration is made at the surgical unit before the patient is accepted for the valve replacement or coronary revascularisation operations.

Open-heart surgery involves considerable trauma, since during the procedure the patient spends some time on cardio-pulmonary bypass, with a machine taking over the heart's function. Ventricular fibrillation is also induced to minimise the spontaneous muscle motion. For these reasons and because of possible postoperative complications, only patients with reasonably well preserved heart function have an acceptable chance of survival. All the parameters described in Chapter 4 have been used, often in some combined

index form, as indicators of ventricular functioning. However the single parameter which appears to have the most prognostic significance is the cardiac ejection fraction. In this chapter, studies of the C.E.F.'s of two groups of patients made at The Princess Margaret Hospital are described.

7.1 METHODS

The first group of patients, numbering 27, all had coronary artery disease confirmed by angiography. Records were made during catheterisation of the left ventricular pressure and E.C.G., before the injection of contrast material, and several minutes after the injection. An Electronics for Medicine DR 8 with an ultraviolet galvonometer recorder was used to make these standard measurements. The end-diastolic pressure was taken as the pressure at the instant of the peak of the R wave on the E.C.G. recording. dP/dt (measured from the pre-injection pressure record) was estimated from the maximum slope at the onset of systole. The severity of disease was gauged from the coronary angiograms and the subsequent cardiologist's report, and a score given to each patient. The basis for obtaining this 'artery score' is described in Appendix VIII.

The second group consisted of 17 patients who underwent catheterisation between January and July 1973 and subsequently were accepted for surgery. Eleven of these had coronary artery disease and had from one to four bypass grafts fitted

(3 also had aneurysms resected). Another 5 patients had one or more valves replaced and 1 patient had a combination of valve replacement and revasularisation. The postoperative course of each patient was studied and given one of three grades. Grade I was excellent recovery, with no reoccurrence of symptoms of heart failure. Grade II was either slight complications immediately following the operation and/or the continuance of mild symptoms (such as angina after exertion). Grade III was operative mortality, defined here as death which could be attributed to the effects of the operation.

Left ventriculography was performed on all patients of both groups. In this process, contrast material is injected by a pneumatic syringe through a catheter directly into the left ventricle. As the injection begins, the x-ray source is energised and the motion of the ventricle observed for a number of beats, until the contrast material has been pumped away and diluted. The resultant angiocardiographic film, taken at 60 frames per second, shows the two-dimensional projection of the ventricular cavity.

The calculator described in Chapters 5 and 6 was used to estimate C.E.F. from the patients' angiocardiographic films. The starting point for the method was to trace the outlines of the left ventricle at systole and at diastole. To facilitate this operation a special screen, which doubled as a table, was constructed and fitted to the existing Tagarno 35 viewer.

7.2 RESULTS

Results of the study for Group I patients are shown in Figures 7-1, 7-2 and 7-3. No attempt was made to correlate results for this group with their prognosis, since most of these patients underwent catheterisation too recently to have had surgery performed at the time of data collection. Instead, the correlation of the parameters dP/dt, E.D.P. (including rise following contrast injection) and artery score, with C.E.F. was investigated.

Figure 7-1 shows dP/dt plotted directly against C.E.F. for the 27 patients. Clearly, there is very little correlation between these two parameters directly, with a correlation coefficient, r^2, of only 0.16. The values of E.D.P. show even less evidence of a direct relationship with C.E.F. ($r^2 = 0.08$). However, comparing the other parameters with each other, with the data grouped according to high or low C.E.F., shows more significant results. Thus Figure 7-2 is dP/dt versus E.D.P. (preangiography) with the points coded for C.E.F. greater or less than 55%. High and low ejection fraction patients can be seen to lie in different, though overlapping, quadrants, whereas the whole group are well spread. The other data presented for Group I is the change of E.D.P. during angiography versus artery score, with similar C.E.F. coding, shown in Figure 7-3. The data for the whole group shows reasonable correlation ($r^2 = 0.33$) as predicted by Brundage.[3] Again the high and low ejection fraction patients occupy

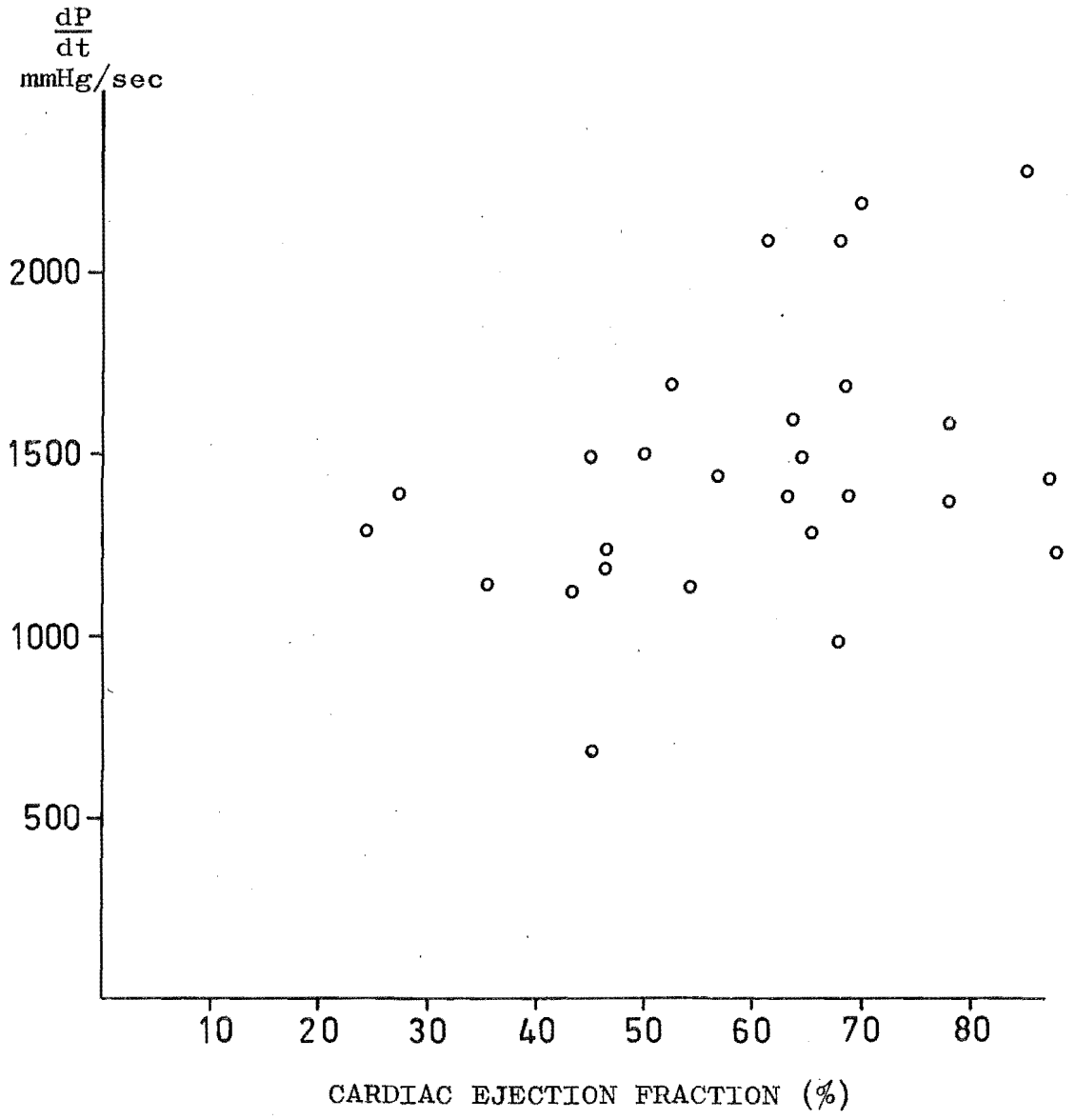

FIGURE 7-1. Group I patients: $\frac{dP}{dt}$ versus C.E.F.

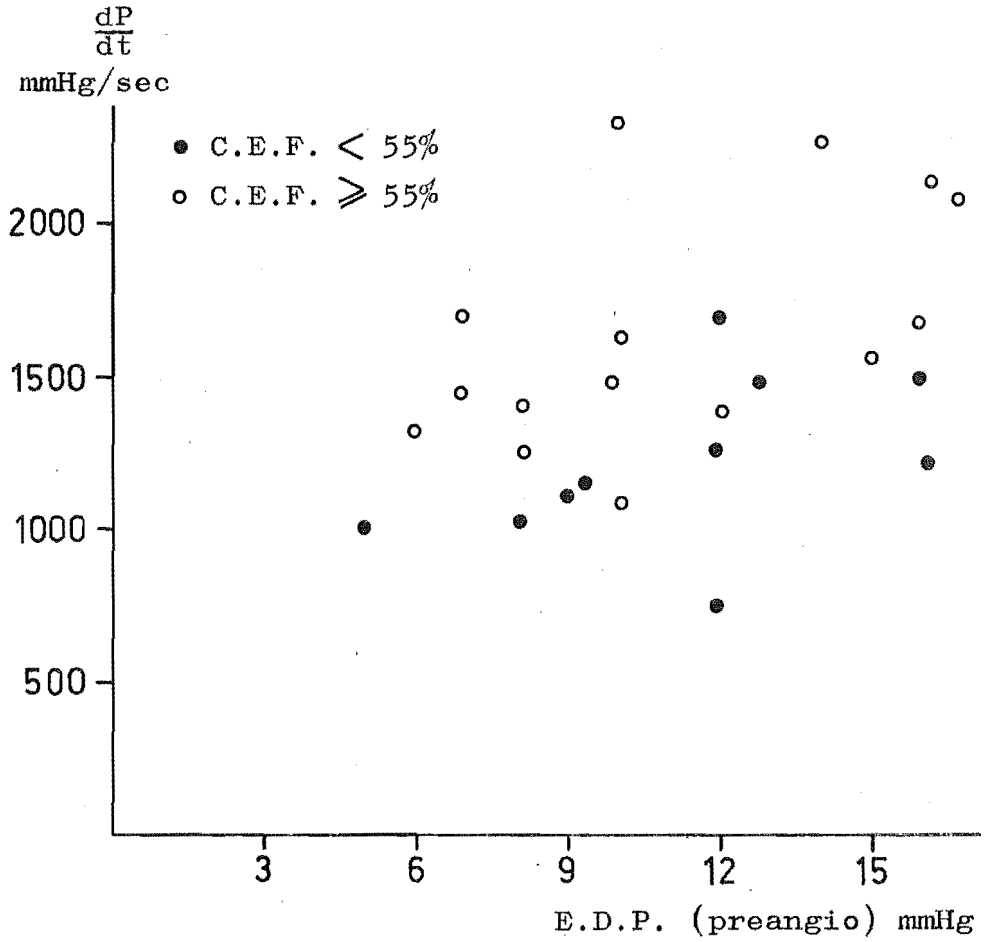

FIGURE 7-2. Group I patients: $\frac{dP}{dt}$ versus E.D.P. (preangio).

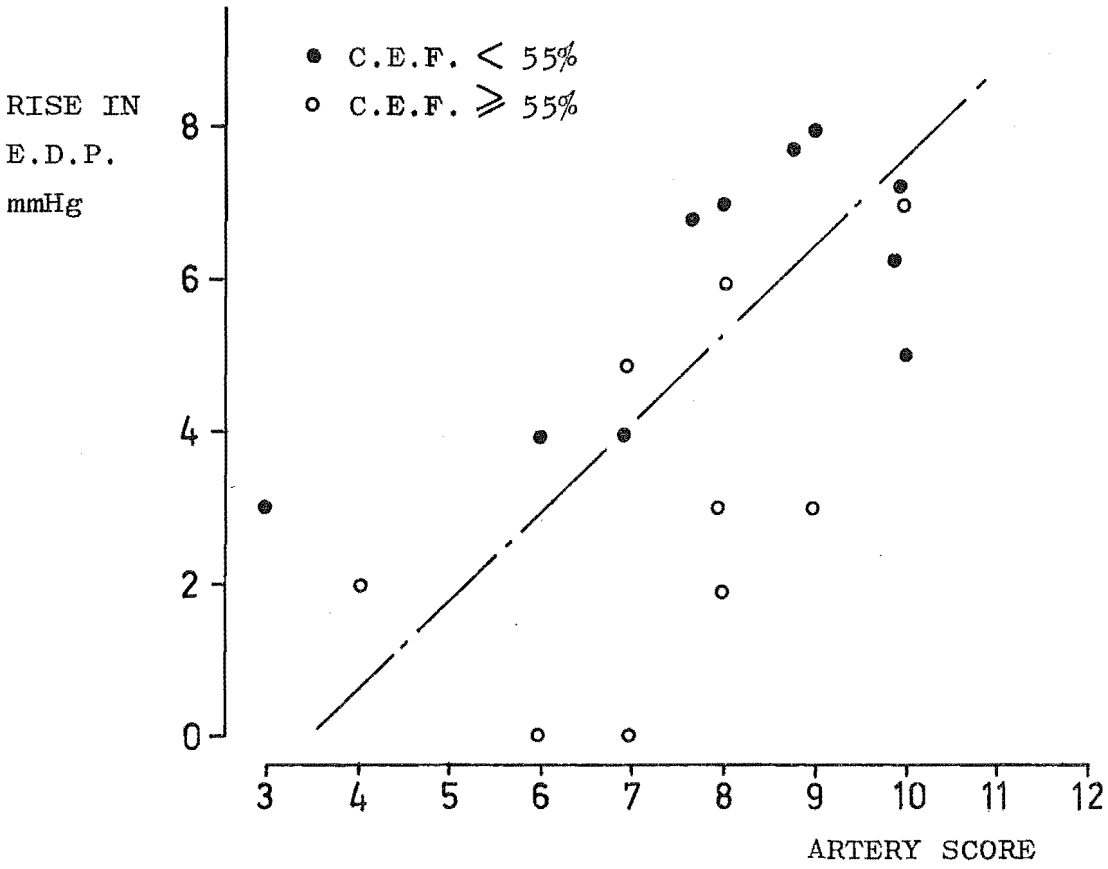

FIGURE 7-3. Group I patients: change in E.D.P. versus artery score.

different quandrants, although with a relatively high degree of overlap in this case.

The results of the study on Group II patients are shown in Figure 7-4, a bar graph of the number of patients with each post-operative grade belonging to various ranges of C.E.F. Grade III outcome (operative mortality) occurred only in patients with ejection fractions less than 40%, while Grade II outcomes were recorded for the patients in the 40% to 50% range. The two other ranges of greater ejection fractions show only one Grade II outcome each, with all the remaining patients having excellent recoveries (Grade I). The size of the sample group is too small to make a realistic statistical analysis of the results, but the correlation between C.E.F. and post-operative recovery is clearly significant.

7.3 DISCUSSION

The investigations carried out with Group I patients (coronary heart disease) illustrate the relationship of the C.E.F. to the other parameters used. An increase in E.D.P. indicates dilation of the heart and increase in V_D. According to the Frank-Starling Law, the result is a larger muscle contraction force and thus an increase in dP/dt for a given muscle condition. Poor muscle can be expected to have a similar relation of dP/dt to E.D.P. to that of good muscle, but with a lower dP/dt for any given E.D.P. Figure 7-2 indicates that, although the points are fairly

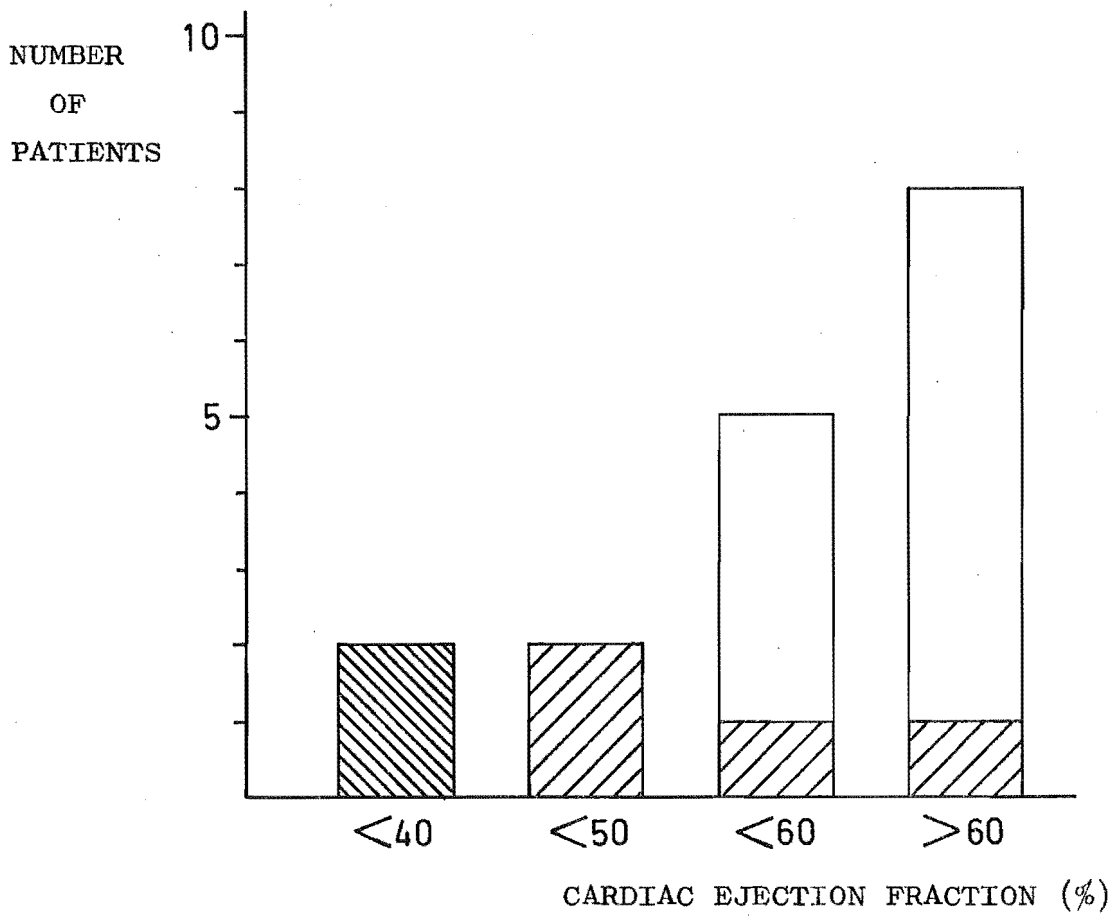

Post-op Grade I: excellent recovery, no symptoms.

Post-op Grade II: slight complications, mild symptoms.

Post-op Grade III: operative mortality

FIGURE 7-4. Group II patients: prognostic significance of the cardiac ejection fraction.

scattered, division according to C.E.F. values separates out two similar groups. Those with a C.E.F. less than 55% lie in a quadrant of low dP/dt relative to E.D.P., while the rest lie in a quadrant of high dP/dt relative to E.D.P. This lends weight to the acceptance of C.E.F. as an indicator of muscle condition.

The amount of work which muscle can perform is governed by the amount of energy available to that muscle. Limiting of the blood supply to the cardiac muscle (ischemia) will therefore limit the heart's ability to cope with extra loads. The injection of fluid into the L.V. during angiography imposes an extra volume load. A normal heart immediately compensates with increased contraction force and clears the extra volume, but an ischemic heart tends to dilate for some time with a corresponding increase in E.D.P. The rise in E.D.P. during angiography of Group I patients (Figure 7-3) shows good correlation with the artery scores, which are likely to be closely related to the degree of ischemia. The hearts of patients with good C.E.F. estimations (greater than 55%) appear to cope better with the increased load than those with poor C.E.F.

The low number of Group II patients with C.E.F. estimations of less than 50% (4 out of 17) reflects the reluctance of the cardiac committees to refer or accept a patient for surgery if he has a low C.E.F. This reluctance is justified in the light of the results obtained in this study. The only mortalities which occurred were patients with very low C.E.F.; of patients with C.E.F. greater than 50%, only 2 out of 13 were Grade II

post-operatively (refer Figure 7-4). It is important to note that both Grades I and II could be classed as success since all Grade II patients experienced a post-operative improvement in health.

The results of this study would appear to suggest that 40% is a reasonable value of C.E.F. on which to base the decision of surgical treatment. However the publication of results of other studies of larger groups has led to the general acceptance of 50% as the cutoff value.[8,15] The acceptance of any definite cutoff requires that a standard technique of C.E.F. estimation be adopted by all parties concerned. At present this is not the case; at least 3 different methods are used within New Zealand.

CHAPTER 8

SUMMARY : CARDIOVASCULAR INSTRUMENTATION

The development of cardiovascular instrumentation has always been aimed at increasing the amount of information which can be obtained about the cardiovascular system from outside the body. This development trend has brought about the advent of many non-invasive monitoring methods. The accuracy of measuring techniques has also improved, allowing more precise diagnoses to be made. All improvements and developments of new techniques lead towards better patient care, whether directly, by ensuring correct medical or surgical treatment and minimum discomfort, or indirectly, by increasing the hospital throughput.

The method proposed for making an assessment of arterial condition, using a relatively inexpensive bedside instrument, is one example of the contribution to clinical diagnosis which is possible by the application of scientific and engineering principles. The same can be said of the C.E.F. calculator, which is designed to provide a method of deriving an important cardiological parameter from angiocardiagrams, with a minimum of time and expensive equipment. These projects belong in the field of bio-medical engineering. This new interdisciplinary field seeks to explore the interaction of medicine, biology and engineering, without being constrained to any one of these.

The emphasis in biomedical engineering is on the collaborative effort of individuals from the different disciplines resulting in the formation of a truly effective problem solving facility.

The results of studies made of the cardiac ejection fractions of patients at The Princess Margaret Hospital show that the acceptance of this parameter as a valuable guide to surgical prognosis is justified. Results also indicate a direct relationship of the parameter to the physical condition of the cardiac muscle. However, in view of the complexities of muscle contraction and the cardiac control mechanisms, it would be unwise to suggest C.E.F. as a true index of myocardial contractility. The need for a standard technique of C.E.F. estimation is evident and it is hoped that the method and calculator described herein may supply such a standard.

ACKNOWLEDGEMENTS

The successful completion of this project would not have been possible without considerable interest and feedback from the medical profession. In this I am indebted to the cardiologists of the Department of Cardiology, The Princess Margaret Hospital and, to The National Heart Foundation of New Zealand for their financial support.

I would like to thank the Department of Electrical Engineering (University of Canterbury), as a whole, for their patience and perseverence. In particular, my thanks to my supervisors, formerly Dr Basil Kerdemelidis, latterly (during the difficult period) Mr Fred Cady, for much advice and assistance. The successful construction of the calculator was made possible by some meticulous engineering from Mr Art Vernon and patient circuit work by Mr Colin Brittenden.

My thanks also to Mrs J.N. Brown for making such a beautiful job of the typing.

REFERENCES

1. ARVIDSSON, H. Angiocardiographic observation in mitral disease. Acta Radiologica, Stockholm, Suppl. 158, 1958: 1-124.

2. BLINKS, J.R. and JEWELL, B.R. The meaning and measurement of myocardial contractility. In Bergel, D.H. Cardiovascular fluid dynamics. London, Academic Press, 1972: 225-260. Vo 1.1.

3. BRUNDAGE, B.H. Left ventricular angiography as a function test. Chest, 64, No. 1, 1973: 70.

4. BRUTSAERT, D.L. The significance of measurement of contractility of the heart. In Snellon, H.A. Quantitation in cardiology. Netherlands, Leiden University Press, 1972: 147-162.

5. CHAPMAN, C.B. and others. Use of biplane cinefluorography for measurement of ventricular volume. Circulation, 18, 1958: 1105.

6. CHARM, S. and KURLAND, G.S. Viscometry of human blood for shear rates of 0-100,000 sec^{-1}. Nature, London, 206, 1965: 617-18.

7. CLARE, C.R. Designing logic systems using state machines. U.S.A., McGraw-Hill, 1973: 116p.

8. COHN, P.F. and others. Left ventricular ejection fraction as a prognostic guide in surgical treatment of coronary and valvular heart disease. American J. of Cardiology, 34, 1974: 136-141.

9. DESILETS, D.T. and BECKENBACH, F.S. Myocardial function from cineangiocardiograms with a digital computer. Fiagnostic Radiology, 99, 1971: 319.

10. DIETMEYER, Logic design of digital systems. Boston, Allyn and Bacon, 1971.

11. DIKEMAN, P. and CHI-NING LIU. Speeding the complex calculations required for assessing left ventricular function of the heart. Hewlett-Packard Jounral, U.S.A., 1974 (March): 18-24.

12. DODGE, H.T. and others. The use of biplane angiocardiography for the measurement of left ventricular volume in man. American Heart J., 60, No. 5, 1960: 762-776.

13. DODGE, H.T. and others. An angiocardiographic method for directly left ventricular stroke volume in man. Circulation Research, 11, 1962: 739-745.

14. DODGE, H.T. and others. Usefulness and limitations of radiographic methods for determining left ventricular volume. American J. of Cardiology, 18, 1966: 10-24.

15. DODGE, H.T. and BAXLEY, W.A. Hemodynamic aspects of heart failure. American J. of Cardiology, 22, 1968: 24-34.

16. FANTON, J.L. A computer-aided hospital system for cardiac catheterization procedures. Hewlett-Packard Journal, U.S.A., 1972(Jan.).

17. FEIGENBAUM, H. Echocardiography. U.S.A., Lea and Febiger, 1972. 239p.

18. FLAX, S.W. and others. Noise and functional limitations of the Doppler blood flowmeter. In Reneman, R.S. Cardiovascular applications of ultrasound. Netherlands, North-Holland, 1974: 18-31.

19. FRANK, E. An accurate, clinically practical system for spatial vectocardiography. Circulation, 13, 1956: 737.

20. FRANKLIN, D.L. and others. Blood flow measurement by backscattered ultrasound. Science, 134, 1961: 564-565.

21. GLEASON, W.L. and others. Studies of the first derivative of the ventricular pressure pulse in man. J. of Clinical Investigation, 41, 1962: 80.

22. GOSLING, R.G. and others. Blood velocity waveforms in the evaluation of atheromatous changes. In Roberts, C. Blood flow measurement. London, Sector Publishing Ltd., 1972; 33-39.

23. GOSLING, R.G. and others. Continuous wave ultrasound as an alternative and complement to X-rays in vascular examination. In Reneman, R.S. (see Reference 18); 266-282.

24. GOW, B.S. The influence of vascular muscle on the viscoelastic properties of blood vessels. In Bergel, D.H. (see Reference 2): 66-110. Vol. 2.

25. GRIBBE, P. Comparison of the angiocardiographic and the direct Fick methods in determining cardiac output. Cardiology, 36, 1960: 20.

26. GRIFFITH, R.L. An algorithm for locating the aortic valve and apex in L.V. angiocardiograms. IEEE Trans. Bio-Med. Eng., BME-21, 1974: 345.

27. GUYTON, A.C. Basic human physiology. U.S.A., Saunders, 1971. 720p.

28. HAGL, S. and others. Influence of stenosis on the velocity profile analysed by a pulsed Doppler ultrasonic flowmeter. In Reneman, R.S. (see Reference 18): 216-225.

29. HALLERMAN, F.J. and others. Comparison of left ventricular volumes by dye dilution and angiographic methods in the dog. American J. of Physiology, 204, 1963: 446-450.

30. HUGENHOLTZ, P.G. and others. Quantitative assessment of left ventricular function. In Snellen, H.A. (see Reference 4): 163-172.

31. KENNEDY, J.W. and others. Quantitative angiocardiography. The normal left ventricle in man. Circulation, 29, 1968: 887.

32. KING, D. and others. Transcutaneous measurement of pulse wave velocity and mean blood pressure in man. In Roberts, C. (see Reference 22): 40-43.

33. KOLIN, A. Electromagnetic flowmeter: principle of method and its application to blood flow measurements. Proc. Exper. Biology and Medicine, 35, 1936: 53-56.

34. KREULEN, T.H. and others. Ventriculographic patterns and hemodynamics in primary myocardial disease. Circulation, 47, 1973: 229-305.

35. LATHI, B.P. Signals, systems and communication. U.S.A., Wiley, 1965. 607p.

36. McCRACKEN, D. and DORN, W.S. Numerical methods and Fortran programming. U.S.A., Wiley, 1964.

37. McDONALD, D.A. Blood flow in arteries. London, Arnold, 1960.

38. MACINTYRE, J. X-ray records from the cinematography. Acta Skiagraphy, 1, 1897: 37.

39. MEESTER, G.T. and others. Measurement of contractile element velocity. A comparison of three methods. In Snellen, H.A. (see Reference 4): 200-203.

40. MILLER, G.A.H. and others. Myocardial function and left ventricular volumes in acquired valvular insufficiency. Circulation, 31, 1965: 344.

41. RENEMAN, R.S. Cardiovascular applications of ultrasound. Netherlands, North-Holland, 1974: 462p.

42. ROSS, J. The assessment of myocardial performance in man by hemodynamics and cineangiography technics. Amer. J. Cardiology, 23, 1969: 511.

43. RUSHMER, R.F. Cardiovascular dynamics. 2nd ed. U.S.A., Saunders, 1961: 502p.

44. SANDLER, H. and others. Calculation of left ventricular volume from single-plane (A-P) angiocardiograms. J. Clinical Investigation, 44, 1965: 1094.

45. SANDLER, H. and DODGE, H.T. The use of single-plane angiocardiograms for the calculations of left ventricular volume in man. Amer. Heart J., 75, 1968: 325.

46. STIMSON, M. and others. Current status of densitometric left ventricular volume computation. In Herron, R.E. Quantitative imagery in biomedical science. Soc. Pho-Opt. Instr. Engineers, 1971.

47. TASTO, M. Motion extraction for left ventricular volume measurement. IEEE Trans. Bio-Med. Eng., BME-21, 1974: 207.

48. WHITMORE, R.L. Rheology of the circulation. Great Britain, Pergamon Press, 1968: 196p.

49. WOODCOCK, J.P. and others. A new non-invasive technique for assessment of superficial femoral artery obstruction. British J. of Surgery, 59, 1972: 226.

50. WOODCOCK, J.P. and others. Physical aspects of blood-velocity measurement by Doppler-shifted ultrasound. In Roberts, C. (see Reference 22): 19-23.

51. VOKONAS, P.S. and others. Dynamic geometry of the left ventricle in mitral regurgitation. Circulation, 48, 1973: 786-796.

52. YAO, S.T. Haemodynamic studies in peripheral arterial disease. British J. of Surgery, 57, 1970: 761.

APPENDIX I

IMPORTANT ABBREVIATIONS AND SYMBOLS USED IN TEXT

ASM,	algorithmic state machine
A-V,	atrio-ventricular
C.E.F.,	cardiac ejection fraction
C.O.,	cardiac output (L/min)
C.P.U.,	central processing unit
dP/dt,	maximum systolic rate of increase in L.V. pressure
E.D.P.,	end-diastolic pressure (L.V., mmHg)
H.R.,	heart rate (beats/min)
L.V.,	left ventricle
S.C.U.,	synchronous control unit
S.V.,	stroke volume (ml)
TTL,	transistor-transistor logic
V_D,	end-diastolic volume (ml)
V_S,	end-systolic volume (ml)
Z.C.D.,	zero-crossing detector
A_i,	ith-bit of accumulator contents
Δf,	Doppler frequency shift
Δf_c, Δf	corresponding to the mean rate of zero crossings
ϕ_1, ϕ_2,	phase-1, phase-2 of calculator clock
h,	pitch of grating used in conjunction with calipers
I_i,	ith-bit of C.P.U. input
N,	preset length of variable-length shift register
R,	correlation factor of blood velocity waveforms
T,	pulse transit time between two arterial sites

τ, sample time of Z.C.D.

u, instantaneous mean blood velocity

U, digital output of Z.C.D. representing u.

x_i, ith intercept length of grating on ventricular outline

X_i, digital representation of x_i

Y_i, ith-bit of the C.P.U. selector output.

APPENDIX II

DERIVATION OF FLOW EQUATIONS

(from Section 2.1)

(a) Parabolic Flow Profile.

The tangential stress S acting on the fluid cylinder (see Figure 2-1(a)) produces a viscous drag force = $S \cdot 2\pi r \cdot 1$. For the velocity to be constant, then

$$\frac{\Delta P}{L} \cdot \pi r^2 = S \cdot 2\pi r$$

The rate of shear, S/η, is equal to the velocity gradient with respect to r (laminar flow). Thus:

$$S = -\eta \frac{du}{dr}$$

Substituting for S:

$$du = -\frac{\Delta P}{2 L \eta} r \, dr$$

Integrating with boundary conditions $u = 0$ when $r = R$,

$$u = \frac{\Delta P}{4 L \eta} (R^2 - r^2)$$

(b) Poiseuille Equation.

Consider a cylindrical annulus of fluid of inner radius r and thickness dr. The quantity of fluid flowing down the annulus in unit time is given by

$$q = u. \; 2\pi r.dr.$$

Substituting for u and integrating from r = 0 to r = R, the total flow rate is given by

$$Q = \frac{\Delta P \, \pi \, R^2}{8 \, L \, \eta} \, .$$

APPENDIX III

DERIVATION OF DOPPLER AMPLITUDE SPECTRA

(from Section 2.3)

(a) Parabolic Flow Profile

Consider the flow velocity $u(r,t)$ to have parabolic profile and arbitrary time dependence. The Doppler shift is proportional to velocity, by equation (2-4), and so can be expressed:

$$\Delta f(r,t) = B(t)\ (1 - (r/R)^2),\ \text{for}\ \ 0 \leqslant r < R.$$

Rearranging and differentiation:

$$dr = \frac{-R}{2\ B(t)}\ \left(1 - \frac{\Delta f}{B(t)}\right)^{-\frac{1}{2}}\ df.$$

The area under the Doppler amplitude spectrum for a small range of frequencies, width df, is dependent on the cross-sectional area of fluid which has the corresponding velocity. Thus:

$$I(f)df = C_1 . 2\pi\ r.dr,$$

and substituting for r and dr

$$I(f) = C_2/_{B(t)},\ \text{for}\ 0 < \Delta f < \Delta f_{max},$$

where C_1 and C_2 are constants.

Thus the amplitude spectrum is flat for the range 0 to Δf_{max}, as shown in Figure 2-7(a). All values of Δf have the same time dependence, $B(t)$, since the profile is

assumed to maintain a constant shape. Thus the area under the amplitude spectrum is given by:

$$I(f).\ \Delta f_{max} = \left(C_2/B(t)\right).\ B(t).1$$
$$= C_2$$

As expected, the area under the spectrum is constant with time.

(b) 'Real' Blood Flow Profile

To illustrate the effect of a flattened profile, consider the profile to be given by

$$u(t) = (1 - (r/R)^4) \times \text{time function, for } 0 < r \leqslant R.$$

The resulting Doppler shift is then

$$\Delta f(r,t) = B(t)\ (1 - (r/R)^4)$$

Rearranging and differentiating:

$$dr = \frac{-R}{4\ B(t)}\ \left(1 - \frac{\Delta f}{B(t)}\right)^{-\frac{3}{4}} df$$

Substituting for r and dr gives

$$I(f) = C3/B(t)\ \left(1 - \Delta f/B(t)\right)^{-\frac{1}{2}}, \text{ for } 0 < \Delta f < \Delta f_{max}.$$

The resulting peaked spectrum is shown in Figure 2-7(b).

(Appendix III cont.)

(c) Parabolic Profile with Narrowbeam

For the inner concentric area, $0 \leqslant r \leqslant w$, all cells with each velocity are illuminated, producing a flat portion of the spectrum:

$$I(f) = {}^{C2}/_{B(t)}, \quad 0 \leqslant \Delta f \leqslant (1 - ({}^{w}/_{R})^{2}) \, \Delta f_{max}.$$

However for $w < r \leqslant R$, each concentric annulus has illuminated cross-sectional area = $4r \sin^{-1}({}^{w}/_{r}).dr$. Thus the spectrum amplitude becomes

$$I(f).dr = C_1.4r \sin^{-1}({}^{w}/_{r}).dr, \quad w < r \leqslant R.$$

Substituting for r and dr

$$I(f) = {}^{C_2}/_{B(t)} \quad \sin^{-1}\left(\frac{w}{R(1 \mp {}^{\Delta f}/_{B(t)})} \right).$$

Again, the modification causes accentuation of the highest frequencies in the Doppler amplitude spectrum, as shown in Figure 2-8.

APPENDIX IV

FIRST-ORDER NUMERICAL INTEGRATION METHODS

(from Section 5-2)

Consider the area under the curve $y = f(x)$ from $x = a$ to $x = b$,

$$I = \int_a^b f(x)\,dx$$

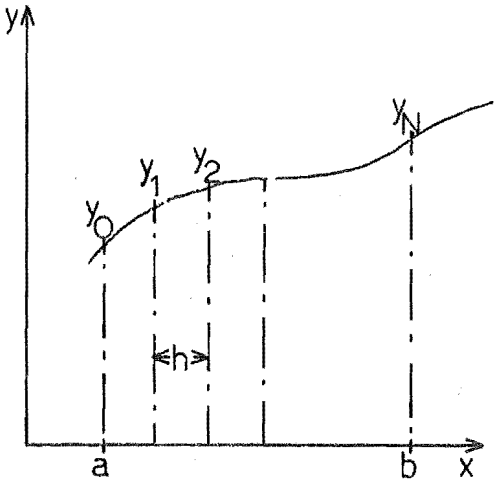

Divide into N small intervals of width h, where

$$h = \frac{b - a}{N}$$

The Trapezoidal Rule estimates the area (integral) by considering the points y_0, y_1, y_2, etc. joined by straight lines, so

$$I = I_h^{TR} = h/2\ (y_0 + 2y_1 + 2y_2 + \ldots + y_N)$$

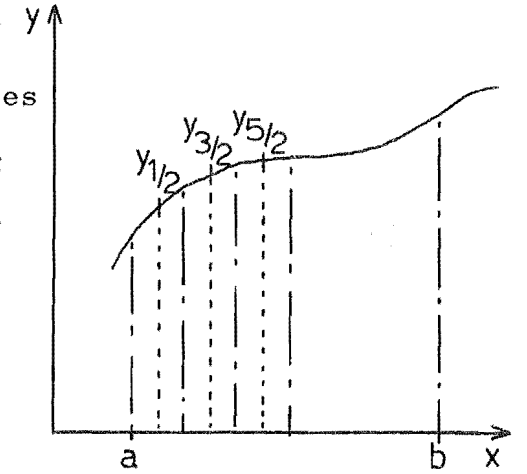

The Rectangular Rule estimates the area from the mid-interval function values

$$I_h^{RR} = h\ (y_{\frac{1}{2}} + y_{\frac{2}{3}} + \ldots + y_{N-\frac{1}{2}}).$$

To a first-order approximation,

$$y_{\frac{1}{2}} = \frac{y_0 + y_1}{2}\ ,\quad y_{\frac{2}{3}} = \frac{y_1 + y_2}{2}\ ,\quad \text{etc.}$$

Substituting,

$$I_h^{RR} = h/2\ (y_0 + 2y_1 + 2y_2 + \ldots + y_N)$$
$$= I_h^{RR}$$

Thus the Rectangular Rule is equivalent to the Trapezoidal Rule.

APPENDIX V

ERROR ANALYSIS OF VOLUME SUMMATION

(from Section 5.4)

To establish a 95% confidence limit on $\sum X_i^2$, for each measurement, consider:

$$x_i = X_i + e_{x_i}$$

where:

$$-\tfrac{1}{2} < e_x \leqslant +\tfrac{1}{2}.$$

The corresponding maximum relative error of each measurement is $\pm$ 1/128. This maximum error is doubled by the squaring process.

Consider the errors produced when 8 measurements are added together. The quantisation interval can be divided up into four possible error ranges, as shown below:

CODE	INTERVAL	PROBABILITY
a	$-\tfrac{1}{2} < e_x \leqslant -\tfrac{1}{4}$	0.25
b	$-\tfrac{1}{4} < e_x \leqslant 0$	0.25
c	$0 < e_x \leqslant +\tfrac{1}{4}$	0.25
d	$+\tfrac{1}{4} < e_x \leqslant +\tfrac{1}{2}$	0.25
Total	$-\tfrac{1}{2} < e_x \leqslant +\tfrac{1}{2}$	1.0

The worst possible case of errors occurs when all 8 errors are in the maximum range with the same sign. The probability of this occurrence is $2 \times (0.25)^8$ and the maximum error produced is $\pm$ 4 quantisation intervals.

The worst 0.05 (5%) of cases were considered. These are tabulated in part below.

COMBINATION TYPE	NO. OF COMBINATIONS N_c	$2 \times N_c \times P$ $P = (0.25)^8$	MAXIMUM ERROR
8 x d	1	.0000306	4.0
7 x d, 1 x c	$^8C_1 = 8$	.000244	3.75
6 x d, 2 x c	$^8C_2 = 28$	.000857	3.50
7 x d, 1 x b	$^8C_1 = 8$	.000244	3.25
.	.	.	.
.	.	.	.
.	.	.	.
3 x d, 4 x c, 1 x b	$^8C_5 \times {}^5C_1 = 280$	.00857	2.25
6 x d, 1 x b, 1 x a	$^8C_2 \times {}^2C_1 = 56$	.00171	2.25

Total = .0516

The 95% confidence limit thus excludes all maximum errors of > 2.0 intervals, so the maximum relative error of each volume summation (considering 8 squared measurements) is:

$$\left|\frac{e_{Vs}}{V_s}\right|, \left|\frac{e_{Vd}}{V_d}\right| \underset{95\%}{\leqslant} \frac{2.0 \times 2}{8 \times 64} = {}^1/128.$$

APPENDIX VI

MNEMONICS USED IN CALCULATOR DESIGN

(from Chapter 6)

Pushbutton Input Qualifiers

NCLR	clear
NINT	integrate
NVSS	syst. vol. store
NVDS	dias. vol. store
NVSD	syst. vol. display
NVDD	dias. vol. display
NCEF	C.E.F. calculation

Type of logic terminal	Mnemonic initial letter	Meaning for terminal equal to	
		1	0
Output	H	active	inactive
	L	inactive	active
Input	Y	true	false
	N	false	true

Other Input Qualifiers

NPB	any pushbutton
NVD	display
NCLS	clear or store
NDC	division complete

S.C.U. Outputs

LACE	accumulator clock enable
HAMS	accumulator mode, shift
HCLA	clear accumulator
HCLD	clear display
HVLE	volume latch enable
HCNT	display counter clock enable
HCMP	complement selector output
SELA	selector address, A
SELB	selector address, B

(Appendix VI cont.)

Flags

YF1 operation performed once

YFCN binary/B.C.D. convert mode

APPENDIX VII

SYNCHRONOUS CONTROL UNIT TEST PROGRAM

(from Section 6.3)

PROGRAM LISTING

Page 1

```
C  CONTROL STATE MACHINE, C.E.F. CALCULATOR
C  LOGIC SYNTHESIS CHECK
C
      DIMENSION IS(6,3),NS(6),IP(8)
@     DO 20 I=1,8
@     IP(I)=1
      NDC=1
C  INPUT IDENTITY OF PUSHBUTTON OPERATED
      WRITE(1,300)
      READ(2,310)N
      IF(N.EQ.0)STOP
      IP(N)=0
C  INPUT THE INITIAL MACHINE STATE AND FLAG CONDITIONS
      WRITE(1,320)
      READ(2,330)((IS(J,I),J=1,6),I=1,3)
      WRITE(1,340)
      MSA=0
      MSK=0
C  START OF STATE MACHINE LOOP
C  ASSIGN INVERSIONS OF STATE VARIABLES
)     DO 70 I=1,6
)     NS(I)=IABS(IS(I,3)-1)
C  ASSIGN INPUT DEPENDENT VARIABLES
      NNPB=IABS(IP(1)*IP(2)*IP(3)*IP(4)*IP(5)*IP(6)*IP(7)-1)
      NVD=IP(5)*IP(6)
      NCLS=IP(1)*IP(3)*IP(4)
C  ASSIGN J,K  INPUTS  IN TERMS OF PRESENT STATE AND INPUTS
      IS(4,1)=IABS(IABS(IS(3,3)*IS(2,3)-1)*IABS(NS(3)*NS(2)*NS(1)*NNP

     CS(5)-1)*IABS(IS(3,3)*NS(1)*NDC*IABS(IP(1)-1)-1)-1)
      IS(4,2)=IABS(NS(3)*NS(2)-1)
      IS(3,1)=IABS(NS(4)*IABS(IS(2,3)*IS(1,3)-1)-1)
      IS(3,2)=IABS(IABS(IS(3,1)-1)*IABS(NS(1)*IABS(NDC-1)-1)-1)
      IS(2,1)=IABS(IABS(NS(3)*IS(1,3)-1)*IABS(IS(4,3)*IS(3,3)*NS(1)*

     C-1)-1)
      IS(2,2)=IABS(NS(4)*IS(1,3)-1)
      IS(1,1)=IABS(IABS(IS(2,3)*NVD-1)*IABS(IS(4,3)*NS(3)*IABS(IP(2)-

     C1)-1)
      IS(1,2)=IS(3,3)*NS(2)
      IS(5,1)=IS(4,3)
      IS(5,2)=NS(3)*NS(2)*NS(1)*IABS(NNPB-1)
      IS(6,1)=IS(4,3)
      IS(6,2)=NS(4)*IS(1,3)
```

(Appendix VII cont.)

PROGRAM LISTING

Page 2

```
C  ASSIGN OUTPUTS IN TERMS OF PRESENT STATE AND INPUTS
       IACE=IABS(IABS(NS(3)*NS(2)*NS(1)-1)*IABS(IS(4,3)*NS(1)-1)-1)
       IAMS=NS(4)*IS(3,3)*IS(1,3)
       ICLA=IS(4,3)*IS(3,3)*NS(1)
       ICLD=IABS(IABS(ICLA-1)*IABS(NS(4)*IS(1,3)-1)-1)
       IVLE=IS(4,3)*NS(3)*NS(2)*IP(2)
       ICNT=NS(4)*IS(3,3)*NS(1)
       ICMP=IABS(IABS(NS(3)*NS(2)-1)*IABS(IS(3,3)*NS(1)-1)-1)
       ISELA=IS(3,1)
       ISELB=IABS(IABS(NS(3)*IS(1,3)-1)*IABS(IS(2,3)*IABS(IP(3)-1)-1)-
C  LIST PRESENT STATE AND CORRESPONDING FLAGS, OUTPUTS
       WRITE(1,350)IS(1,3),IS(2,3),IS(3,3),IS(4,3),IS(5,3),IS(6,3),IA(

     CAMS,ICLA,ICLD,IVLE,ICNT,ICMP,ISELA,ISELB
C  FIND NEXT MACHINE STATE AND FLAGS FROM J,K INPUTS
       DO 100 I=1,6
100    IS(I,3)=IABS(IABS(NS(I)*IS(I,1)-1)*IABS(IS(I,3)*IABS(IS(I,2)-1:

      C-1)
       IF(MSA.GT.2)GO TO 200
       MPA=IS(1,3)+IS(2,3)+IS(3,3)+IS(4,3)
       IF(MPA.EQ.0)MSA=MSA+1
       MPK=IS(1,3)+IS(2,3)+IABS(IS(3,3)-1)+IS(4,3)
       IF(MPK.EQ.0)MSK=MSK+1
       IF(MSK.LT.3)GO TO 150
       NDC=0
C  NEXT STATE NOW BECOMES PRESENT STATE, REPEAT
50     GO TO 60
200    GO TO 10
300    FORMAT(/14HPUSHBUTTON NO?)
10     FORMAT(I1)
20     FORMAT(/14HINITIAL STATE?)
30     FORMAT(6I1)
40     FORMAT(/3X,5HSTATE,5X,5HFLAGS,5X,7HOUTPUTS/2X,7HD C B A,3X,6HF1

     CN,3X,17HL M N O P Q R S T)
350    FORMAT(2X,4(I1,1X),3X,I1,2X,I1,4X,9(I1,1X))
       END
```

(Appendix VII, cont.)

EXAMPLES OF RESULTS*

```
PUSHBUTTON NO?      7
INITIAL STATE?      000000
          STATE       FLAGS          OUTPUTS
        D C B A     F1   FCN    L M N O P Q R S T
        0 0 0 0      0    0     1 0 0 0 0 0 1 0 0
        0 0 0 1      0    0     1 0 0 0 1 0 1 1 0
        0 0 1 1      1    1     1 0 1 1 0 0 1 1 0
        0 1 0 0      1    1     0 0 0 0 0 0 0 0 0
        1 0 0 0      1    1     0 0 0 1 0 0 1 0 1
        1 1 0 0      1    0     0 0 0 1 0 0 0 1 1
        1 1 1 0      1    0     0 1 0 1 0 0 0 1 0
        1 1 0 1      1    0     0 0 0 0 0 0 0 1 1
        1 0 1 0      1    1     0 1 0 1 0 0 0 0 0
        0 0 1 0      1    0     0 0 0 0 0 1 1 0 0
        0 0 1 0      1    0     0 0 0 0 0 1 1 0 0
        0 0 1 0      1    0     0 0 0 0 0 1 1 0 0
        0 0 0 0      1    0     1 0 0 0 0 0 1 0 0

PUSHBUTTON NO?      5
INITIAL STATE?      000000
          STATE       FLAGS          OUTPUTS
        D C B A     F1   FCN    L M N O P Q R S T
        0 0 0 0      0    0     1 0 0 0 0 0 1 0 0
        0 0 0 1      0    0     1 0 0 0 1 0 1 1 0
        0 0 1 1      1    1     1 0 1 1 0 0 1 1 0
        0 1 0 0      1    1     0 0 0 0 0 0 0 0 1
        0 0 0 0      1    1     1 0 0 0 0 0 1 0 0

PUSHBUTTON NO?      8
INITIAL STATE?      000000
          STATE       FLAGS          OUTPUTS
        D C B A     F1   FCN    L M N O P Q R S T
        0 0 0 0      0    0     1 0 0 0 0 0 1 0 0
        0 0 0 0      0    0     1 0 0 0 0 0 1 0 0
        0 0 0 0      0    0     1 0 0 0 0 0 1 0 0
```

*Pushbutton and output coding

Pushbuttons: 1 NCLR, 2 NINT, 3 NVSS, 4 NVDS, 5 NVSD, 6 NVDD, 7 NCEF, 8 no pushbutton.

Outputs: L LACE, M HAMS, N HCLA, O HCLD, P HVLE, Q HCNT, R HCMP, S SELA, T SELB.

APPENDIX VIII

CORONARY ARTERY SCORING

(from Section 7.1)

The score is awarded on the basis of the three major coronary supply vessels, the anterior descending and circumflex branches of the left coronary artery and the right coronary artery. Each is scored according to:

1 = normal artery

2 = irregularity up to 50% lumenal restriction

3 = generalised narrowing with more than 50% in one or more areas or single area of 80%

4 = complete obstruction.

Minimum score = 3

Maximum score = 12.